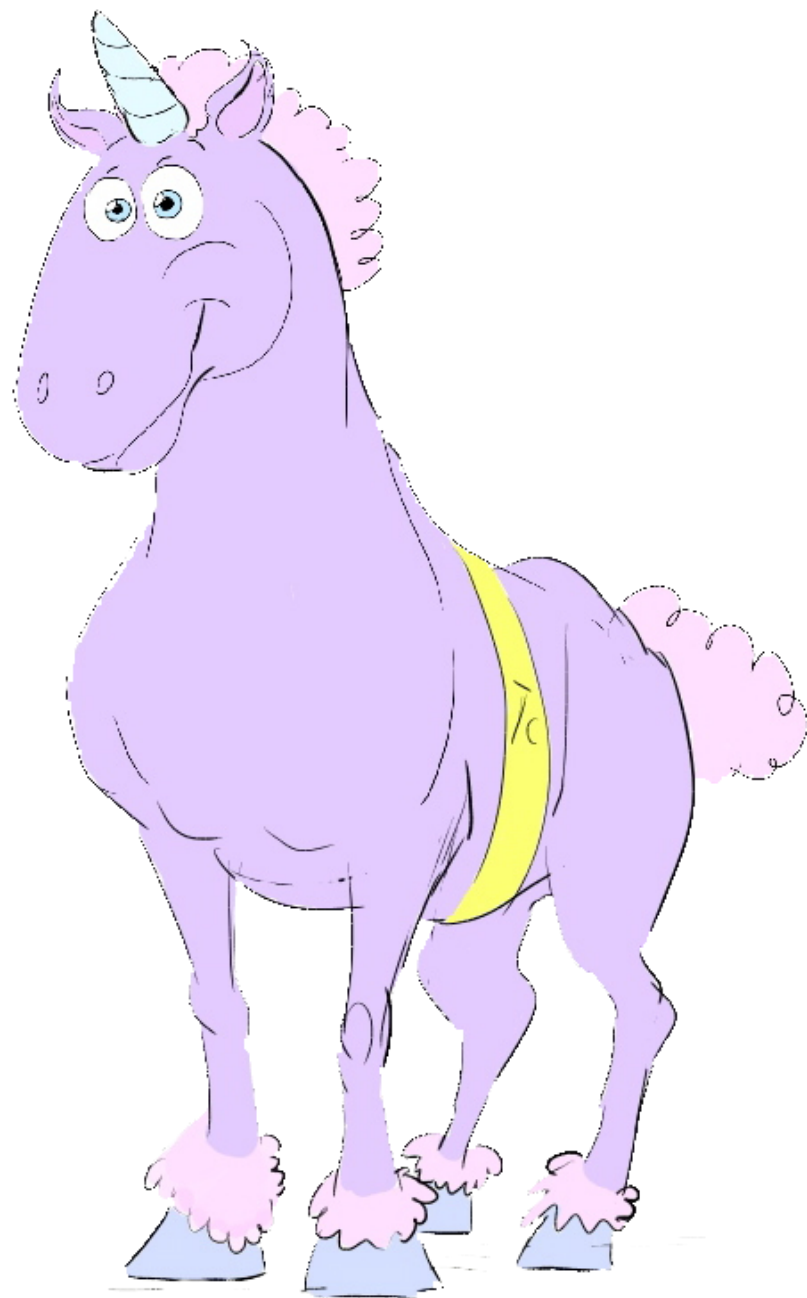


Attitude Control and Fault Detection for AAUSAT3



Anders Bech Borchersen
Bjørn Eskildsen
Kasper Worre Foged
Jonas Lauridsen





Title:

Attitude Control and Fault Detection for AAUSAT3

Theme:

Modeling and Regulation

Project period:

February 1st - June 1st, 2010

Project group: 10gr832

Group members:

Anders Bech Borchersen

Bjørn Eskildsen

Kasper Worre Foged

Jonas Lauridsen

Supervisor:

Rafael Wisniewski

Number of copies: 7

Number of report pages: 94

Appended documents:

(9 appendix, 1 CD-ROM)

Total number of pages: 119

Finished: June 2010

Abstract:

AAUSAT3 is the third student cubesat satellite developed at Aalborg University. The mission objective is to evaluate the possibility of receiving AIS messages from the ships in the waters around Greenland, which for high reliability requires an Attitude Determination and Control System.

This report studies kinematics and dynamics of the AAUSAT3 and describes the design of three controllers. For detumbling the satellite (B-dot controller) and for reference frame pointing (inertial and nadir pointing controllers) by LQR-design. The designed controllers have been tested for stability, using stability theory for periodic systems.

Due to the hostile space environment, some sensors and actuators can possibly fail and thus Fault Detection and Isolation (FDI) is designed. For fault analysis, a Failure Mode and Effect Analysis (FMEA) is conducted, while residuals are generated by a bank of Unknown Input Observers and evaluated using the CUSUM algorithm. The information from the FDI is used in a supervisor which carries out reconfiguration regarding controllers, sensors, and actuators.

By using an advanced simulation model the designed system is validated. All three controllers are able to stabilize the satellite, when affected by environmental disturbances and noisy sensors. Both the inertial and nadir pointing controller are able to hold the satellite below an error angle of 50° 90% of the time. The FDI is able to detect all the tested simulated faults, but not all faults were isolated correctly and some detection times did not satisfy the requirement.

Preface

This report describes the project developed by Group 832 on the 8th semester, Intelligent Autonomous Systems. Department of Control, Institute of Electronic Systems, Aalborg University. The target group for the report is primarily supervisors and students attending 8th semester Control Engineering.

When using references in the text, equations are denoted "(no.)" and figures are denoted "Fig. no.". Units in calculations are given in square brackets, while units used in the body text are denoted in *italic*. Source references are given with square brackets and possibly page reference and nomenclature is defined on vi. All sources are listed in the Bibliography on page 118.

A composed CD containing used data sheets, source code, MATLAB scripts, Simulink Models, and Internet sources, is attached in Appendix J.

Acknowledgements

The group would like to thank Kasper Fuglsang Jensen and Kasper Vinther for introduction of the Simulink simulation environment of the satellite and for borrowing the nomenclature and notation list, and Jakob Foged for drawing the report cover.

Author Signatures

Anders Bech Borchersen

Bjørn Eskildsen

Jonas Lauridsen

Kasper Worre Foged

Table of Contents

Preface	iii
1 Introduction	1
1.1 The AAU Cubesat Project	1
1.2 The AAUSAT3 project	1
1.3 Subsystems of the AAUSAT3	2
1.4 The report structure	4
2 Attitude Determination and Control System on AAUSAT3	5
2.1 Sensors and Actuators	7
2.2 Software	12
2.3 Controllers and FDI	14
2.4 Requirement Specification	15
3 Modeling	17
3.1 Reference Frames	17
3.2 Magnetic Field Model	21
3.3 Satellite Dynamics and Kinematics	22
3.4 Model for Nadir Pointing	25
3.5 Energy Optimizing Control Torque	29
3.6 Introduction of Reference	30
3.7 Simulation Environment	31
3.8 Model Validation	35
4 Controllers	40
4.1 Detumbling Controller	40
4.2 Reference Frame Pointing Controllers	44
5 Fault Analysis	52
5.1 Failure Mode and Effects Analysis	52
5.2 Severity Occurrence Analysis	56
6 Fault Detection and Isolation	58
6.1 Simple FDI Methods	59
6.2 Unknown Input Observer	61
6.3 Model Based FDI Overview	66
6.4 Autonomous Supervisor	75
7 Acceptance Test	80
7.1 Test of the B-dot Controller	80
7.2 Test of Constant Gain Controller	81

7.3	Test of FDI system	84
8	Closure	91
8.1	Conclusion	91
8.2	Perspective and Further Work	92
A	General Rotational Kinematics	94
A.1	Euler Angles	94
A.2	Euler's Eigenaxis	96
A.3	Quaternions	98
A.4	The Angular Velocity	98
B	Quaternion Algebra	99
B.1	Quaternion Multiplication	99
B.2	Quaternion Addition and Subtraction	100
B.3	Quaternion Complex Conjugate	100
B.4	Quaternion Norm and Inverse	101
B.5	Quaternion Rotation of a Vector	101
C	Dynamic Equations for Nadir pointing	102
D	Linearization of Model Equations	103
D.1	Linearization of Kinematics	103
D.2	Linearization of Dynamics	105
D.3	The Linearized Model	106
E	The State Transition Matrix	107
E.1	The Time-independent System	107
E.2	Time-dependent Periodic System and Floquet Theory	107
F	Lyapunov Stability	109
G	Fault Propagation Calculations	110
H	CUSUM Algorithm Calculations	112
I	Simulation Environment	115
J	CD Content	117
	Bibliography	118

Nomenclature

Acronyms

ACS	Attitude Control System.
ADS	Attitude Determination System.
ADCS	Attitude Determination and Control System.
AIS	Automatic Identification System.
CAM	CAMera system.
CAN	Controller Area Network.
CoM	Center of Mass.
EPS	Electrical Power Supply.
FDI	Fault Detection and Isolation.
FP	Flight Planner.
FTC	Fault Tolerant Control.
GPS	Global Positioning System.
GND	Ground Station.
I ² C	Inter-Integrated Circuit.
IGRF	International Geomagnetic Reference Model.
IO	Input Output.
JD	Julian Date.
LEO	Low Earth Orbit.
LOG	data LOGging system.
MCC	Mission Control Center.
NORAD	North American Aerospace Defense Command.
PCB	Printed Circuit Board.
P-POD	Poly Picosatellite Orbital Deployer.
SGP	Simplified General Perturbation.
SPI	Serial Peripheral Interface.
SWIS	SoftWare Image Server.
TLE	Two-Line orbital Element set.
UHF	Ultra High Frequency.

Reference Frames

ECI	(i)	Earth Centered Inertial reference frame.
ECEF	(e)	Earth Centered Earth Fixed reference frame.
ORF	(o)	Orbit Reference Frame.
SBRF	(s)	Satellite Body Reference Frame.
CRF	(c)	Controller Reference Frame.

Notation

The following mathematical notations are used.

Vectors are written as:

$$\mathbf{v}$$

Matrices are written as:

$$\underline{\mathbf{M}}$$

The reference frame a vector belongs to is indicated as

$${}^c\mathbf{v}$$

where c denotes the CRF. Rotations are written

$${}^s_c\mathbf{q}$$

which is a rotation from the CRF to the SBRF described by a quaternion. A direct cosine matrix is defined as

$${}^s\underline{\mathbf{C}}_c \quad (1)$$

A direct cosine matrix based on a quaternion is defined as

$$\underline{\mathbf{C}}({}^s_c\mathbf{q}) \quad (2)$$

The transpose is denoted

$$\mathbf{v}^T$$

The complex conjugate is denoted

$$\mathbf{q}^*$$

The inverse of a matrix is written as

$$\underline{\mathbf{M}}^{-1}$$

Unit vectors are typed as

$$\hat{\mathbf{u}}$$

Label assignment to variables and constants are written as a subscript as

$$\mathbf{q}_{label}$$

A tilde is the small signal value and a line indicates the operating point value

$$\tilde{i}, \bar{i}$$

Time derivatives are denoted with a dot as

$$\dot{x}$$

Symbols

Symbol	Description	Unit
A	Surface area	$[m^2]$
A_{mt}	Area enclosed by magnetorquer	$[m^2]$
\mathbf{A}_{mt}	Perpendicular vector to A_{mt}	$[m^2]$
\mathbf{I}_{sat}	Inertia matrix of the satellite	$[kgm^2]$
i_o	Inclination of the orbit plane	$[deg]$
I_{mt}	Current through magnetorquer	$[A]$
\mathbf{L}	Angular momentum	$[Nm \cdot s]$
m_a	Arbitrary mass	$[Kg]$
\mathbf{m}_{pm}	Magnetic dipole moment of the permanent magnet	$[Am^2]$
\mathbf{N}_{ctrl}	Control torque	$[Nm]$
\mathbf{N}_{dist}	Disturbance torque	$[Nm]$
\mathbf{N}_{pm}	Torque caused by permanent magnet	$[Nm]$
ω	Angular velocity vector ($\omega_1, \omega_2, \omega_3$)	$[rad/s]$

Terminology

ARM7	refers to the 32 [bit] Atmel ARM microcontroller AT91SAM7A3.
Apogee	is the point where a satellite reaches the greatest distance to the Earth during its orbit.
Attitude	is the orientation of a satellite in a certain reference frame.
AVR8	refers to the 8 [bit] Atmel microcontroller AT91CAN128.
Ecliptic	plane represents Earth's orbit around the Sun. It is inclined at an approximate angle of 23 [deg] to the equator.
Eclipse	is the transit of Earth blocking all or some of the Sun's radiation as seen from a satellite.
Epoch	is a moment in time for which the position or the orbital elements of a celestial body are specified.
Geoid	is the equipotential surface which would coincide exactly with the mean ocean surface of the Earth.
Geostationary	is the state where a satellite appears stationary in the ECEF. This is approximately an altitude of 35 900 [km] above the Earth's equator and a speed matching the rotation of the Earth.
Mean anomaly	of a satellite, moving with a constant angular speed, is the angle it has traveled since perigee measured in radians.
Nadir	is the direction towards the center of the Earth.
Orbital rate	is the mean angular velocity of a satellite during an orbit around the Earth.
Latitude	is the angular distance north or south of the Earth's equator, measured in degrees.
Longitude	is the angular distance east or west from the prime meridian at Greenwich, measured in degrees.
Pitch, roll, yaw	are the angles describing the attitude of a satellite in a reference frame. Pitch is the rotation about the y-axis, roll refers to rotation about the x-axis and yaw is the rotation about the z-axis.
Perigee	is the point where a satellite reaches the smallest distance to the Earth during its orbit.
System engineering group	is a design and planning group, consisting of members of the AAUSAT3 team.
Vernal Equinox	is where the ecliptic plane crosses the equator going from south to north. Equinox happens twice a year and vernal is the spring equinox (northern hemisphere spring).

continued...

Zenith

of a satellite is the unit vector in the CRF pointing away from the center of the Earth.

Color standard

In Fig. 1, the different colors in the block diagrams is explained.

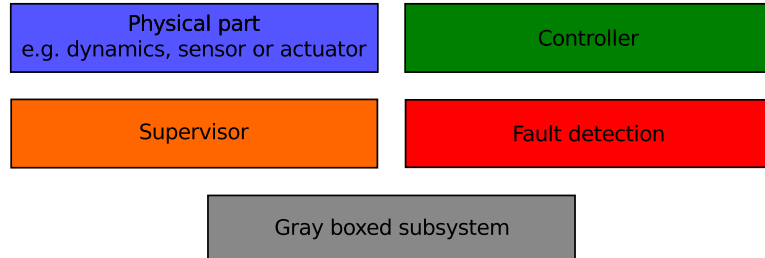


Figure 1: The colors in the block diagrams

Chapter 1

Introduction

1.1 The AAU Cubesat Project

The purpose of the AAU CubeSat project is to introduce students to knowledge in space worthy technologies and to involve them in the design, construction, and implementation process of pico-size satellites. The project was initiated in the summer of 2001, with the launch of the first satellite "AAU Cubesat" in April 2003. The success of AAU Cubesat was limited to receiving a beacon from the satellite[team 10a]. The second satellite AAUSATII was launched April 28 2008 and is still functional thought the number of successful packages being received is reduced due to the fact that the satellite is tumbling[team 10c].

As the development of the cubesat satellites is a large students project the AAUSAT Cubesat Project is a cooperation between several students group involving the institutes of Electronic Systems, Mechanical Engineering, Computer Science, and Energy Technology[team 10a].

The cubesat concept is developed at California Polytechnic State University and Standford University in 1999. This concept limits the satellite dimension to $10 \times 10 \times 10 \text{ cm}$ and the mass to 1 kg [team 10d]. AAUSAT3 is expected to measure $10 \times 10 \times 11 \text{ cm}$.

1.2 The AAUSAT3 project

This section is based on [team 10b].

The AAUSAT3 sat is the third cubesat projects developed by students at Aalborg University and is scheduled to launch in the beginning of 2011. The main objective of the project is to develop a working satellite and secondly to have the payloads function in orbit.

The objective for the primary payload is to receive Automatic Identification System (AIS) messages from the ships in the waters around Greenland. This mission objective is given by The Royal Danish Administration of Navigation and Hydrography (RDANH) now known as Danish Maritime Safety Administration (DaMSA), who which to have the safest seaways in the world. As the waters around Greenland covers an enormous area in a hostile environment the use of ground stations, for AIS monitoring, is both expensive an insufficient for an effective monitoring of the waters. As secondary payload a GPS module will be implemented, such that it is possible to evaluate at which satellite locations, the AIS data was received. Also a camera is applied as secondary payload. However it is likely that the camera will not be implemented, due to time issues.

For total mission success the satellite should fulfill the following mission goals which is defined by the AAUSAT3 system engineering group:

- The satellite is capable of monitoring all of Greenland, and the open sea around, in one

pass.

- The ship traffic data around Greenland can be downloaded via UHF in subsequent passes over Aalborg.
- The satellite can receive GPS coordinates to evaluate received AIS data.
- The satellite can detumble itself and point the antennas in certain directions using an Attitude Determination and Control System (ADCS).

1.3 Subsystems of the AAUSAT3

The communication between the different subsystem of the AAUSAT3 is based on non-centralized communication and thus functioning as a distributed system over CAN bus. The reason for this structure is to ensure that a non-working part of the satellite will confine the problem and thereby limit the affect to a dysfunctional subsystem if possible. For the satellite to meet the demand listed above a whole range of different subsystems are required to operate in orbit and on the ground. These are:

- EPS (Electrical Power Supply)
- LOG (Data Logging)
- FP (Flight Planner)
- UHF (Ultra High Frequency radio link)
- AIS-1 (Automatic Identification System 1)
- AIS-2 (Automatic Identification System 2)
- ADCS (Attitude Determination and Control System)
- GPS (Global Positioning System)
- CAM (Camera)
- SWIS (SoftWare Image Server)
- GND (Ground Station)
- MCC (Mission Control Center)

EPS The Electrical Power Supply delivers, monitor and control the power to the subsystems. This includes the current to voltage conversions, which is needed for charging the batteries and supplying the subsystems from the solar cells.

LOG The Data Logger saves log data from the different subsystems, which cannot immediately be transferred via the UHF to the ground stations, in the internal memory of the system.

FP The Flight Planner is the over all state machine for the satellite. This is where it is decided which subsystems should be turned on and at what power level they should be turned off again. The FP is autonomous so if nothing is received from the GND it will automatically start performing predefined assignments.

UHF The Ultra High Frequency radio link, enables the communication between ground stations and the subsystem of the satellite. Any information from subsystem to ground is transmitted via the UHF and vice versa.

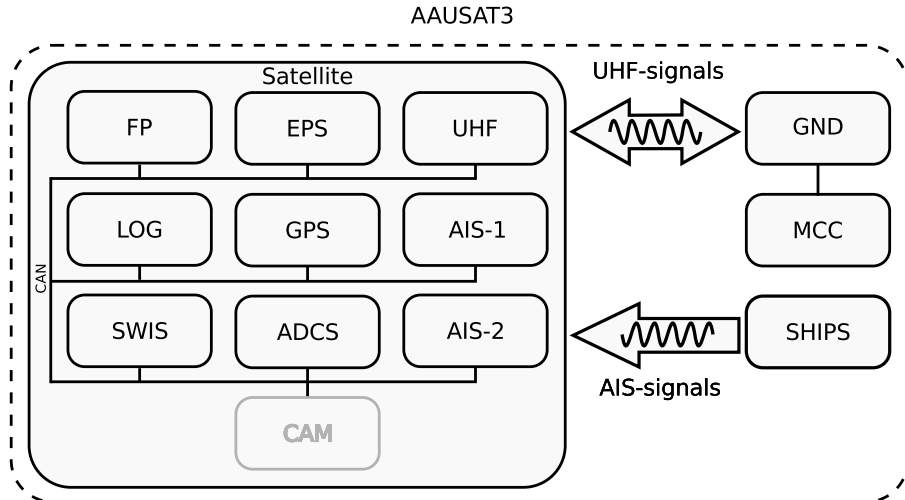


Figure 1.1: Communication between subsystems of AAUSAT3, ships sending AIS-messages, and Mission Control Center

AIS-1 and AIS-2 The Automatic Identification System is the satellite primary payload. It is able to detect AIS-messages send from ships and to analyse the quality of the radio link. Furthermore it analysis the data onboard (AIS-1) of forward it to the UHF, which will transfer the data to the ground station (AIS-2).

ADCS The Attitude Determination and Control System control the attitude of the satellite in orbit and thus prevents the satellite from tumbling (detumbling mode) or rotates it to a desired attitude (pointing mode). The actuation is performed by 3-axis coils and a permanent magnet. By controlling the attitude of the satellite a reliable and steady communication between ships, satellite and ground station can be achieved. Also the camera can be turned to a desired attitude

GPS The GPS is a secondary payload used to control the correctness of the received AIS messages. Also it can be used to estimate the orbit propagation of the satellite.

CAM The Camera is a secondary payload which objective is to take pictures of the Earth. The camera need the ADCS to be able to point towards the Earth to take pictures. The purpose of taking pictures is manly to give increase the publicity about the project. The camera is illustrated by a gray box as it is questionable whether it will be implemented in time for the launch.

SWIS The Software Image Server is a software module placed onboard the AAUSAT3. The module is used to store different software images for the subsystems. This is used for uploading new software to the satellite and change back to a stable version in case of failure in the newly uploaded software.

GND The Ground Station handles radio communication with the satellite over the UHF-connection radio link, control the modem, and the direction of the ground antennas.

MCC The Mission Control Center is the user interface to the satellite, the MCC is also where data is stored in a database and presented to the satellite controllers which then decided what commands to send to the satellite. The commands is then send from the MCC to the Ground station to the satellite.

A drawing of the AAUSAT3 with the subsystem connection is seen in Fig. 1.1.

1.4 The report structure

The mission objective is to evaluate the possibility of receiving AIS-messages from the ships and transmitting these to the ground station. The secondary objective is to take pictures of the surface of the Earth. Both payloads are dependent on a well functioning attitude control (ADCS). In the hostile space environment, it is likely that some sensors and actuators will fail, thus it is advantageous to be able to detect faults in the transducers and be able to control the satellite without using these faulty transducers to ensure a successful mission. This leads to the problem statement:

How to develop a Fault Detection and Isolation (FDI) and Control for the ADCS system of the AAUSAT3?

Such a design procedure involves a number of widespread assignment, why an overview of the project is presented chapterwise in the following.

In **Chapter 2** the structure of the ADCS for the AAUSAT3 is presented, which includes the hardware, software, and controller platform along with a requirement specification for the controllers and the FDI.

Chapter 3 concerns with the modeling of the kinematics and the dynamics of two different models for the aausat3. a short description of the applied reference frames, and a magnetic field model are presented. lastly the aausat3 kinematic and dynamic models are validated.

in **Chapter 4** three controllers are studied a B-dot detumbling controller, a controller with an attitude reference wrt. the Earth Inertial Frame (see Section 3.1.1), and a controller with an attitude reference wrt. the Orbit Reference Frame (see Section 3.1.3).

In **Chapter 5** a fault analysis is performed describing common fault scenarios on sensors and actuators. Based on the fault scenarios a fault propagation scheme is presented, which illustrates how occurring hardware faults propagate. The Fault analysis concludes with a severity analysis.

In **Chapter 6** a Fault Detection and Isolation is performed. A residual generation is performed by the use of Unknown Input Observers and the fault are isolated to by CUSUM algorithms and a fault decision logic. Also a Supervisory Controller is designed such that a decision, can be made given occurring scenarios.

In **Chapter 7** an Acceptance Test is performed for the FDI and the three controllers.

Chapter 8 summarize the report and concludes on the result from the acceptance test. Also perspectives are presented along with future work needed for the designed FDI and attitude control to be implemented on the satellite.

Chapter 2

Attitude Determination and Control System on AAUSAT3

In this chapter the general structure of the Attitude Determination and Control System (ADCS) on AAUSAT3 is introduced. The purpose of the ADCS is to have the attitude of the satellite stabilized while orbiting. This is achieved by first detumbling the satellite and then pointing it towards specific direction. The states of the ADCS system is shown in Fig. 2.1.

Off The ADCS is turned off by the EPS or the FP.

Diagnostics When the ADCS is turned on by either EPS or FP it runs diagnostic procedure before it starts any controlling.

Idle/sleep Diagnostics is over waitng for a signal to start the controllers.

Detumbling The ADCS controls the satellite so it follows the magnetic field while orbiting (rotating with 0.0022 rad/s or $\approx 0.12 \text{ deg/s}$).

Pointing On commands from EPS or FP the satellite is poitned towards a specific direction or point. When the satellite is detumbled.

When the satellite is in the poitning state it is in one of the three substates. The substates for pointing is shown in Fig. 2.2.

Inertial pointing The ADCS points the satellite such that it follows the inertial coordinate system at all the time (see Section 3.1.1).

Nadir Pointing The ADCS points the satellite antennas towards Nadir at all the time.

Fixed Pointing The ADCS points one side to a specified point(e.g. Aalborg when the satellite is within range).

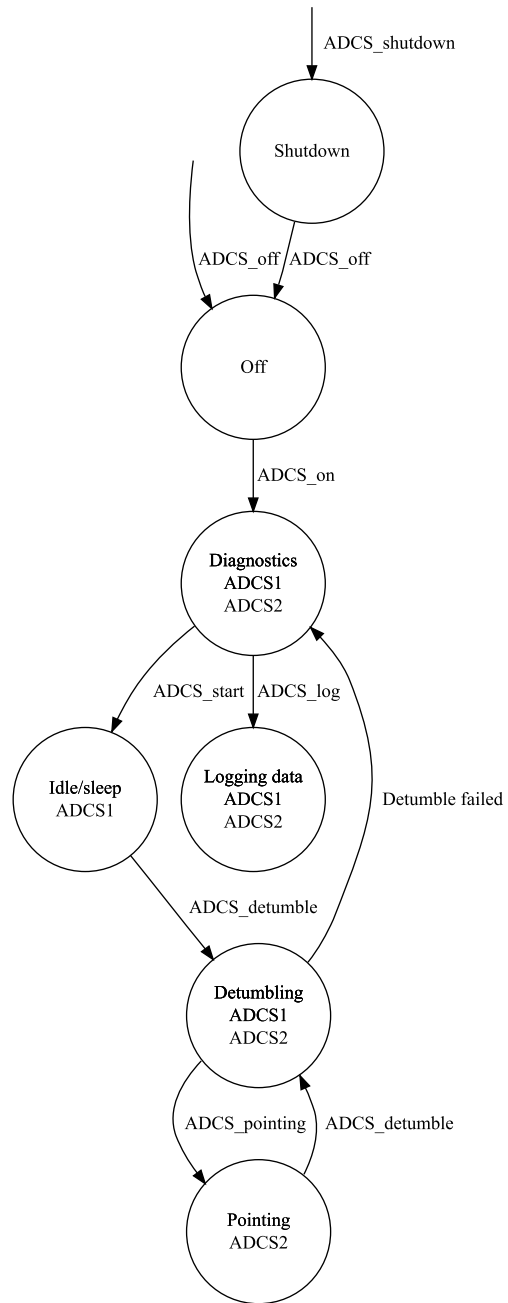


Figure 2.1: Over all states for the ADCS

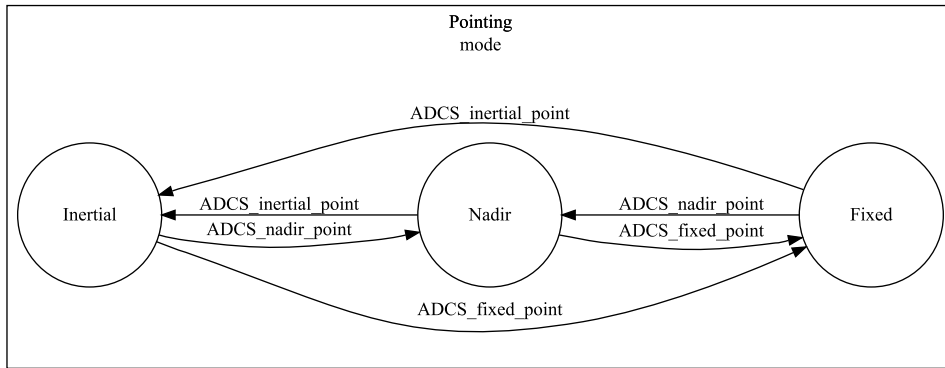


Figure 2.2: States for the ADCS when pointing

2.1 Sensors and Actuators

The hardware design of the ADCS has been performed by group 09gr935, which the hardware description in this section is based on [Jensen 10]. A diagram of the hardware layout is illustrated in Fig. 2.3. It has been decided to divide the ADCS into two separate systems ADCS1 and ADCS2. The two systems share actuators but the sensors are separated between the two systems as shown in Fig. 2.3.

ADCS1 is running on the AVR8-microprocessor since it is very insensitive to ambient

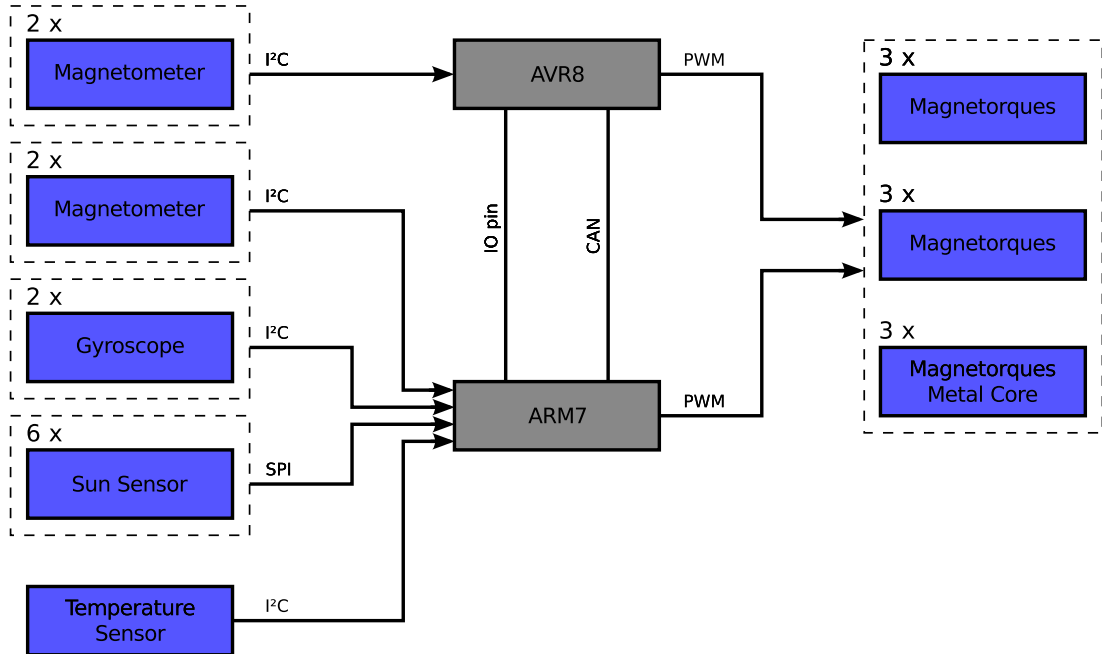


Figure 2.3: Overview diagram of the hardware layout in the ADCS

temperatures and has a very low power consumption [Atmel 06]. Thereby ADCS1 should be very stable and thus suitable for the AAUSAT3. ADCS1 is only capable of detumbling the satellite since the AVR8 is not a powerful microcontroller, and thus can not respect

the real time requirements for advanced algorithms, which is needed when the satellite is operating in pointing mode. Therefore ADCS1 only has the magnetometers connected, since these are able to handle the detumbling of the satellite. ADCS2 has to run both the pointing control and the detumbling control modes. ADCS2 thus runs on an ARM7-microcontroller to utilize the extra calculation power which is needed for pointing. More sensors are connected to the ARM7 since this is also needed for pointing the satellite.

2.1.1 Magnetometer

Having a spacecraft orbiting at a low altitude (as AAUSAT3), it is possible to measure the magnetic field of the earth relative to the spacecraft body frame using magnetometers, without being affected by a considerable noise level. For that reason, the AAUSAT3 is equipped with two different kind of magnetometers and a total of four magnetometers. One of each kind is connected to the AVR8 and one of each kind is connected to the ARM7. All the magnetometers are digital and the communication protocol between the microprocessors and the magnetometers is I²C. The two types of magnetometers are the Honeywell HMC6343 [Hor 08] and the Honeywell HMC5843 [Hor 09].

2.1.2 Sun Sensor

To be able to estimate the position of the sun relative to the Spacecraft Body Frame (see Section 3.1.4), the AAUSAT3 is equipped with 6 sun sensors (one on each side of the satellite). These are SLCD-61N8 photo diodes [Sil 04], which signals are transmitted to the ARM7 by SPI.

2.1.3 Gyroscopes

To measure the angular velocity of the different axis of the body frame, the AAUSAT3 is equipped with both a 1-axis gyroscope (IDG-1215 [Inv 09]) and a 2-axis gyroscope (ISZ-1215 [Inv 08]) to cover all the three axis. The gyroscopes provides an analog output, which is sampled by an ADC (ADS1115 [Tex 09]) and transmitted to the ARM7 using I²C.

2.1.4 Temperature Sensors

The temperature inside the satellite is measured using the temperature sensor (DS75LXU+ [Max 07]). Information regarding the temperature can be used to fault detection or feed-forward in hardware configurations.

2.1.5 GPS

The purpose of the onboard GPS receiver is to provide TLE-information such that the orbit propagation, via the SPG4, can be updated frequently (see Section 2.2.1). The GPS is named "Phoenix GPS Receiver" and is sponsored by "Deutsches Zentrum für Luft- und Raumfahrt" for experimental tests.

2.1.6 Permanent Magnet

AAUSAT3 is equipped with a permanent magnet which is fixed mounted in the SBRF (see Section 3.1.4). The permanent magnet north pole points in the direction of the negative z-axis (see Fig. 2.4), such that the AIS- and UHF-antennas are parallel to the earth's

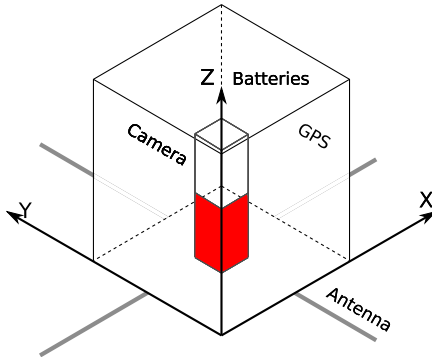


Figure 2.4: Placement of permanent magnet in Spacecraft Body Reference Frame

surface when flying over the north magnetic pole. The purpose of the permanent magnet is to ensure that the antennas on the satellite (AIS and UHF) is pointing towards the northern hemisphere, which is beneficial in order to communicate with the ground station in Aalborg and the ships around Greenland. By introducing the permanent magnet, it is possible to reduce the consumption of energy to magnetorquers, when pointing the antennas towards the ground station in Aalborg and the ships near Greenland which is the primary mission of the AAUSAT3, while the permanent magnet cause increased consumption of energy to magnetorquers when the satellite is near equator.

Permanent Magnet Design

The magnet, that is chosen is an N35 sintered neodymium magnet with a given magnetic dipole moment \mathbf{m}_{pm} of $0.0030 \text{ A} \cdot \text{m}^2$. The magnetic field strength of the earth is assumed to vary between $20\,000 \text{ nT}$ and $50\,000 \text{ nT}$, during an orbit, in an altitude of 600 km (see Fig. 3.8). The worst case for controlling the satellite is when the earth magnetic field strength is low because the torque that the actuators can produce is lowest there.

The torque that the permanent magnet contributes with, \mathbf{N}_{pm} , is given by (2.1)[Wertz 78, p. 643]:

$$\begin{aligned}\mathbf{N}_{pm} &= \mathbf{m}_{pm} \times \mathbf{B}_E \\ &= \|\mathbf{m}_{pm}\| \|\mathbf{B}_E\| \sin(\theta_{bpm}) \quad [\text{Nm}]\end{aligned}\tag{2.1}$$

θ_{bpm} : The angle between \mathbf{B}_E and \mathbf{m}_{pm}

The maximum torque can be obtained at an angle of $\theta_{bpm} = 90^\circ$ in which the torque, for the smallest value of \mathbf{B}_E , is 60 nNm and 150 nNm for the largest \mathbf{B}_E . For this reason the magnetorquer with a combined torque of up to 400 nNm per axis should be sufficient to counter the permanent magnet torque if it is needed.

2.1.7 Magnetorquers

AAUSAT3 is equipped with two sets of magnetorquers. These are mounted on three different sides of the satellite, which enables actuation in all three axis of the satellite body. The magnetorquers are all driven by a SI9988 H-bridge [Vis 04]. The magnetorques

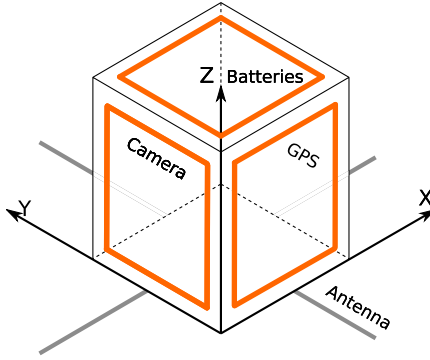


Figure 2.5: Placement of magnetorques in Spacecraft Body Reference Frame

are the primary actuator for the ADCS and has been designed by 09gr925. It is by group 925 chosen that each magnetorquer should produce a torque of 200 nNm in order to be able to detumble and to operate in tracking mode under environment disturbances, under low magnetic field strength on earth. This contributes with a total torque of 400nNm on each axis. The location of the magnetorquers are seen in Fig. 2.5.

Magnetorquers Design

The torque that each of the magnetorquer contributes \mathbf{N}_{mt} , is given as [Serway 04, p. 917]

$$\mathbf{N}_{mt} = \mathbf{m}_{mt} \times \mathbf{B}_E \quad [\text{Nm}] \quad (2.2)$$

\mathbf{m}_{mt} : The magnetic dipole moment from the magnetorquer.

\mathbf{B}_E : The geomagnetic field strength of the earth.

The magnetic dipole moment \mathbf{m}_{mt} is given by [Serway 04, p. 917]

$$\mathbf{m}_{mt} = n_w I_{mt} \mathbf{A}_{mt} \quad [\text{Am}^2] \quad (2.3)$$

n_w : The number of windings

I_{mt} : The current through the coil

\mathbf{A}_{mt} : The vector that is perpendicular to as the area enclosed by the magnetorquer. With the length proportional to the enclosed area.

Now (2.2) and (2.3) can be collected to

$$\mathbf{N}_{mt} = n_w I_{mt} |\mathbf{A}_{mt}| |\mathbf{B}_E| \sin(\theta) \quad (2.4)$$

θ : The angle between \mathbf{A}_{mt} and \mathbf{B}_E

The current I_{mt} is determined by the impedance of the coil and the applied PWM (Ohms law). The impedance of the coil is given as a real part $R(T)$ that is dependent of the temperature and an imaginary part Z_L . By substituting I_{mt} with $\frac{\text{PWM}}{R+Z_L}$, (2.4) is rewritten to

$$\mathbf{N}_{mt} = n_w \frac{\text{PWM}}{R(T) + Z_L} |\mathbf{A}_{mt}| |\mathbf{B}_E| \sin(\theta) \quad (2.5)$$

$R(T)$: The coil resistance, dependant on temperature

Z_L : The coil inductance

By Laplace transforming the coil Z_L can be substituted with sL , and the final transfer function can be written as (2.6)

$$\frac{N_{mt}}{PWM} = \frac{n_w}{R(t) + sL} |A_{mt}| |B_E| \sin(\theta) \quad (2.6)$$

For the magnetorquer to provide the required 200 nNm the following design for each magnetorquer is applied.

- 250 winding
- An area of 75x75 mm^2
- A PWM controlled voltage of $\pm 1.25 V$
- Calculated worst case resistance $120 \Omega @ 70 {}^\circ C$, which implies a current of 10.4 mA .
- A duty-cycle of 88% provides 200 nNm

The rest of the time is reserved for the measuring by the magnetometers, because it is undesired to have the magnetorquers actuating doing measurements.

2.1.8 Magnetorquers with Metal Core

To have redundant actuators and for experiment purposes magnetorquers with metal cores are mounted on the PCB. These magnetorquers are considerably more powerful than the ones without a metal core, consumes less power and are smaller. On the other hand the permeability of different iron cores varies a lot (600 - 7600) Furthermore the solution including the iron core is harder to implement, such that the magnetic moment points in the right direction. Also it has not been tested in space before by the AAUSAT team. Thus it is not included in the rest of this project only the design of them is briefly described below.

Magnetorquers with Metal Core Design

For obtaining 400 nNm the following design is applied

- 200 windings
- at a diameter of 0.13 mm
- permeability assumed to be 1000
- A PWM controlled voltage of $\pm 1.25 V$
- Calculation maximal resistance of $25.21 m\Omega @ 70 {}^\circ C$, which implies a current at 49.6 A

Since this is way too high a current an external resistance of 62.5 ω is added which implies a current at 20 mA . The 400 nNm torque can be obtained at 27% duty cycle.

2.1.9 Actuations and Measurements

Because the magnetorques will distort the measurements of the Earth magnetic field substantial, it is chosen to alternate between actuating with the magnetorques and measuring the Earth's magnetic field. A period of 100 ms is chosen for the actuation and measurement, in which the magnetorquers has a duty cycle of 88%. This is due to a required discharge time of the magnetorquers, leaving enough time for the magnetometer measurement.

2.2 Software

This section is based on the ADCS software layout predesigned by group 09gr935 [Jensen 10]. The layout is illustrated in Fig. 2.6. It is chosen to regard the attitude determination

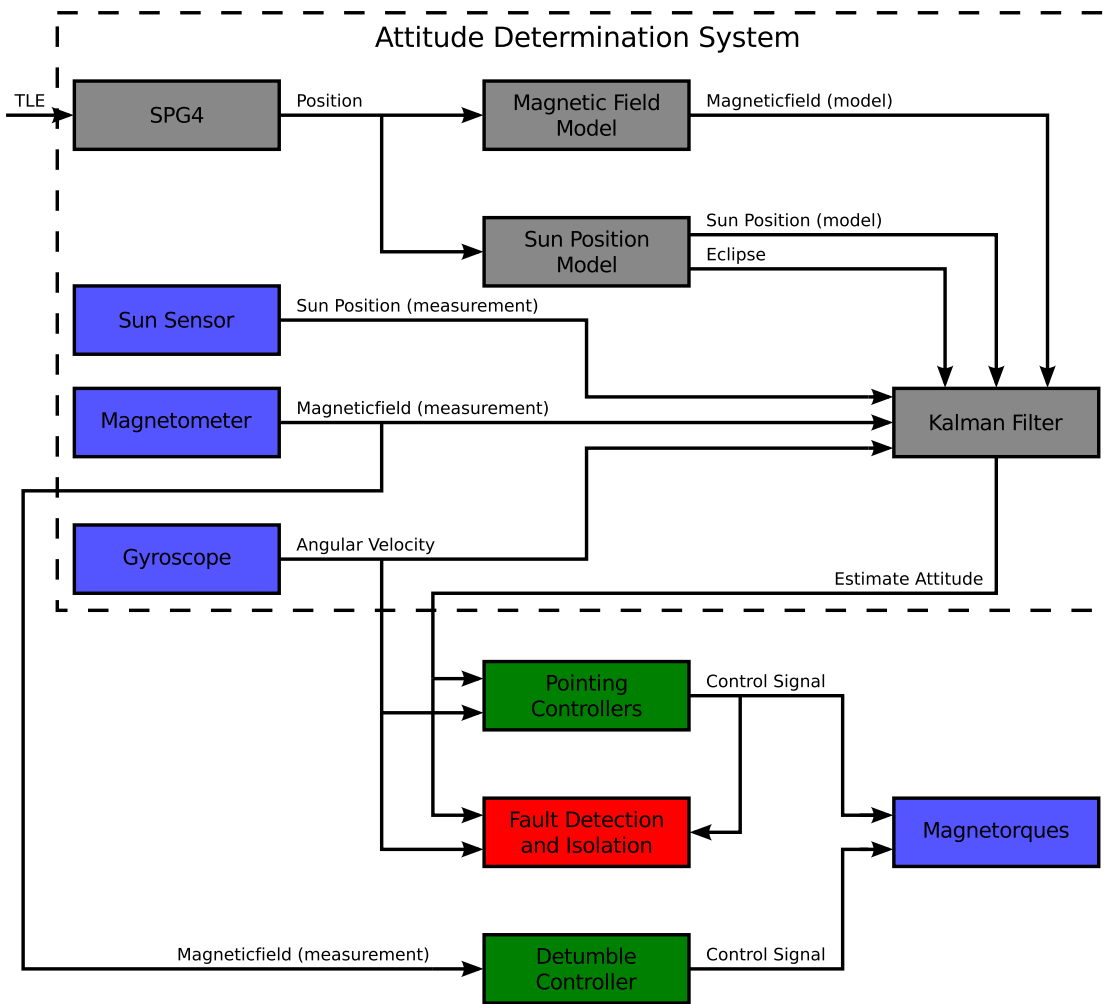


Figure 2.6: Overview diagram of the software in the ADCS

system (ADS) of the satellite as a gray box. That is describing the general functions of the ADS blocks briefly. Furthermore for the FDI design, the different blocks of the ADS will be regarded as one.

2.2.1 SGP4

When the satellite passes the USA¹, NASA² and NORAD³ record the altitude, the direction and the velocity of the satellite, along with other parameters. Together with the time of observation, this information is saved as a packet in the two-line elements (TLE) format and published on the Internet for free accessibility. The most recent TLE-data is then uploaded to the satellite, when it passes the mission control center in Aalborg. If an on board GPS receiver is present on the satellite, the needed TLE-data can also be generated (estimated) using this. The Simplified General Perturbations Satellite Orbit Model 4 (SGP4) is a model which purposes is to predict the orbital position of the satellite at a specified time. This model is mainly used for Low Earth Orbit (LEO) spacecrafts (spacecrafts with orbital time less than 225 minutes), which correspond with the orbital time of AAUSAT3 (approximately 97 minutes). SGP4 uses the uploaded TLE data as a known starting point, and is considered fairly precise for a couple of days. It is expected that new TLE data can be uploaded to AAUSAT3 every day.

2.2.2 Magnetic Field and Sun Position Model

On board the satellite, a model of the Earth's magnetic field is implemented. The magnetic field model is based on the International Geomagnetic Reference Field (IGRF) model. By using the estimate of the position from the SGP4- and the IGRF-model, it is possible to determine the expected magnetic field for the satellite's given position.

Also, a model of the suns position is implemented. By using the estimate of the position from the SGP4 and the sun positioning model, it is possible to determine the expected position of the sun relative to the position of the satellite and thereby whether the satellite is in eclipse.

2.2.3 Kalman Filter

By estimates and measurements of the magnetic field, the position of the sun, and by the measurements of the satellite angular velocity the current attitude of the satellite is estimated by a Kalman filter. The real quaternion and the quaternion estimated by the Kalman filter are plotted in Fig. 2.7.

It is noted in Fig. 2.7, that when the satellite is out of eclipse, the estimation of the quaternion is almost identical to the real quaternion. When the satellite enters eclipse, the estimate diverges from the real quaternion because the sun sensors are not available, but when it again exits eclipse, the estimate quickly converges to the real quaternion.

¹USA - United States of America - a federal constitutional republic comprising fifty states and a federal district
- Situated mostly in the North American continent

²NASA - National Aeronautics and Space Administration

³NORAD - North American Aerospace Defense Command

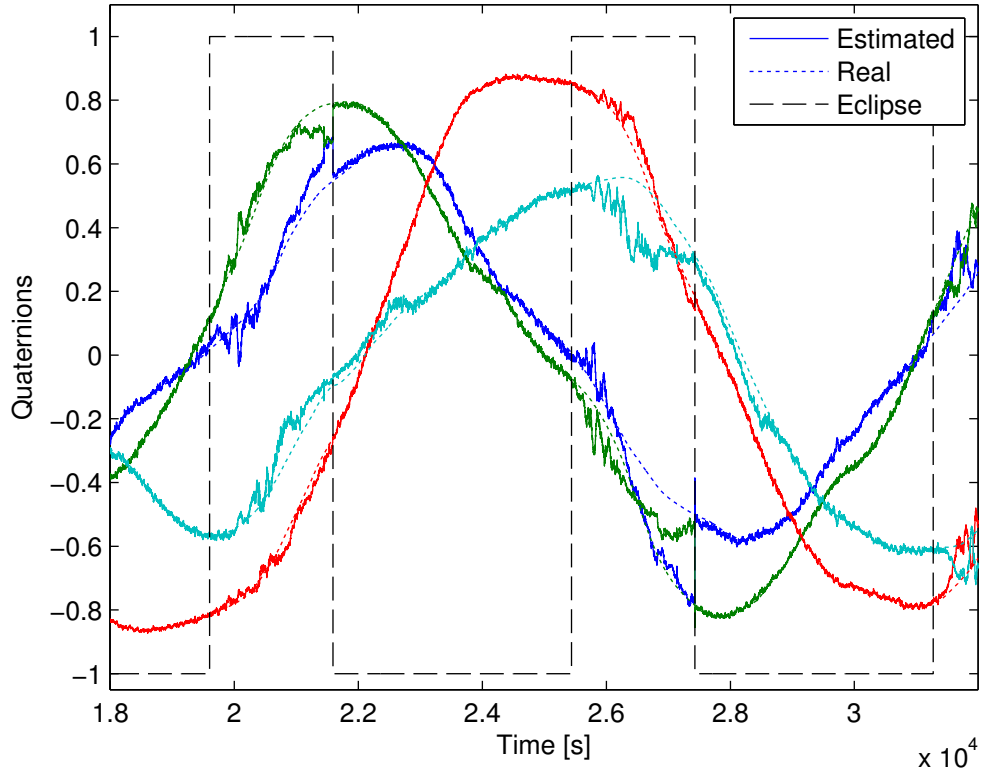


Figure 2.7: The estimated and real quaternion

2.3 Controllers and FDI

The controllers and Fault Detection and Isolation (FDI) for AAUSAT3 is briefly introduces here. The ADCS of the satellite operates in two control modes, a detumbling and a pointing mode. As described in the beginning of this chapter there are three different pointing controllers. In this report only the Nadir pointing controller and inertial pointing controller are studied along with a detumbling controller, which is briefly introduced here.

2.3.1 Detumbling Controller

The detumbling mode is used when the satellite has a high angular velocity ($> 0.12 \text{ circ/s}$), which it is very likely after the launch from the P-POD. The purpose of the detumbling controllers is only to lower the angular velocity of the satellite. The detumbling controller only make use of the magnetometers and the actuators, and can thus be used by the ADCS1. The detumbling controller is further described in Section 4.1

2.3.2 Pointing Controllers

When the satellite's angular velocity is sufficiently low and enough power is available, the control mode can be changed to pointing mode. In this mode, the satellite should be able to point the antenna side of the satellite, towards a specified direction for instance it could point towards the center of the earth (nadir) or an other reference frame. The design of the pointing controllers is described further in Section 4.2.

2.3.3 Fault Detection and Isolation

The purpose of the Fault Detection and Isolation is to be able to detect a faulty transducer in the system and isolate the origin of the fault. The fault analysis and design of a FDI algorithm is described in Chapter 5 and in Chapter 6. When a fault has been detected the supervisor designed in Section 6.4 decides how to handle the fault. The supervisor thereby link the FDI to the controllers such that AAUSAT3 can remain in control even in case of a faulty transducer.

2.4 Requirement Specification

To evaluate whether the satellite attitude control and fault detection provides satisfactory results, performance requirements are defined. As later described in respectively chapter 4 and 6, three different controllers and a model based FDI is designed. The requirements for these, are described here.

2.4.1 Detumbling Controller Requirement

The detumbling rate of the satellite is defined as the satellite turning two times around each of its control frame axis, wrt. the ECI-frame during one orbit, giving the rate

$$^c\omega_{ci_{detumbled}} = 2 \frac{2\pi[\text{rad}]}{5830[\text{s}]} = 0.0022 \left[\frac{\text{rad}}{\text{s}} \right] \quad (2.7)$$

It is assumed that the satellite will have a angular rate of no more than 0.1 [rad/s] when deployed from the P-POD[Green 06, p. 174]. The detumbling controller is defined to perform satisfactory if the angular velocity is no more than 20% higher than the detumbling rate, within one orbit thus

$$^c\omega_{ci_{max}} = 1.20 \cdot 0.0022 \left[\frac{\text{rad}}{\text{s}} \right] = 0.0026 \left[\frac{\text{rad}}{\text{s}} \right] \quad (2.8)$$

An additionally requirement is that the velocity after one orbit, should be under 0.0026 rad/s in 90% of the time for all three axes, when including sensor dynamics and environmental disturbances.

2.4.2 Nadir Pointing Controller

For the nadir pointing controller, the operating point is defined as the alignment of the CRF-frame and the ORF-frame which is also the desired reference. The demands for the nadir pointing controller are:

- The eigenvector angle between ORF and CRF should be within 50° within four orbits in at least 90% of the time, for the simulation that includes environment disturbances and sensor dynamics.

Additionally the start angle between ORF and CRF should be 180° around the eigenvector which is defined as $\begin{bmatrix} \frac{1}{\sqrt{3}} & \frac{1}{\sqrt{3}} & \frac{1}{\sqrt{3}} \end{bmatrix}$. The start velocity of the satellite is defined as the worst case detumbling rate which in Section 7.1 is found to be 0.004 rad/s.

2.4.3 Inertial Pointing Controller

For the inertial pointing controller, the operating point is defined as the alignment of the CRF-frame and the ECI-frame which is also the desired reference. The demands for the nadir pointing controller are:

- The eigenvector angle between ECI and CRF should be within 50° within four orbits in at least 90% of the time, for the simulation that includes environment disturbances and sensor dynamics.

Additionally the start angle between ECI and CRF should be 180° around the eigen vector that is defined as $\left[\frac{1}{\sqrt{3}} \frac{1}{\sqrt{3}} \frac{1}{\sqrt{3}} \right]$. The start velocity of the satellite is defined as the worst case detumbling rate which in Section 7.1 is found to be 0.004 rad/s .

2.4.4 Fault Detection Requirement

The requirement for the FDI, is that it should be possible to detect the five worst faults in the actuators and sensors within 500s.

The worst faults is determined in the SO analysis in Section 5.2 which leads to the following requirements:

$(f_{error_{ads_1}})$ The FDI should detect if the ADS instantly outputs a faulty estimate of the satellite attitude, which is defined as a 0.5° rotation of the real attitude, rotated around the eigenvector $\left[\frac{1}{\sqrt{3}} \frac{1}{\sqrt{3}} \frac{1}{\sqrt{3}} \right]$.

$(f_{error_{ads_2}})$ The FDI should detect and isolate if the ADS slowly outputs an increasingly faulty estimate of the satellite attitude. This is defined as an increasing rotational rate of $0.01^\circ/\text{s}$ of the real attitude, rotated around the unit eigenvector $\left[\frac{1}{\sqrt{3}} \frac{1}{\sqrt{3}} \frac{1}{\sqrt{3}} \right]$.

(f_{scg_g}) The FDI should detect and isolate, if the gyroscope in one axis is instantly short circuited to ground.

(f_{bias_g}) The FDI should detect and isolate if the gyroscope in one axis is instantly biased with $0.1^\circ/\text{s}$.

$(f_{scgmt,1-3})$ The FDI should detect and isolate if the magnetorquers dipole moment, in one plane of the satellite, is instantly reduced to zero.

$(f_{scsmmt,1-3})$ The FDI should detect and isolate if the magnetorquers dipole moment, in one plane of the satellite, is instantly increased to its maximum level.

Chapter 3

Modeling

In this chapter all issues related to modeling is described. This includes a section that describes the used reference frames, the magnetic field model that is based on the IGRF model. Additionally, the general kinematics and dynamics for the satellite, are described which leads to the linearized models that is used for nadir and inertial pointing in Section 4.2.1. Also, the simulation environment that is used to test the designed controllers is described and a validation of the model is described.

3.1 Reference Frames

This section explains the different types of coordinate systems, that is reference frames which are used to describe the behaviour of the satellite relative to its context. Describing the satellite attitude and angular velocity in a given coordinate system wrt. a different coordinate systems will ease the calculation of the kinematic and dynamic equations. All the coordinate systems/reference frames stated below are right-handed Cartesian coordinate systems in 3-dimensions. The described frames are:

- ECI - Earth Centered Initial Reference Frame
- ECEF - Earth Centered Earth Fixed Reference Frame
- ORF - Orbit Reference Frame
- SBRF - Spacecraft Body Reference Frame
- CRF - Controller Reference Frame

3.1.1 ECI - Earth Centered Initial Reference Frame

The ECI is defined relative to the rotation axis of the Earth, which points towards the geographic North Pole as shown in Fig. 3.1. The origin is placed in the center of the Earth, and the X-axis, which is perpendicular to the Z-axis, points towards the center of sun, one time each year at vernal equinox, which is illustrated in Fig. 3.1. The Y-axis is the cross product of the Z- and X-axes. In this way, the plane spanned by the X- and Y-axis is the equatorial plane. It should be noted that this frame does not rotate like the ECEF frame, because it is fixed relative to the sun.

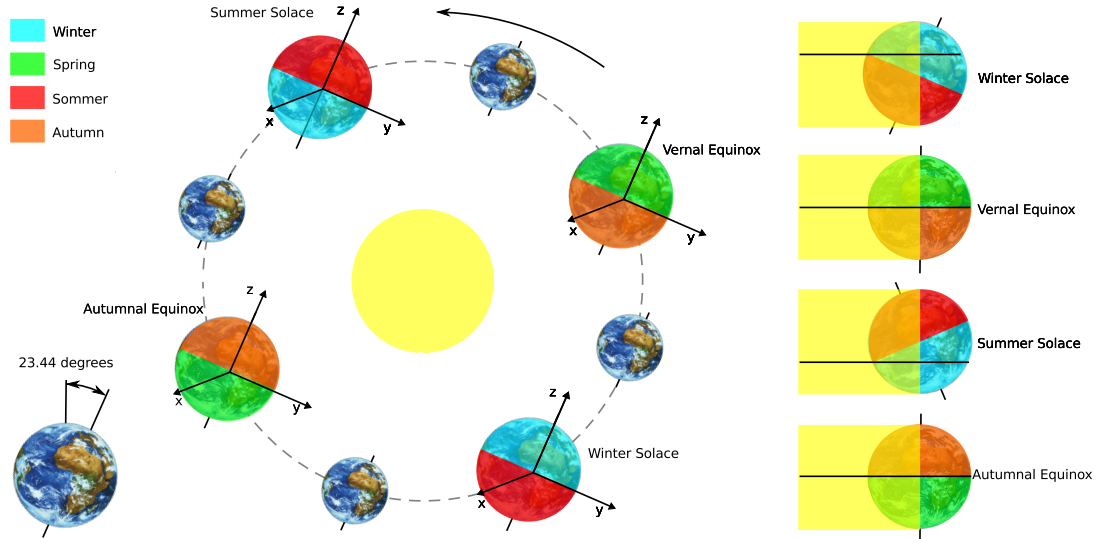


Figure 3.1: Earth Centered Initial Reference Frame, which is defined as the Z-axis pointing towards the north pole and X-axis pointing towards the center of sun, one time each year at vernal equinox

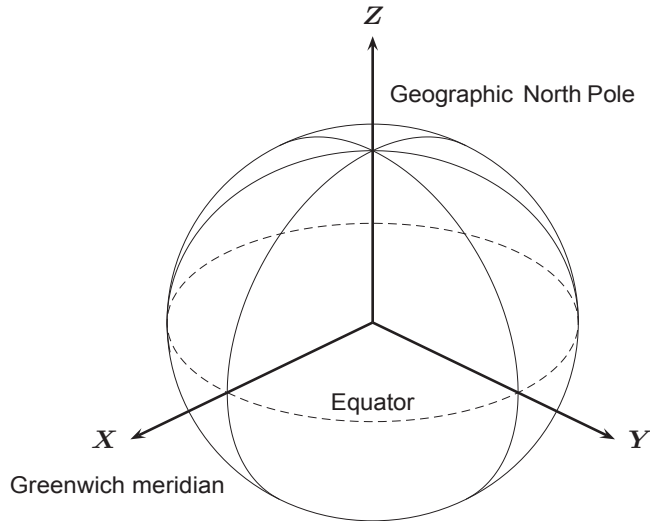


Figure 3.2: Earth Centered Earth Fixed Reference Frame, where the Z-axis points towards to North pole, and the X-axis points towards Greenwich meridian.

3.1.2 Earth Centered Earth Fixed Reference Frame

Like the ECI reference frame, the ECEF has its origin in the center of the Earth and the Z-axis points in the direction of the geographic North Pole. This frame is fixed to the Earth in which the X-axis is defined as pointing towards Greenwich meridian and Equator meets (latitude and longitude = 0°), illustrated in Fig. 3.2. The Y-axis is the cross product of the Z- and X-axes.

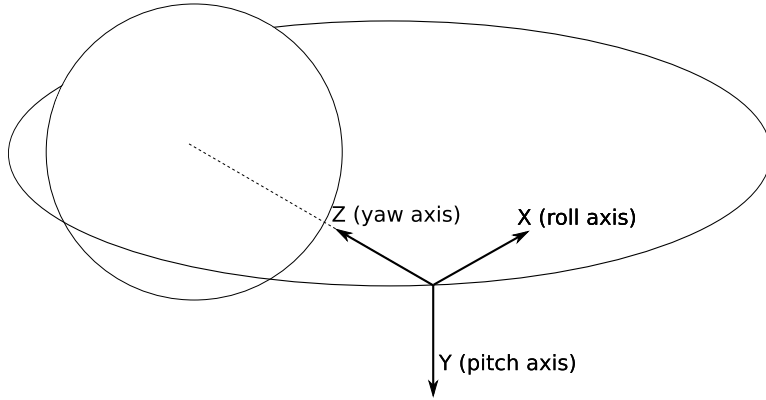


Figure 3.3: Orbit Reference Frame, defined as the Z-axis points towards the center of the earth and the Y-axis is perpendicular to the orbit plane

3.1.3 Orbit Reference Frame

The ORF describes the rotation of the satellite relative to the orbit. The origin of the ORF is placed in the CoM of the satellite. The Z-axis points toward nadir (the center of the Earth) and the Y-axis is perpendicular to the orbit plane. The X-axis is given as the cross product of the Z- and Y-axis. The ORF is illustrated in Fig. 3.3. As the X-axis is a cross product of the Z- and Y-axis, it will be parallel to the orbit velocity vector only if the orbital trajectory is circular. Given the position vector in the ECI frame iR and the velocity vector of the orbiting satellite seen from the ECI frame iV , the ORF basis can be described as:

$$\begin{aligned} {}^oZ &: \frac{-{}^iR}{\|{}^iR\|} \\ {}^oY &: \frac{{}^oZ \times {}^iV}{\|{}^oZ \times {}^iV\|} \\ {}^oX &: \frac{{}^oY \times {}^oZ}{\|{}^oY \times {}^oZ\|} \end{aligned} \quad (3.1)$$

The vectors iR and iV are illustrated in Fig. 3.4.

3.1.4 Spacecraft Body Reference Frame

The SBRF is fixed to the body of the spacecraft. This frame is used to describe the position of the onboard hardware on the satellite, as in Fig. 2.4 and Fig. 2.5. The SBRF is illustrated in Fig. 3.5 in which the placements of some components are also shown.

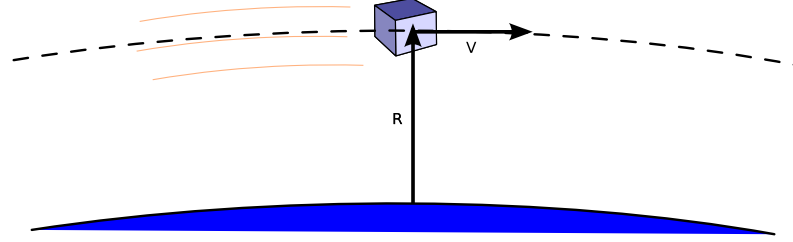


Figure 3.4: Velocity and position vectors of the orbiting satellite seen from ECI

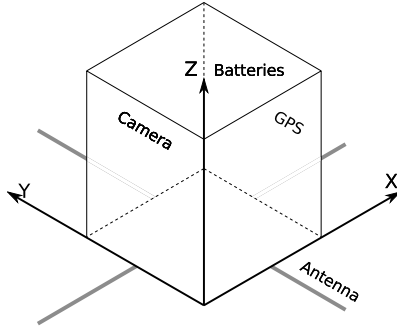


Figure 3.5: Spacecraft Body Reference Frame. Used to describe the position of the hardware, mounted on the satellite

3.1.5 Controller Reference Frame

The CRF is fixed to the body of the spacecraft in which the origin is placed in the CoM of the spacecraft. The axis of the CRF is the principle axis of the satellite, in which the X-axis denote the minor axis of inertia, the Z-axis denotes the major axis of inertia and the Y-axis is the cross product of the X- and Z-axis.

Moments of Inertia for CRF

The inertia-product and -moments of the AAUSAT3 SBRF has been found by [Jensen 10] using a CAD program. As the CRF axis is defined by the principal axis of inertia, the principal-axis moment of inertia-matrix should be used. It is found by the eigenvalues of the inertia-product matrix [Wie 98, mangler], and is given by

$${}^c\mathbf{I} = \begin{bmatrix} 1.7464 \cdot 10^{-3} & 0 & 0 \\ 0 & 2.2092 \cdot 10^{-3} & 0 \\ 0 & 0 & 2.2388 \cdot 10^{-3} \end{bmatrix} \quad (3.2)$$

For future use, ${}^c\mathbf{I}$ is simply denoted by \mathbf{I} .

Also, a quaternion describing the rotation between the SBRF and CRF is found by [Jensen 10].

3.2 Magnetic Field Model

The International Geomagnetic Reference Field (IGRF) is a standard mathematical description of the Earth's main magnetic field. The IGRF model is a result of observations made by satellites and earth stations around the world and is given by (3.3)

$$V(r, \phi, \theta) = a \sum_{\ell=1}^L \sum_{m=0}^{\ell} \left(\frac{a}{r} \right)^{\ell+1} (g_{\ell}^m \cos m\phi + h_{\ell}^m \sin m\phi) P_{\ell}^m(\theta) \quad (3.3)$$

in which the following letters represent

r : The distance to the center of the earth

a : The Earth's radius

L : The maximum degree of the expansion

ϕ : The East longitude

θ : The colatitude (the polar angle)

g_{ℓ}^m and h_{ℓ}^m : Gauss constants

$P_{\ell}^m(\theta)$: The Schmidt normalized associated Legendre functions of degree ℓ and order m

The Gauss constants are updated every 5. year, both because of new available measurements and because of the time variation of the magnetic field. A simulation of the magnetic field (using the 10th order IGRF model) in the AAUSAT3's ORF and ECI is illustrated in 3.6 and 3.7.

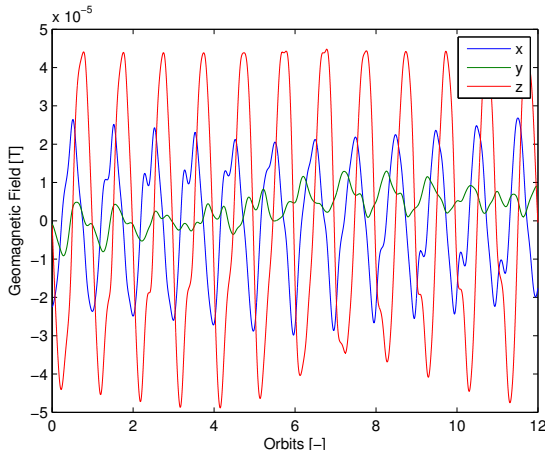


Figure 3.6: The magnetic field in the ORF

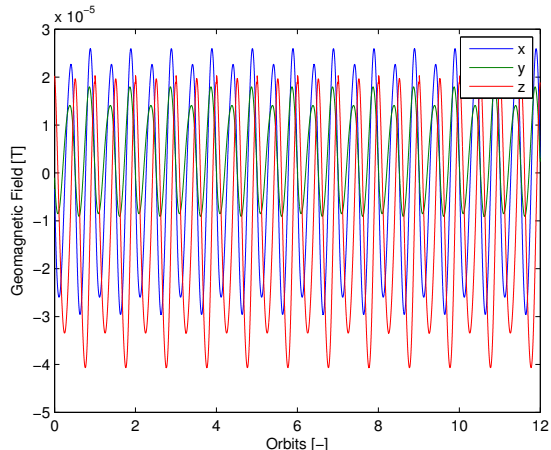


Figure 3.7: the magnetic field in the ECI

It is observed in Fig. 3.6 and 3.7, that the magnetic field is very periodic and symmetrical around the earth in the path of the satellite. At higher altitudes (above 30000 km), the solar winds cause the magnetic field of the earth to become more asymmetrical.

The magnetic field strength, in an altitude of 600 km is seen in Fig. 3.8[Korhonen 10] in which it is seen that the geomagnetic fields strength varies from between 20,000 nT to 50,000 nT.

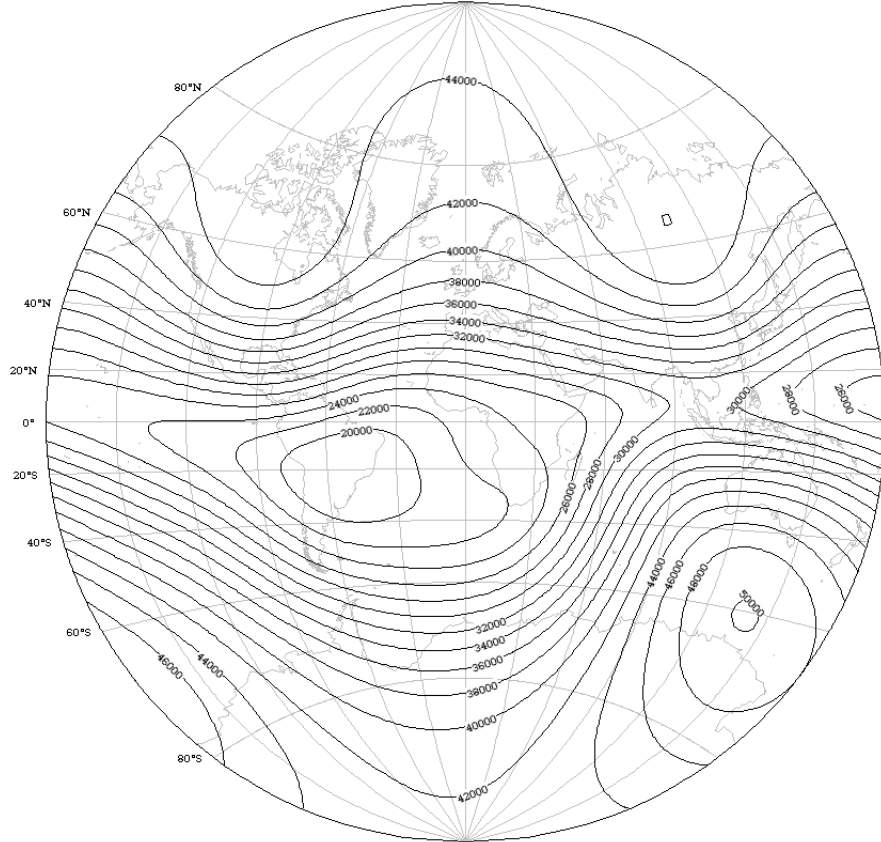


Figure 3.8: The geomagnetic fields strength in an altitude of 600 km, represented by the 10th order IGRF-model

3.3 Satellite Dynamics and Kinematics

In this section the kinematic and dynamic equations for the satellite is presented. The kinematic differential equations is a general description of kinematics between frames, while the dynamic differential equations describes the dynamics of the satellite CRF seen from ECI.

3.3.1 Kinematic Differential Equations

This section is based on [Wie 98] and [Bak 02].

As described in Appendix A, the rotation between reference frames can be described by a direction cosine matrix such that

$${}^b \underline{C}_a \begin{bmatrix} \mathbf{a}_1 \\ \mathbf{a}_2 \\ \mathbf{a}_3 \end{bmatrix} = \begin{bmatrix} \mathbf{b}_1 \\ \mathbf{b}_2 \\ \mathbf{b}_3 \end{bmatrix} \quad (3.4)$$

As $\underline{\mathbf{C}}$ maps between orthogonal unit vectors $\underline{\mathbf{C}}$ is an orthonormal matrix thus $\underline{\mathbf{C}}^T = \underline{\mathbf{C}}^{-1}$.

$$\begin{bmatrix} \mathbf{a}_1 \\ \mathbf{a}_2 \\ \mathbf{a}_3 \end{bmatrix} = {}^b\underline{\mathbf{C}}_a^T \begin{bmatrix} \mathbf{b}_1 \\ \mathbf{b}_2 \\ \mathbf{b}_3 \end{bmatrix} \quad (3.5)$$

Differentiating this with respect to the time ($\underline{\mathbf{C}}$ is function of time) yields by the product rule:

$$\begin{aligned} \underline{\mathbf{0}} &= {}^b\dot{\underline{\mathbf{C}}}_a^T \begin{bmatrix} \mathbf{b}_1 \\ \mathbf{b}_2 \\ \mathbf{b}_3 \end{bmatrix} + {}^b\underline{\mathbf{C}}_a^T \begin{bmatrix} \dot{\mathbf{b}}_1 \\ \dot{\mathbf{b}}_2 \\ \dot{\mathbf{b}}_3 \end{bmatrix} \\ &= {}^b\dot{\underline{\mathbf{C}}}_a^T \begin{bmatrix} \mathbf{b}_1 \\ \mathbf{b}_2 \\ \mathbf{b}_3 \end{bmatrix} + {}^b\underline{\mathbf{C}}_a^T \begin{bmatrix} \boldsymbol{\omega} \times \mathbf{b}_1 \\ \boldsymbol{\omega} \times \mathbf{b}_2 \\ \boldsymbol{\omega} \times \mathbf{b}_3 \end{bmatrix} \end{aligned} \quad (3.6)$$

In which $\boldsymbol{\omega}$ is the angular velocity vector in reference frame B wrt. A, given in B coordinates such that:

$$\boldsymbol{\omega} = {}^b\boldsymbol{\omega}_{ba} = \omega_1 \mathbf{b}_1 + \omega_2 \mathbf{b}_2 + \omega_3 \mathbf{b}_3 \quad (3.7)$$

Here the cross-product can be replaced by a skew-symmetric matrix $\underline{\mathbf{S}}(\boldsymbol{\omega})$ such that:

$$\begin{aligned} \underline{\mathbf{0}} &= {}^b\dot{\underline{\mathbf{C}}}_a^T \begin{bmatrix} \mathbf{b}_1 \\ \mathbf{b}_2 \\ \mathbf{b}_3 \end{bmatrix} - {}^b\underline{\mathbf{C}}_a^T \underbrace{\begin{bmatrix} 0 & -\omega_3 & \omega_2 \\ \omega_3 & 0 & -\omega_1 \\ -\omega_2 & \omega_1 & 0 \end{bmatrix}}_{\underline{\mathbf{S}}(\boldsymbol{\omega})} \begin{bmatrix} \mathbf{b}_1 \\ \mathbf{b}_2 \\ \mathbf{b}_3 \end{bmatrix} \\ &= \left({}^b\dot{\underline{\mathbf{C}}}_a^T - {}^b\underline{\mathbf{C}}_a^T \underline{\mathbf{S}}(\boldsymbol{\omega}) \right) \begin{bmatrix} \mathbf{b}_1 \\ \mathbf{b}_2 \\ \mathbf{b}_3 \end{bmatrix} \\ &\Downarrow \\ \underline{\mathbf{0}} &= {}^b\dot{\underline{\mathbf{C}}}_a^T - {}^b\underline{\mathbf{C}}_a^T \underline{\mathbf{S}}(\boldsymbol{\omega}) \end{aligned} \quad (3.8)$$

By taking the transpose on both sides of (3.8) and applying the skew-symmetric identity; $\underline{\mathbf{S}}(\boldsymbol{\omega}) = -\underline{\mathbf{S}}(\boldsymbol{\omega})^T$, the kinematic differential equations are given by:

$$\underline{\mathbf{0}} = {}^b\dot{\underline{\mathbf{C}}}_a + \underline{\mathbf{S}}(\boldsymbol{\omega}) {}^b\underline{\mathbf{C}}_a \quad (3.9)$$

Solving (3.9) yields:

$$\omega_1 = \dot{C}_{21}C_{31} + \dot{C}_{22}C_{32} + \dot{C}_{23}C_{33} \quad (3.10)$$

$$\omega_2 = \dot{C}_{31}C_{11} + \dot{C}_{32}C_{12} + \dot{C}_{33}C_{13} \quad (3.11)$$

$$\omega_3 = \dot{C}_{11}C_{21} + \dot{C}_{12}C_{22} + \dot{C}_{13}C_{23} \quad (3.12)$$

The direct cosine matrix is represented by quaternions (see Section A) as no kinematic singularities occurs, as opposed to euler angles. Also, no trigonometric functions need to be evaluated. By substituting (A.24) into (3.10), (3.11), and (3.12) yields:

$$\omega_1 = 2(\dot{q}_1 q_4 + \dot{q}_2 q_3 - \dot{q}_3 q_2 - \dot{q}_4 q_1) \quad (3.13)$$

$$\omega_2 = 2(\dot{q}_2 q_4 + \dot{q}_3 q_1 - \dot{q}_1 q_3 - \dot{q}_4 q_2) \quad (3.14)$$

$$\omega_3 = 2(\dot{q}_3 q_4 + \dot{q}_1 q_2 - \dot{q}_2 q_1 - \dot{q}_4 q_3) \quad (3.15)$$

As the eigenaxis is constrained by (A.16), the quaternion is constrained by:

$$\begin{aligned} q_1^2 + q_2^2 + q_3^2 + q_4^2 &= \left(e_1 \sin\left(\frac{\theta}{2}\right)\right)^2 + \left(e_2 \sin\left(\frac{\theta}{2}\right)\right)^2 + \left(e_3 \sin\left(\frac{\theta}{2}\right)\right)^2 + \left(\cos\left(\frac{\theta}{2}\right)\right)^2 \\ &= (e_1^2 + e_2^2 + e_3^2) \sin^2\left(\frac{\theta}{2}\right) + \cos^2\left(\frac{\theta}{2}\right) \\ &= \sin^2\left(\frac{\theta}{2}\right) + \cos^2\left(\frac{\theta}{2}\right) = 1 \end{aligned} \quad (3.16)$$

By differentiating (3.16), a forth equation is derived:

$$2(\dot{q}_1 q_1 + \dot{q}_2 q_2 + \dot{q}_3 q_3 + \dot{q}_4 q_4) = 0 \quad (3.17)$$

Writing (3.13), (3.14), (3.15), and (3.17) in matrix form yields:

$$\begin{bmatrix} \omega_1 \\ \omega_2 \\ \omega_3 \\ 0 \end{bmatrix} = 2 \begin{bmatrix} q_4 & q_3 & -q_2 & -q_1 \\ -q_3 & q_4 & q_1 & -q_2 \\ q_2 & -q_1 & q_4 & -q_3 \\ q_1 & q_2 & q_3 & q_4 \end{bmatrix} \begin{bmatrix} \dot{q}_1 \\ \dot{q}_2 \\ \dot{q}_3 \\ \dot{q}_4 \end{bmatrix} \quad (3.18)$$

Which can be rewritten to (where $\boldsymbol{\omega} = [\omega_1 \omega_2 \omega_3]^T$):

$$\underbrace{\begin{bmatrix} \dot{q}_1 \\ \dot{q}_2 \\ \dot{q}_3 \\ \dot{q}_4 \end{bmatrix}}_{\dot{\mathbf{q}}} = \frac{1}{2} \underbrace{\begin{bmatrix} \mathbf{S}(\boldsymbol{\omega}) & \boldsymbol{\omega} \\ -\boldsymbol{\omega}^T & 0 \end{bmatrix}}_{\Omega} \underbrace{\begin{bmatrix} q_1 \\ q_2 \\ q_3 \\ q_4 \end{bmatrix}}_{\mathbf{q}} \quad (3.19)$$

3.3.2 Dynamics Differential Equations

As the satellite is considered as a rigid body, it has six degrees of freedom (DOF). Three of the DOF describe the orbital position of the satellites in three axis and the other three DOF describe the rotation in three axis, which is considered in this section.

Eulers second law states that the torque (\mathbf{N}) applied to the satellite is defined as the time derivative of the angular momentum (\mathbf{L}) [Wertz 78, p. 498]:

$$\dot{\mathbf{L}} = \mathbf{N} \quad (3.20)$$

The satellite control frame is denoted by (c) and the ECI-frame is denoted by (i). By the direction cosine matrix ${}^c\underline{\mathbf{C}}_i$, the angular momentum vector can be rotated from the ECI frame to the CRF frame.

$${}^c\mathbf{L} = {}^c\underline{\mathbf{C}}_i {}^i\mathbf{L} \quad (3.21)$$

Differentiating L yields:

$${}^c\dot{\mathbf{L}} = {}^c\dot{\underline{\mathbf{C}}}_i {}^i\mathbf{L} + {}^c\underline{\mathbf{C}}_i {}^i\dot{\mathbf{L}} \quad (3.22)$$

The following relationship is known [Bak 02]:

$${}^c\dot{\underline{\mathbf{C}}}_i = -{}^c\boldsymbol{\omega}_{ci} \times {}^c\underline{\mathbf{C}}_i \quad (3.23)$$

Substitution (3.23) into (3.22) yields:

$$\begin{aligned} {}^c\dot{\mathbf{L}} &= -{}^c\omega_{ci} \times {}^c\underline{\mathbf{C}}_i {}^i\mathbf{L} + {}^c\underline{\mathbf{C}}_i {}^i\dot{\mathbf{L}} \\ &= -{}^c\omega_{ci} \times {}^c\mathbf{L} + {}^c\mathbf{N} \end{aligned} \quad (3.24)$$

The angular momentum is given as:

$$\mathbf{L} = \underline{\mathbf{I}}\boldsymbol{\omega} \quad (3.25)$$

Where $\underline{\mathbf{I}}$ is the matrix that consist of the principle axis of inertia in the CRF. Substituting (3.25) into (3.24) yields:

$$\begin{aligned} \underline{\mathbf{I}}{}^c\dot{\boldsymbol{\omega}}_{ci} &= -{}^c\omega_{ci} \times \underline{\mathbf{I}}{}^c\omega_{ci} + {}^c\mathbf{N} \\ &\Downarrow \\ {}^c\dot{\boldsymbol{\omega}}_{ci} &= \underline{\mathbf{I}}^{-1} (-{}^c\omega_{ci} \times \underline{\mathbf{I}}{}^c\omega_{ci} + {}^c\mathbf{N}) \end{aligned} \quad (3.26)$$

By inserting the skewmetric matrix $\underline{\mathbf{S}}(\omega)$ and substitute the existing torque \mathbf{N} , with the torque caused by the disturbances ${}^c\mathbf{N}_{dist}$ and the torque caused by the controller, ${}^c\mathbf{N}_{ctrl}$ yields the final dynamic equations for the satellite

$$\begin{aligned} {}^c\dot{\boldsymbol{\omega}}_{cici} &= \underline{\mathbf{I}}^{-1} (-{}^c\underline{\mathbf{S}}({}^c\omega_{ci}) \underline{\mathbf{I}}{}^c\omega_{ci} + {}^c\mathbf{N}) \\ &= \underline{\mathbf{I}}^{-1} (-{}^c\underline{\mathbf{S}}({}^c\omega_{ci}) \underline{\mathbf{I}}{}^c\omega_{ci} + {}^c\mathbf{N}_{dist} + {}^c\mathbf{N}_{ctrl}) \end{aligned} \quad (3.27)$$

3.3.3 Inertial Reference Pointing Equations

(3.19) and (3.27) are combined in a single matrix, describing the dynamic differential equations for the CRF wrt. the ECI.

$$\begin{bmatrix} \dot{\mathbf{q}}_i^c \\ {}^c\dot{\boldsymbol{\omega}}_{ci} \end{bmatrix} = \begin{bmatrix} \frac{1}{2}{}^c\Omega_{ci} \mathbf{q}_i^c \\ \underline{\mathbf{I}}^{-1} (-{}^c\underline{\mathbf{S}}(\omega) \underline{\mathbf{I}}{}^c\omega_{ci} + {}^c\mathbf{N}_{dist} + {}^c\mathbf{N}_{ctrl}) \end{bmatrix} \quad (3.28)$$

The linearized state space model of the system, deduced in Appendix D.3, is represented as (with the frame notation ommited):

$$\begin{bmatrix} \dot{\tilde{\mathbf{q}}}_{1:3} \\ \dot{\tilde{\boldsymbol{\omega}}} \end{bmatrix} = \begin{bmatrix} -\underline{\mathbf{S}}(\bar{\omega}) & \frac{1}{2}\mathbf{1}_{3x3} \\ \mathbf{0}_{3x3} & \underline{\mathbf{I}}^{-1} [\underline{\mathbf{S}}(\underline{\mathbf{I}}\bar{\omega}) - \underline{\mathbf{S}}(\bar{\omega})\underline{\mathbf{I}}] \end{bmatrix} \begin{bmatrix} \tilde{\mathbf{q}}_{1:3} \\ \tilde{\boldsymbol{\omega}} \end{bmatrix} + \begin{bmatrix} \mathbf{0}_{3x3} \\ \underline{\mathbf{I}}^{-1} \end{bmatrix} [\tilde{\mathbf{N}}_{ctrl}] \quad (3.29)$$

Because the operating point for the inertial pointing controller is ${}^c\bar{\omega}_{ci} = [0 \ 0 \ 0]^T$, the model can be simplified to:

$$\begin{bmatrix} \dot{\tilde{\mathbf{q}}}_{1:3} \\ \dot{\tilde{\boldsymbol{\omega}}} \end{bmatrix} = \begin{bmatrix} \mathbf{0}_{3x3} & \frac{1}{2}\mathbf{1}_{3x3} \\ \mathbf{0}_{3x3} & \mathbf{0}_{3x3} \end{bmatrix} \begin{bmatrix} \tilde{\mathbf{q}}_{1:3} \\ \tilde{\boldsymbol{\omega}} \end{bmatrix} + \begin{bmatrix} \mathbf{0}_{3x3} \\ \underline{\mathbf{I}}^{-1} \end{bmatrix} [\tilde{\mathbf{N}}_{ctrl}] \quad (3.30)$$

3.4 Model for Nadir Pointing

For the antennas signal range to point in the direction of the earth, a controller which ensures that a given side of the satellite point toward the center of the earth is analysed in Section 4.2. For this study, a model which describes the kinematics and dynamics of the CRF wrt. ORF is derived.

3.4.1 Kinematic Differential Equations

The general linearized kinematic equation (D.16) is represented as:

$$\dot{\tilde{\mathbf{q}}}_{1:3} = -\underline{\mathbf{S}}(\bar{\omega})\tilde{\mathbf{q}}_{1:3} + \frac{1}{2}\tilde{\boldsymbol{\omega}} \quad (3.31)$$

Adding frame indexes for nadir pointing, this can be rewritten to:

$${}^c_o\dot{\tilde{\mathbf{q}}}_{1:3} = -\underline{\mathbf{S}}({}^c\bar{\omega}_{co}){}^c_o\tilde{\mathbf{q}}_{1:3} + \frac{1}{2}{}^c\tilde{\boldsymbol{\omega}}_{co} \quad (3.32)$$

By inserting the operating point ${}^c\bar{\omega}_{co} = [0 \ 0 \ 0]^T$, the equation is simplified to:

$${}^c_o\dot{\tilde{\mathbf{q}}}_{1:3} = \frac{1}{2}{}^c\tilde{\boldsymbol{\omega}}_{co} \quad (3.33)$$

3.4.2 Dynamic Differential Equations

In order to find the model for nadir pointing, the dynamic equation (3.28) must be rewritten such that it describes the ${}^c\dot{\boldsymbol{\omega}}_{co}$ instead of ${}^c\dot{\boldsymbol{\omega}}_{ci}$.

For the nadir pointing controller the operating point is:

$${}^c\bar{\omega}_{co} = [0 \ 0 \ 0]^T \quad (3.34)$$

$${}^c_o\bar{\mathbf{q}} = [0 \ 0 \ 0 \ 1]^T \quad (3.35)$$

By means of these operating points, it is derived that:

$$\begin{aligned} {}^c_o\mathbf{q} &= {}^c_o\tilde{\mathbf{q}} {}^c_o\bar{\mathbf{q}} \\ &= {}^c\tilde{\mathbf{q}} \end{aligned} \quad (3.36)$$

and

$$\begin{aligned} \boldsymbol{\omega}_{co} &= \tilde{\boldsymbol{\omega}}_{co} + \bar{\boldsymbol{\omega}}_{co} \\ &= \tilde{\boldsymbol{\omega}}_{co} \end{aligned} \quad (3.37)$$

Also, it should be noted that ${}^o\boldsymbol{\omega}_{oi}$ is assumed to be:

$${}^o\boldsymbol{\omega}_{oi} = \begin{bmatrix} 0 \\ \omega_0 \\ 0 \end{bmatrix} \quad (3.38)$$

where ω_0 is the constant orbital rate. This is a good approximation, as the orbit is nearly circular. The velocity ${}^c\boldsymbol{\omega}_{co}$ can be written as:

$${}^c\boldsymbol{\omega}_{ci} = {}^c\boldsymbol{\omega}_{co} + {}^c\boldsymbol{\omega}_{oi} \quad (3.39)$$

$$\begin{aligned} \Updownarrow \\ {}^c\boldsymbol{\omega}_{co} &= {}^c\boldsymbol{\omega}_{ci} - {}^c\boldsymbol{\omega}_{oi} \\ &= {}^c\boldsymbol{\omega}_{ci} - \underline{\mathbf{C}}_o {}^o\boldsymbol{\omega}_{oi} \end{aligned} \quad (3.40)$$

Using (3.34), the velocity ${}^c\boldsymbol{\omega}_{ci}$ can be rewritten as:

$$\begin{aligned} {}^c\boldsymbol{\omega}_{ci} &= {}^c\bar{\boldsymbol{\omega}}_{ci} + {}^c\tilde{\boldsymbol{\omega}}_{ci} \\ &= {}^c\bar{\boldsymbol{\omega}}_{co} + {}^c\bar{\boldsymbol{\omega}}_{oi} + {}^c\tilde{\boldsymbol{\omega}}_{ci} \\ &= \mathbf{0} + \underline{\mathbf{C}}_o {}^o\bar{\boldsymbol{\omega}}_{oi} + {}^c\tilde{\boldsymbol{\omega}}_{ci} \end{aligned} \quad (3.41)$$

By substituting (3.41) into (3.40) the orbital rate dismisses, such that

$$\begin{aligned} {}^c\boldsymbol{\omega}_{co} &= {}^c\underline{\mathbf{C}}_o {}^o\bar{\boldsymbol{\omega}}_{oi} + {}^c\tilde{\boldsymbol{\omega}}_{ci} - {}^c\underline{\mathbf{C}}_o {}^o\boldsymbol{\omega}_{oi} \\ &= {}^c\tilde{\boldsymbol{\omega}}_{ci} \end{aligned} \quad (3.42)$$

Because of the operating point in (3.34) is zero, the small signal values ${}^c\tilde{\boldsymbol{\omega}}_{co}$ and ${}^c\tilde{\boldsymbol{\omega}}_{ci}$ are also equal.

$${}^c\tilde{\boldsymbol{\omega}}_{co} = {}^c\tilde{\boldsymbol{\omega}}_{ci} \quad (3.43)$$

The dynamic equation (3.27) deduced in Section 3.3.2 is represented as:

$${}^c\dot{\boldsymbol{\omega}}_{ci} = \underline{\mathbf{I}}^{-1} (-\underline{\mathbf{S}}({}^c\boldsymbol{\omega}_{ci}) \underline{\mathbf{I}} {}^c\boldsymbol{\omega}_{ci} + {}^c\mathbf{N}) \quad (3.44)$$

The term $\underline{\mathbf{I}}^{-1} {}^c\mathbf{N}$ is explained in Section 3.5 and thus omitted in this section. By inserting (3.39), (3.44) can be rewritten to (ommitting the term $\underline{\mathbf{I}}^{-1} {}^c\mathbf{N}$):

$${}^c\dot{\boldsymbol{\omega}}_{ci_{cross}} = \underline{\mathbf{I}}^{-1} \underline{\mathbf{S}}({}^c\underline{\mathbf{C}}_o {}^o\boldsymbol{\omega}_{oi} + {}^c\boldsymbol{\omega}_{co}) \underline{\mathbf{I}} ({}^c\underline{\mathbf{C}}_o {}^o\boldsymbol{\omega}_{oi} + {}^c\boldsymbol{\omega}_{co}) \quad (3.45)$$

In Appendix C, equation (3.45) is extended and $\underline{\mathbf{C}}_o({}^c\mathbf{q})$ is approximated by $\underline{\mathbf{1}} + \underline{\mathbf{S}}({}^c\tilde{\mathbf{q}})$, because the ${}^c\mathbf{q}$ is assumed to be around [0 0 0 1].

Because the model needs to be linear, all constant and quadratic terms can be dismissed, such that (3.45) can be rewritten to:

$$\begin{aligned} {}^c\dot{\boldsymbol{\omega}}_{ci_{cross}} &= \underbrace{\underline{\mathbf{I}}^{-1} \underline{\mathbf{S}}({}^o\tilde{\boldsymbol{\omega}}_{oi}) \underline{\mathbf{I}} \underline{\mathbf{S}}({}^c\tilde{\mathbf{q}}) {}^o\boldsymbol{\omega}_{oi}}_{1a} + \underbrace{\underline{\mathbf{I}}^{-1} \underline{\mathbf{S}}(\underline{\mathbf{S}}({}^c\tilde{\mathbf{q}}) {}^o\boldsymbol{\omega}_{oi}) \underline{\mathbf{I}} {}^o\boldsymbol{\omega}_{oi}}_{1b} \\ &\quad + \underbrace{\underline{\mathbf{I}}^{-1} \underline{\mathbf{S}}({}^o\boldsymbol{\omega}_{oi}) \underline{\mathbf{I}} {}^c\boldsymbol{\omega}_{co}}_2 + \underbrace{\underline{\mathbf{I}}^{-1} \underline{\mathbf{S}}({}^c\boldsymbol{\omega}_{co}) \underline{\mathbf{I}} {}^o\boldsymbol{\omega}_{oi}}_3 \end{aligned} \quad (3.46)$$

For state space representation it is necessary to have the state variable vector on the right side, that in this case is either ${}^c\boldsymbol{\omega}_{co}$ or ${}^c\mathbf{q}$. As an example, expression (3.46, 1a), which is a linear term, and can to be rewritten to:

$$\underline{\mathbf{X}} {}^c\mathbf{q} \quad (3.47)$$

The matrix $\underline{\mathbf{X}}$ is found be inserting ${}^c\mathbf{q} = [1 \ 0 \ 0]^T$, ${}^c\mathbf{q} = [0 \ 1 \ 0]^T$, ${}^c\mathbf{q} = [0 \ 0 \ 1]^T$ one at a time in (3.46, 1a) which gives the basis vectors for $\underline{\mathbf{X}}$. Expression 1b and 3 in (3.46) is solved by the same approach.

Using kinematics, the left side of (3.46) needs to be rewritten using the differentiated (3.39):

$${}^c\dot{\boldsymbol{\omega}}_{co} = {}^c\dot{\boldsymbol{\omega}}_{ci} - {}^c\dot{\boldsymbol{\omega}}_{oi} \quad (3.48)$$

In which ${}^c\dot{\boldsymbol{\omega}}_{oi}$ is the only undetermined term, which is found as:

$$\begin{aligned} {}^c\dot{\boldsymbol{\omega}}_{oi} &= \underline{\mathbf{C}}({}^c\dot{\mathbf{q}}) {}^o\boldsymbol{\omega}_{oi} \\ &\approx \underline{\mathbf{S}}({}^c\dot{\mathbf{q}}) {}^o\boldsymbol{\omega}_{oi} \\ &\approx -\underline{\mathbf{S}}({}^o\boldsymbol{\omega}_{oi}) {}^c\dot{\mathbf{q}} \end{aligned} \quad (3.49)$$

The term ${}^c\dot{\mathbf{q}}$ approximates by the linearized kinematic equation (3.33) such that

$${}^c\dot{\boldsymbol{\omega}}_{oi} \approx -\underline{\mathbf{S}}({}^o\boldsymbol{\omega}_{oi}) \frac{1}{2} {}^c\tilde{\boldsymbol{\omega}}_{co} \quad (3.50)$$

Now the final dynamic model only relies on ${}^c\tilde{\boldsymbol{\omega}}_{co}$ and ${}^c\tilde{\mathbf{q}}$.

3.4.3 Dynamics (an alternative approach)

The model equations for the dynamic part ${}^c\omega_{ci_{cross}}$ has also be studied by an alternative approach, which is described in this section. The result is denoted ${}^c\omega_{ci_{cross_2}}$

The cross coupling from Section 3.3.2 can be rewritten as:

$$\begin{aligned} \underline{\mathbf{I}}^{-1} (-{}^C\underline{\mathbf{S}}(\omega) \underline{\mathbf{I}} {}^C\boldsymbol{\omega}) &= \begin{bmatrix} \frac{I_y {}^c\omega_{ci_y} \omega_{ci_z} - I_z {}^c\omega_{ci_y} \omega_{ci_z}}{I_x} \\ \frac{I_x {}^c\omega_{ci_x} \omega_{ci_z} - I_z {}^c\omega_{ci_x} \omega_{ci_z}}{I_y} \\ \frac{I_x {}^c\omega_{ci_x} \omega_{ci_y} - I_y {}^c\omega_{ci_x} \omega_{ci_y}}{I_z} \end{bmatrix} \\ &= \begin{bmatrix} \sigma_x {}^c\omega_{ci_y} \omega_{ci_z} \\ \sigma_y {}^c\omega_{ci_z} \omega_{ci_x} \\ \sigma_z {}^c\omega_{ci_x} \omega_{ci_y} \end{bmatrix} \end{aligned} \quad (3.51)$$

Where $\sigma_x = \frac{I_y - I_z}{I_x}$, $\sigma_y = \frac{I_z - I_x}{I_y}$ and $\sigma_z = \frac{I_x - I_y}{I_z}$.

Because ${}^o\boldsymbol{\omega}_{oi} = [0 \ \omega_0 \ 0]^T$, and ${}^o\mathbf{C}_o \approx \underline{\mathbf{S}}({}^o\mathbf{q}) + \underline{\mathbf{1}}$ for small rotations between ORF and CRF, (3.39) can be reduced to:

$$\begin{aligned} {}^c\boldsymbol{\omega}_{ci} &= (\underline{\mathbf{S}}({}^o\mathbf{q}) + \underline{\mathbf{1}}) {}^o\boldsymbol{\omega}_{oi} + {}^c\tilde{\boldsymbol{\omega}}_{ci} \\ &= \underline{\mathbf{S}}({}^o\mathbf{q}) {}^o\boldsymbol{\omega}_{oi} + {}^o\boldsymbol{\omega}_{oi} + {}^c\tilde{\boldsymbol{\omega}}_{ci} \\ &= -\underline{\mathbf{S}}({}^o\boldsymbol{\omega}_{oi}) {}^o\mathbf{q} + {}^o\boldsymbol{\omega}_{oi} + {}^c\tilde{\boldsymbol{\omega}}_{ci} \\ &= -\begin{bmatrix} 0 & 0 & \omega_0 \\ 0 & 0 & 0 \\ -\omega_0 & 0 & 0 \end{bmatrix} {}^o\mathbf{q} + [0 \ \omega_0 \ 0]^T + {}^c\tilde{\boldsymbol{\omega}}_{ci} \end{aligned} \quad (3.52)$$

By applying (3.36), the small value for quaternions can be substituted into (3.52), which now can be rewritten to

$$\begin{bmatrix} {}^c\omega_{ci_x} \\ {}^c\omega_{ci_y} \\ {}^c\omega_{ci_z} \end{bmatrix} = \begin{bmatrix} -\omega_0 {}^o\tilde{q}_3 \\ 0 \\ \omega_0 {}^o\tilde{q}_1 \end{bmatrix} + \begin{bmatrix} 0 \\ \omega_0 \\ 0 \end{bmatrix} + \begin{bmatrix} {}^c\tilde{\omega}_{ci_x} \\ {}^c\tilde{\omega}_{ci_y} \\ {}^c\tilde{\omega}_{ci_z} \end{bmatrix} \quad (3.53)$$

By substituting with the linearized expression from (3.53) and neglecting 2. order terms, (3.51) can be rewritten to

$$\begin{aligned} \begin{bmatrix} \sigma_x {}^c\omega_{ci_y} {}^c\omega_{ci_z} \\ \sigma_y {}^c\omega_{ci_z} {}^c\omega_{ci_x} \\ \sigma_z {}^c\omega_{ci_x} {}^c\omega_{ci_y} \end{bmatrix} &\approx \begin{bmatrix} \sigma_x (\omega_0 + {}^c\tilde{\omega}_{ci_y})(\omega_0 {}^o\tilde{q}_1 + {}^c\tilde{\omega}_{ci_z}) \\ \sigma_y (\omega_0 {}^o\tilde{q}_1 + {}^c\tilde{\omega}_{ci_z})(-\omega_0 {}^o\tilde{q}_3 + {}^c\tilde{\omega}_{ci_x}) \\ \sigma_z (-\omega_0 {}^o\tilde{q}_3 + {}^c\tilde{\omega}_{ci_x})(\omega_0 + {}^c\tilde{\omega}_{ci_y}) \end{bmatrix} \\ &\approx \begin{bmatrix} \sigma_x (\omega_0^2 {}^o\tilde{q}_1 + \omega_0 {}^c\tilde{\omega}_{ci_z}) \\ 0 \\ \sigma_z (-\omega_0^2 {}^o\tilde{q}_3 + {}^c\tilde{\omega}_{ci_x} \omega_0) \end{bmatrix} \end{aligned} \quad (3.54)$$

By applying (3.43), the expression becomes

$${}^c\dot{\boldsymbol{\omega}}_{ci_{cross_2}} = \begin{bmatrix} \sigma_x (\omega_0^2 {}^o\tilde{q}_1 + \omega_0 {}^c\tilde{\omega}_{ci_z}) \\ 0 \\ \sigma_z (-\omega_0^2 {}^o\tilde{q}_3 + {}^c\tilde{\omega}_{ci_x} \omega_0) \end{bmatrix} = \begin{bmatrix} \sigma_x (\omega_0^2 {}^o\tilde{q}_1 + \omega_0 {}^c\tilde{\omega}_{co_z}) \\ 0 \\ \sigma_z (-\omega_0^2 {}^o\tilde{q}_3 + {}^c\tilde{\omega}_{co_x} \omega_0) \end{bmatrix} \quad (3.55)$$

Now ${}^c\dot{\boldsymbol{\omega}}_{ci_{cross_2}}$ is found which only relies on ${}^c\tilde{\boldsymbol{\omega}}_{co}$ and ${}^o\tilde{\mathbf{q}}$

3.5 Energy Optimizing Control Torque

The last contribution of the state space model, which is seen in (3.29) is the same for both the nadir and inertial pointing model. The contribution is given as

$$\begin{bmatrix} \mathbf{0}_{3 \times 3} \\ \underline{\mathbf{I}}^{-1} \end{bmatrix} \begin{bmatrix} \tilde{\mathbf{N}}_{ctrl} \end{bmatrix} \quad (3.56)$$

The only controllable torque available on the satellite is the contribution from the magnetorquers ${}^c\mathbf{N}_{ctrl}$ that are described in (2.2) in Section 2.1.7 (cross product between the geomagnetic field vector ${}^c\mathbf{B}$ and the magnetic dipole moment vector ${}^c\mathbf{m}$). It is obvious that the torque contribution from the magnetorquers is largest when ${}^c\mathbf{B}$ and ${}^c\mathbf{m}$ are perpendicular to each other. Likewise, if ${}^c\mathbf{B}$ and ${}^c\mathbf{m}$ vectors are close to parallel, the torque is close to zero. It is beneficial to save energy from the ineffective magnetorquers and use more power on effective magnetorquers. A method to solve this problem, is to map the control signal, from the controller ${}^c\tilde{\mathbf{m}}$ to ${}^c\mathbf{m}$ such that ${}^c\mathbf{m}$ is perpendicular to the earth magnetic field, which is shown in (3.57).

$${}^c\mathbf{m} = \frac{{}^c\tilde{\mathbf{m}} \times {}^c\mathbf{B}}{\|{}^c\mathbf{B}\|} \quad (3.57)$$

The cross product is divided by $\|{}^c\mathbf{B}\|$ to make ${}^c\mathbf{m}$ a unitary vector. By applying (3.57) the efficiency will be improved. The direction of the control signal ${}^c\mathbf{m}$ can be chosen arbitrary from the controller.

Because the coils are placed perpendicular on the x-, y- and z-axis of the SBRF, the ${}^c\mathbf{m}$ signal needs to be mapped to ${}^s\mathbf{m}$. This is done using

$${}^s\mathbf{m} = {}^s\underline{\mathbf{C}}_c {}^c\mathbf{m} \quad (3.58)$$

For designing the controller, the magnetorquers are rewritten as:

$${}^c\mathbf{N}_{ctrl} = {}^c\mathbf{m} \times {}^c\underline{\mathbf{C}}_r {}^r\mathbf{B} \quad (3.59)$$

Where ${}^c\underline{\mathbf{C}}_r$ is the transformation matrix between the reference frame (denoted by r) and the CRF. The reference frame is ECI for inertial reference pointing and ORF for nadir reference pointing. For angles close to zero, the transformation matrix (A.24) can be approximated as:

$${}^c\underline{\mathbf{C}}_r \approx \underline{\mathbf{1}}_{3 \times 3} + \underline{\mathbf{S}}({}^r\tilde{\mathbf{q}}) \quad (3.60)$$

It is assumed that the term $\underline{\mathbf{S}}({}^r\tilde{\mathbf{q}})$ diminishes when feedback is applied and thus can be neglected, such that the torque can be rewritten as:

$${}^c\mathbf{N}_{ctrl} \approx {}^c\mathbf{m} \times {}^r\mathbf{B} \quad (3.61)$$

The mapping in (3.57) implies that the torque $\tilde{\mathbf{N}}$ from (3.29) to be effective is not substituted by the cross product ${}^c\tilde{\mathbf{m}} \times {}^r\mathbf{B}$, but with the double cross product $\frac{{}^c\tilde{\mathbf{m}} \times {}^r\mathbf{B}}{\|{}^r\mathbf{B}\|} \times {}^r\mathbf{B}$. This implies that the contribution, that corresponds to the input matrix and input is given as:

$$\begin{bmatrix} \mathbf{0}_{3 \times 3} \\ \underline{\mathbf{I}}^{-1} \end{bmatrix} \begin{bmatrix} \tilde{\mathbf{N}}_{ctrl} \end{bmatrix} = \underline{\mathbf{B}}(t) \tilde{\mathbf{m}}_{mt} \quad (3.62)$$

where the input matrix $\underline{\mathbf{B}}(t)$ is given by

$$\underline{\mathbf{B}}(t) = \begin{bmatrix} 0 & 0 & 0 \\ 0 & 0 & 0 \\ 0 & 0 & 0 \\ \underline{\mathbf{I}}^{-1} \begin{bmatrix} -{}^r B_y^2(t) - {}^r B_z^2(t) & {}^r B_x(t) {}^r B_y(t) & {}^r B_x(t) {}^r B_z(t) \\ {}^r B_x(t) {}^r B_y(t) & -{}^r B_x^2(t) - {}^r B_z^2(t) & {}^r B_y(t) {}^r B_z(t) \\ {}^r B_x(t) {}^r B_z(t) & {}^r B_y(t) {}^r B_z(t) & -{}^r B_x^2(t) - {}^r B_y^2(t) \end{bmatrix} \end{bmatrix} \quad (3.63)$$

3.6 Introduction of Reference

The model derived in Section 3.4.2, can only be used for control when it is wanted to coincide the CRF to the ORF.

In order to define another direction of the satellite relative to the ORF, a model is derived for pointing where CRF and an arbitrary reference frame should coincide. It is needed to have the possibility to some times point the antenna toward the earth and other times the camera. The antenna and camera is defined relative to the SBRF. To have the camera points towards nadir, the SBRF must be rotated 90° around the Y-axis of ORF. For obtaining that the antenna points towards nadir, the SBRF must be rotated 180° around the Y-axis of ORF. In both cases, the rotation can be defined by the quaternion

$${}_o^{s_{ref}} \mathbf{q} = \left[0 \ \sin\left(\frac{\theta}{2}\right) \ 0 \ \cos\left(\frac{\theta}{2}\right) \right] \quad (3.64)$$

Where s_{ref} is the frame that the SBRF should coincidence with, and θ is the rotated angle. In order to simplify calculations, it is convenient to represent the reference frame (denoted by r), by the one that should coincidence with CRF. This is done by

$${}_o^{s_{ref}} \mathbf{q} {}_s^c \mathbf{q} = {}_o^{c_{ref}} \mathbf{q} = {}_o^r \mathbf{q} \quad (3.65)$$

Where ${}_s^c \mathbf{q}$ is a constant quaternion, that describes the rotation from SRBF to CRF.

In the implementation, the rotation from the reference frame to CRF, which should be used as input to the controller, is calculated as

$${}_r \mathbf{q} = {}_o^r \mathbf{q} {}_o^c \mathbf{q} \quad (3.66)$$

The velocity ${}^c \boldsymbol{\omega}_{cr}$, which should be used as input to the controller, can be rewritten as

$${}^c \boldsymbol{\omega}_{cr} = {}^c \boldsymbol{\omega}_{ci} + {}^c \boldsymbol{\omega}_{ir} \quad (3.67)$$

$$\begin{aligned} &= {}^c \boldsymbol{\omega}_{ci} - {}^c \boldsymbol{\omega}_{ri} \\ &= {}^c \boldsymbol{\omega}_{ci} - {}^c \underline{\mathbf{C}}_r {}^r \boldsymbol{\omega}_{ri} \end{aligned} \quad (3.68)$$

while ${}^r \boldsymbol{\omega}_{ri}$ can be expressed as

$$\begin{aligned} {}^r \boldsymbol{\omega}_{ri} &= {}^r \boldsymbol{\omega}_{ro} + {}^r \boldsymbol{\omega}_{oi} \\ &= {}^r \boldsymbol{\omega}_{ro} + {}^r \underline{\mathbf{C}}_o {}^o \boldsymbol{\omega}_{oi} \end{aligned} \quad (3.69)$$

where ${}^r\underline{C}_o$ and ${}^o\omega_{oi}$ are constants and ${}^r\omega_{ro}$ is zero. The model equation (3.44) can be extended by substituting ${}^c\omega_{ci}$ by $({}^c\omega_{cr} + {}^c\omega_{ri})$:

$$\begin{aligned} {}^c\dot{\omega}_{ci} &= \underline{I}^{-1}\underline{S}({}^c\omega_{ci})\underline{I}{}^c\omega_{ci} \\ &= \underline{I}^{-1}\underline{S}({}^c\omega_{cr} + {}^c\omega_{ri})\underline{I}({}^c\omega_{cr} + {}^c\omega_{ri}) \\ &= \underline{I}^{-1}\underline{S}({}^c\omega_{cr} + {}^c\underline{C}_r{}^r\omega_{ri})\underline{I}({}^c\omega_{cr} + {}^c\underline{C}_r{}^r\omega_{ri}) \end{aligned} \quad (3.70)$$

By comparing (3.45) to the found equation (3.70), it is seen that the only difference is that ORF replaced the reference frame. As the only difference between these two frames is a constant rotation, the solution that is used for (3.45) is also valid for (3.70) just with ORF is replaced by the reference frame. The solution for ${}^c\dot{\omega}_{ci}$ yields:

$$\begin{aligned} {}^c\dot{\omega}_{ci_{cross3}} &= \underbrace{\underline{I}^{-1}\underline{S}({}^r\omega_{ri})\underline{I}\underline{S}({}^c\dot{q}_r){}^r\omega_{ri}}_{1a} + \underbrace{\underline{I}^{-1}\underline{S}(\underline{S}({}^c\dot{q}_r){}^r\omega_{ri})\underline{I}{}^r\omega_{ri}}_{1b} \\ &\quad + \underbrace{\underline{I}^{-1}\underline{S}({}^r\omega_{ri})\underline{I}{}^c\omega_{cr}}_2 + \underbrace{\underline{I}^{-1}\underline{S}({}^c\omega_{cr})\underline{I}{}^r\omega_{ri}}_3 \end{aligned} \quad (3.71)$$

Now ${}^c\dot{\omega}_{ci_{cross3}}$ is found, ${}^c\omega_{ir}$ needs to be found in order to obtain the final model equation ${}^c\omega_{cr} = {}^c\omega_{ci} + {}^c\omega_{ir}$.

${}^c\omega_{ir}$ differentiated yields:

$${}^c\dot{\omega}_{ir} = -({}^c\dot{\underline{C}}_r{}^r\omega_{ir} + {}^c\underline{C}_r{}^r\dot{\omega}_{ir}) = -{}^c\dot{\underline{C}}_r{}^r\omega_{ri} \quad (3.72)$$

For small angles between the CRF and the reference frame, (3.72) can be rewritten to

$$\begin{aligned} {}^c\dot{\omega}_{ir} &\approx -\underline{S}({}^c\dot{q}_r){}^r\omega_{ri} \\ &\approx \underline{S}({}^r\omega_{ri}){}^c\dot{q}_r \end{aligned} \quad (3.73)$$

${}^c\dot{q}_r$ can be approximated the same way as in Section 3.4.1.

$${}^c\dot{q}_r \approx \frac{1}{2}{}^c\tilde{\omega}_{cr} \quad (3.74)$$

By inserting (3.74) in (3.73) yields:

$$\begin{aligned} {}^c\dot{\omega}_{ir} &\approx \underline{S}({}^r\omega_{ri}){}^c\dot{q}_r \\ &\approx \underline{S}({}^r\omega_{ri})\frac{1}{2}{}^c\tilde{\omega}_{cr} \end{aligned} \quad (3.75)$$

Now the final linearized model equation that describes ${}^c\omega_{cr}$ has been derived.

3.7 Simulation Environment

In order to verify the performance of the satellite, the environment in which the satellite is operating must be examined. This simulation environment is created by previous groups working with the ADCS on different AAU-cubesat projects. In general the simulation environment calculates a combined disturbance torques acting on the satellite, which (among others) are affected by the Julian Date, the TLE, and the satellite attitude. As the report mainly focus on the fault detection and control of the satellite, the description is not thorough, but should provide an overview of which elements are considered when simulating the controllers. An overall diagram is displayed in Fig. 3.9. Here the satellite attitude and angular velocity refers to the attitude and angular velocity in SBRF seen

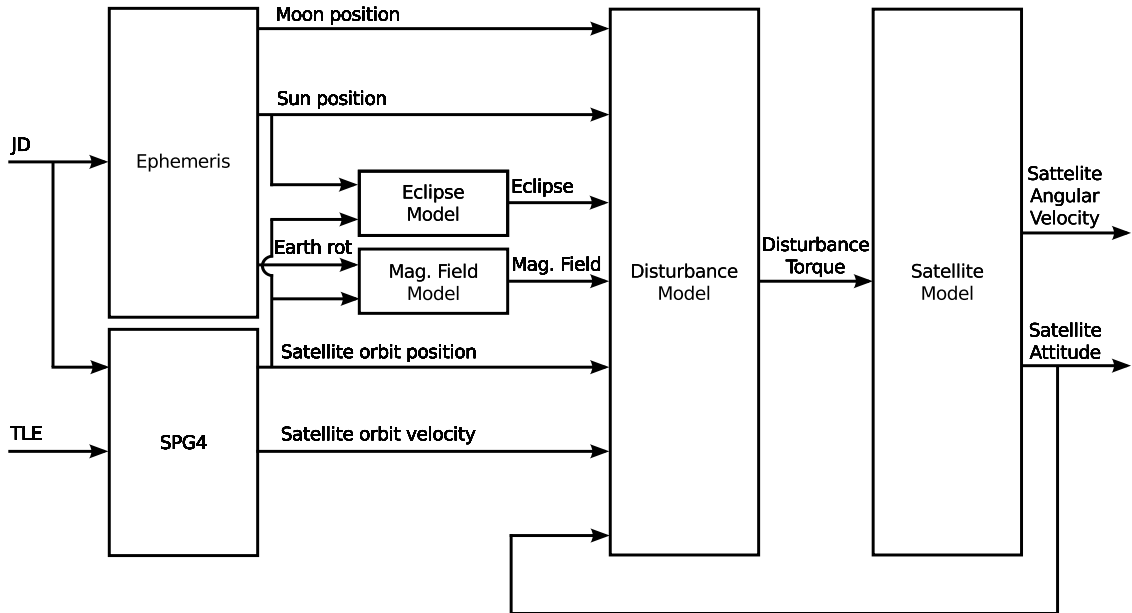


Figure 3.9: Overview of simulation environment for AAUSAT3

from ECI and the orbit position and velocity are the position and velocity represented in ECI.

The SPG4-box is described in Section 2.2.1 and calculates how the satellite is positioned in space, represented in the inertial frame.

3.7.1 Ephemeris

To be able to describe the motion of the satellite, the Ephemeris must be considered. The Ephemeris provides the position of astronomical object at a given time. The astronomical objects which has the largest effect on the satellite motion is the Earth, the sun and the moon.

Earth Rotation

The direction of the Earth rotation is defined as the rotation between the ECI-frame and the ECRF-frame, around their common z-axis. The rotated angle is thus given by the angle between the x-axis of the ECI-frame (axis described by the vernal equinox) and the Greenwich median axis, in the direction of the Earth rotation.

JD - The Julian Date

In order to calculate the rotation of the earth at a given time, the time, in which the two frame-axis are aligned must be known. For this the Julian Date (*JD*) is used and refers to the number of days since 12:00 January 1, 4713 B.C. Greenwich time.

Sun and Moon position

The position of a body in space can be calculated by several methods. The simulating environment make use of Kepler's Equation of motion for determination the sun position.

Eclipse and Magnetic Field Model

From the Sun position and the satellite position, it is possible to calculate when the satellite will be operating in eclipse, which is done by the Eclipse Model. The Eclipse disturbance is simply a boolean number. The Magnetic Field vector acting on the satellite is determined by the Magnetic Field model which uses the satellite position and the rotation of the earth.

3.7.2 Disturbance Model

The total attitude disturbance torque acting on the satellite is calculated by the disturbance model. This model includes four environmental torques which are the dominant sources of disturbing torques [Wertz 78, p. 566]. These are:

- Gravity gradient torque
- Solar radiation torque
- Aerodynamic drag torque
- Magnetic residual torque

Gravity Gradient Torque

The gravity gradient torque disturbance which is included in the simulation environment includes:

- The gravitation force from the Earth
- The gravitation force from the Sun
- The gravitation force from the Moon
- The Earths zonal harmonics

Here the satellite attitude is of relevance as the different gravitational forces will make it subject to different torques due its non-symmetric mass distribution. The orbital position is of relevance both with respect to the position of the Sun and Moon. Also as the orbit is not completely spherical, the gravitational torque-contribution from the earth will vary. The zonal harmonics is an term used for the variation in the gravitation field, which is caused by the earths non-uniform mass-distribution. The zonal harmonics only depends on the satellite latitude, why the satellites position in orbit is relevant. Of the four above mentioned contribution to the gravitational disturbance torque, the gravitational force from the earth is by far the largest[Wertz 78, p. 566 - 570].

Solar Radiation Torque

Solar radiation on the surface of the satellite causes a disturbance torque, which practically is altitude independent due to the satellites very small difference in distance from the sun and as the radiation varies with the inverse square of that distance. There are several sources of radiation such as Earth Albedo (reflection from the earth), solar illumination, and earth radiation. But the major radiation torque is cause by the direct solar radiation. In the simulation environment the earth albedo and the solar radiation is applied. For

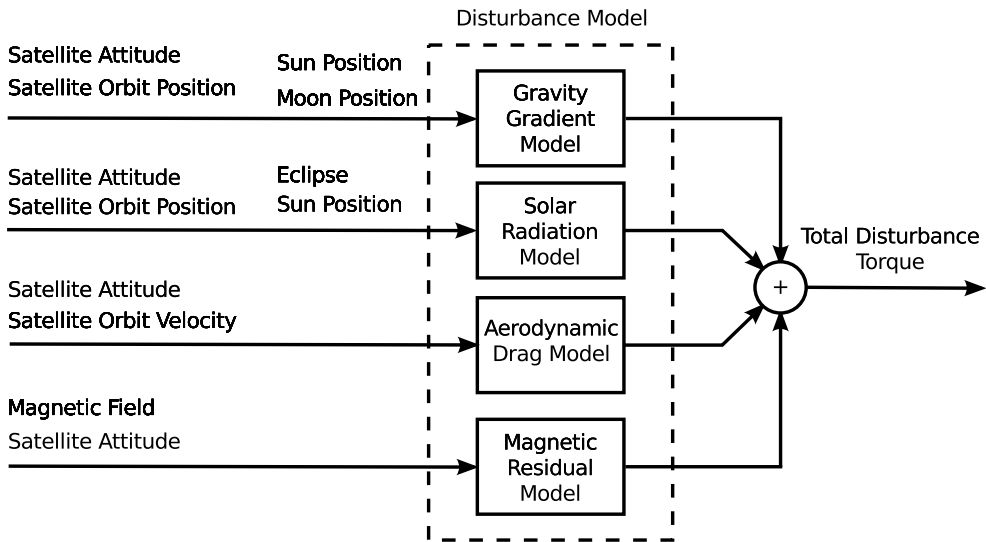


Figure 3.10: Overview of the simulation disturbance model

this reason the satellite attitude, orbit position, sun position and whether the satellite is in solar eclipse is used as input arguments for the Solar Radiation Model[Wertz 78, p. 570 - 571].

Aerodynamic Drag Torque

The friction which is caused by the interaction between the surface of the satellite and the atmosphere causes a disturbance torque. For spacecraft below an altitude of 400 km, the major environmental disturbance is due to aerodynamic draft. The AAUSAT3 will be operating at an altitude of approximately 600 km. The force acting on the surface of the satellite and thereby the disturbance torque is modelled by the energy absorbed from particles colliding with the satellite surface [Wertz 78, p. 573].

Magnetic Residual Torque

The interaction between the earths geomagnetic field and the satellites residual magnetic field provides a disturbance torque. The largest residuals is caused by:

- The satellites magnetic moments, caused by permanent and induced magnetism from currents in the satellites PCBs
- Eddy Current, caused by conductors exposed to a changing magnetic field
- Hysteresis from ferromagnetic materials

The first of the three mention above, is expected to affect the satellite with the largest disturbance torque [Wertz 78, p. 575]. For the simulation the permanent magnet dipole moment is applied together with a Gaussian noise disturbance vector. As the residual torque depends on the interaction between the geomagnetic field and the magnetic residual of the satellite, the magnetic residual model uses the magnetic field vector and satellite attitude as input. The disturbance model is illustrated in Fig. 3.10.

3.8 Model Validation

To verify to what degree the linear models for the Inertial and Nadir pointing deduced in Section 3.3.3 and Section 3.4 diverge from the non-linear model applied in the simulating environment, each linear model is compared to the non-linear. For this validation the input matrices ($\underline{\mathbf{B}}$) from the linear models are not considered directly. Instead a worst-case scenario of the applied torque is used as input, why the linear model, represented by a block in Fig. 3.11, does not represent the entire state space model, but merely the system matrix $\underline{\mathbf{A}}$.

The worst case scenario torque is defined as the maximum torque required for controlling the satellite in high magnetic field intensity. For the verification, the torque is applied to a single axis by a torque step with a magnitude given by [Jensen 10, p. 51]

$$\begin{aligned}\mathbf{N}_{tot} &= \mathbf{N}_{per} + \mathbf{N}_{track} + \mathbf{N}_{dist} \\ &= (145.2 + 146.4 + 51.88)[nNm] = 343.48[nNm]\end{aligned}\quad (3.76)$$

\mathbf{N}_{per} : Maximum torque from permanent magnet

\mathbf{N}_{track} : Maximum torque needed for tracking (pointing)

\mathbf{N}_{dist} : Environmental disturbance torque

3.8.1 Validation Procedure

The step is applied as input for both the linear and non-linear models. The initial condition for the attitude and angular velocities are given by

$$\boldsymbol{\omega}_{lin} = \boldsymbol{\omega}_{unlin} = [0\ 0\ 0]^T \quad (3.77)$$

$$\mathbf{q}_{lin} = \mathbf{q}_{ulin} = [0\ 0\ 0\ 1]^T \quad (3.78)$$

$$(3.79)$$

As the output vector of the linear model is reduced to six entries, the last value (q_4) is derived from the first three quaternions by (q_4 calculator box)

$$q_{4lin} = 1 - \sqrt{q_{1lin}^2 + q_{2lin}^2 + q_{3lin}^2} \quad (3.80)$$

The quaternion error is then computed by

$$\mathbf{q}_{err} = (\mathbf{q}_{lin})^{-1} \mathbf{q}_{unlin} \quad (3.81)$$

To evaluate the error by a meaningful quantity, the difference in the eigenaxis rotation (error angle θ_{err}) from the models attitude output is studied, and is obtained merely by the real part of the error quaternion (q_{4err})

$$\theta_{err} = 2 \arccos(q_{4err}) \quad (3.82)$$

Also the angular rate error is studied and is given by

$$\boldsymbol{\omega}_{err} = \boldsymbol{\omega}_{lin} - \boldsymbol{\omega}_{ulin} \quad (3.83)$$

In Fig. 3.11 the model validation procedure is illustrated.

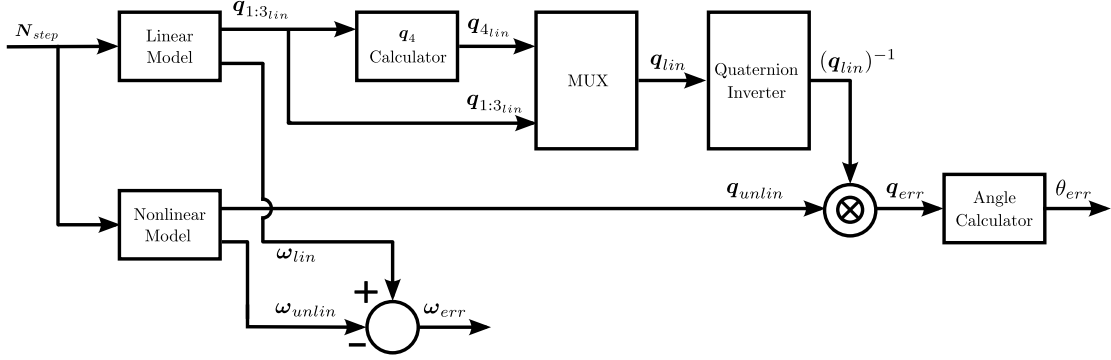


Figure 3.11: The procedure of the model validation, with a torque pulse as input and the eigenaxis angle error and the angular rate error as outputs

N_{step} : The applied torque step

q_{lin} : The attitude of the linear system

$q_{1:3lin}$: The imaginary part of q_{lin}

q_{4lin} : Real part of q_{lin}

q_{unlin} : The attitude of the nonlinear system

q_{err} : The attitude error between the linear and nonlinear models, expressed as the quaternion error

θ_{err} : The attitude error between the linear and nonlinear models, expressed as an eigenaxis error

ω_{lin} : The angular rate of the linear system

ω_{unlin} : The angular rate of the nonlinear system

ω_{err} : The angular rate error of between the linear and nonlinear system

3.8.2 Validation of Inertial Pointing Model

In Fig. 3.12 a comparison of the linear and nonlinear model attitude, for the inertial pointing model, is plotted. As the torque is only affecting a rotation around the x-axis, the eigenaxis is given by $e = [1 \ 0 \ 0]^T$, and the quaternion is thus expected to be $q_i^c = [\sin(\theta/2) \ 0 \ 0 \ \cos(\theta/2)]$. It can be seen from Fig. 3.12 that both q_2 and q_3 are zero for both the linear and nonlinear model and that the eigenaxis angle error is diverging with time.¹ Another thing which is noted is that the quaternion in the linear model is not constrained by a norm of one. In Fig. 3.13 a comparison of the angular velocities from the linear and nonlinear models, of the inertial pointing model, is plotted. As expected the velocity is increasing with time on the x-axis alone. It is seen from the lowest graph in Fig. 3.13 that the angular velocity error is practically zero.

3.8.3 Validation of Nadir Pointing Model

In Fig. 3.14, a comparison of the linear and nonlinear model attitude, for the nadir pointing model, is plotted. It is noticed that the step pulse is affecting the rotation of both the x- and the z-axis, which is caused by the cross coupling of (3.54). Though the rotation around the z-axis is small, especially for the first 200 s. The output of the two

¹The graph of the eigenaxis error saturates at 360° due to the undefined value for $\arccos(q_4)$, for $1 < q_4 < -1$

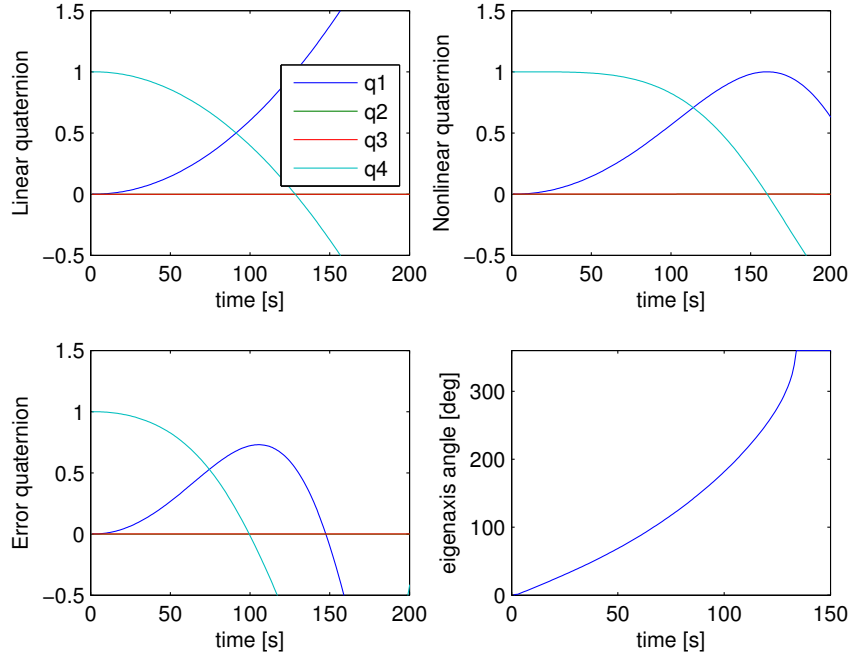


Figure 3.12: The linear and nonlinear, inertial model, attitude output and output error, when affected by a worst case torque step on the x-axis

described Nadir pointing models appeared to be so similar that only the one described in Section 3.4.3 is represented in this section. In Fig. 3.15, a comparison of the angular velocities from the linear and nonlinear models, of the nadir pointing model, is plotted. It is seen that the angular velocity error is more significant than for the inertial model. From Fig. 3.12 and Fig. 3.14 it is seen that the attitude for the linear and nonlinear models are reasonably close doing the first seconds, though with time the error (θ_{err}) diverges "fast" for both models. Thus it seems that the linear model performs satisfactory, while close to the operating point. The angular rate error (ω_{err}) is almost zero for the inertial pointing model while the nadir pointing model has a higher angular error rate, which is first noticeable for the high eigenaxis angle error.

It should be noted that the model validation does not concern with any validation of the non-linear model, which is considered as a truth model.

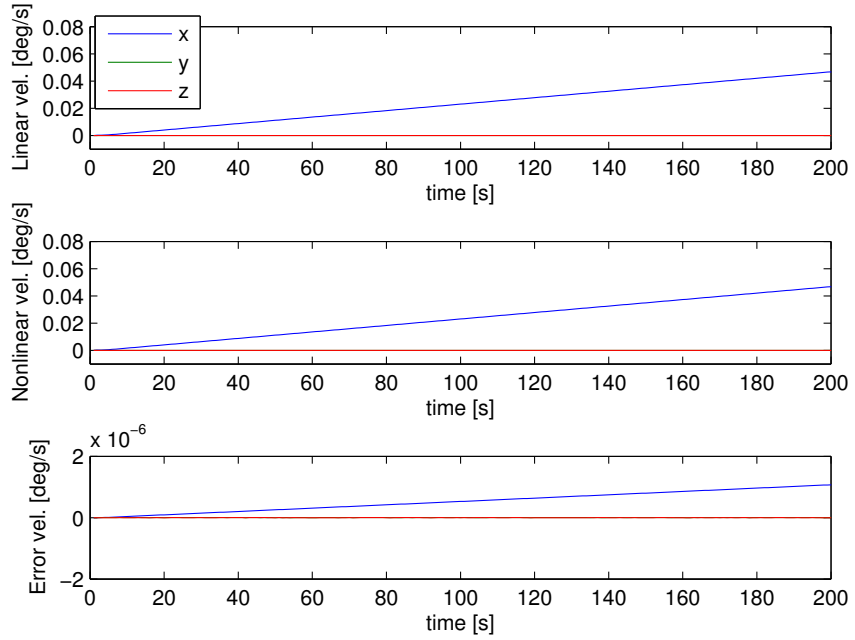


Figure 3.13: The linear and nonlinear, inertial model, angular velocity output and output error, when affected by a worst case torque step on the x-axis

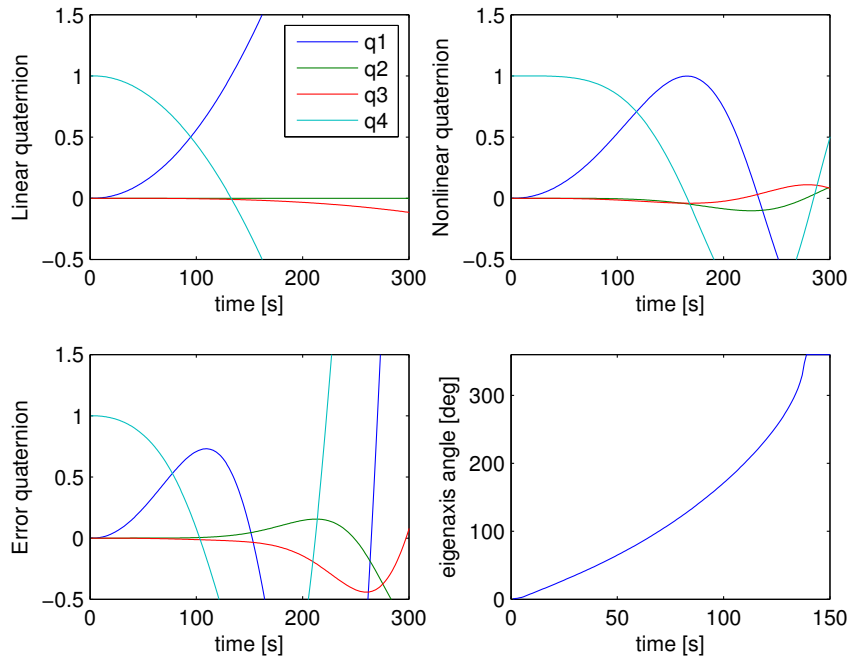


Figure 3.14: The linear and nonlinear, nadir model, attitude output and output error, when affected by a worst case torque step on the x-axis

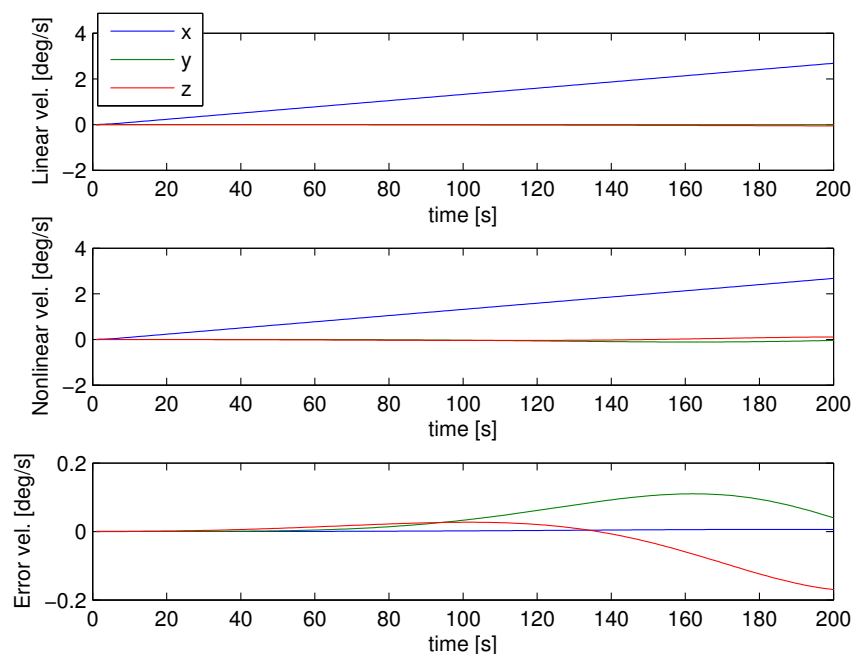


Figure 3.15: The linear and nonlinear, nadir model, angular velocity output and output error, when affected by a worst case torque step on the x-axis

Chapter 4

Controllers

In this chapter three controllers are described: One which is used for detumbling the satellite and two which are used for pointing according to a certain reference frame. The detumbling controller makes use of the rate of change in the B-field vector, and is thus called a B-dot controller. The two reference frame pointing controllers are constant gain controllers, which assumes that the B-field is constant. These two controllers point the satellite in the direction of the earth centeret inertial frame (ECI) and the orbit reference frame (ORF), and are called "Inertial pointing controller" and "Nadir pointing controller" respectively.

4.1 Detumbling Controller

When the satellite is released from the P-POD (Poly Picosatellite Orbital Deployer) it is expected to have an angular rate that is too high for the constant gain controller to stabilize it (tumbling). For this reason a detumbling controller is used. The definition for the satellite to be detumbeled is that it should follow the earths geomagnetic field, while moving around the earth.

The satellite is expected to operating at an altitude of 600 km and the orbit time is approximately 5830 s . As the geomagnetic field will cause the satellite to rotate twice around its axis in one orbit, the detumbling rate is as mentioned earlier given by

$$\text{detumble rate} = 2 \cdot \frac{2\pi \text{ [rad]}}{5830 \text{ [s]}} = 0.0022 \left[\frac{\text{rad}}{\text{s}} \right] \quad (4.1)$$

The radio transmission between the ground station and the satellite is crucial to the mission success, but the antenna has very wide angle of communication, which implies low pointing requirements for the ADCS. The essential mission requirements could be satisfied by an detumbling controller, in which focus should be on robustness and a simple design.

A simple controller which satisfies this is the B-dot controller. The idea of the B-dot controller is to control the rate of change of the B-field vector, such that the angular velocity is lowered to the detumbling rate. This is done by the derivative of the magnetometers measurements.

4.1.1 The B-dot controller

To determine if the B-dot controller is stable, a Lyapunov candidate function is used (see Chapter F). For the rate of the B-field vector and thereby the angular velocity to decrease,

the kinetic energy must dissipate from the satellite, why the Lyapunov candidate function describes the kinetic energy from the rotation of satellite, given by

$$E_{kin}(^c\boldsymbol{\omega}_{ci}) = \frac{1}{2} {}^c\boldsymbol{\omega}_{ci}^T \underline{\mathbf{I}} {}^c\boldsymbol{\omega}_{ci} \quad (4.2)$$

For simplicity, for the rest of this section ${}^c\boldsymbol{\omega}_{ci}$ is written as $\boldsymbol{\omega}$. Differentiating (4.2), and exploiting the fact that $\underline{\mathbf{I}}$ is a diagonal matrix yields

$$\begin{aligned} \dot{E}_{kin}(\boldsymbol{\omega}) &= \frac{1}{2} (\dot{\boldsymbol{\omega}}^T \underline{\mathbf{I}} \boldsymbol{\omega} + \boldsymbol{\omega}^T \underline{\mathbf{I}} \dot{\boldsymbol{\omega}}) \\ &= \frac{1}{2} (\dot{\boldsymbol{\omega}}^T \underline{\mathbf{I}} \boldsymbol{\omega} + \dot{\boldsymbol{\omega}}^T \underline{\mathbf{I}} \boldsymbol{\omega}) \\ &= \dot{\boldsymbol{\omega}}^T \underline{\mathbf{I}} \boldsymbol{\omega} \end{aligned} \quad (4.3)$$

Substituting the non-linear dynamic equation from (3.27) into (4.3) yields

$$\begin{aligned} \dot{E}_{kin}(\boldsymbol{\omega}) &= (\underline{\mathbf{I}}^{-1} (-\underline{\mathbf{S}}(\boldsymbol{\omega}) \underline{\mathbf{I}} \boldsymbol{\omega} + \mathbf{N}_{dist} + \mathbf{N}_{ctrl}))^T \underline{\mathbf{I}} \boldsymbol{\omega} \\ &= (-\underline{\mathbf{S}}(\boldsymbol{\omega}) \underline{\mathbf{I}} \boldsymbol{\omega} + \mathbf{N}_{dist} + \mathbf{N}_{ctrl})^T \underline{\mathbf{I}}^{-1} \underline{\mathbf{I}} \boldsymbol{\omega} \\ &= (-\underline{\mathbf{S}}(\boldsymbol{\omega}) \underline{\mathbf{I}} \boldsymbol{\omega})^T \boldsymbol{\omega} + (\mathbf{N}_{dist}^T + \mathbf{N}_{ctrl}^T) \boldsymbol{\omega} \\ &= (\underline{\mathbf{I}} \boldsymbol{\omega})^T \cdot -\underline{\mathbf{S}}(\boldsymbol{\omega})^T \boldsymbol{\omega} + (\mathbf{N}_{dist}^T + \mathbf{N}_{ctrl}^T) \boldsymbol{\omega} \end{aligned} \quad (4.4)$$

By applying the identity $\underline{\mathbf{S}}(\boldsymbol{\omega}) = -\underline{\mathbf{S}}(\boldsymbol{\omega})^T$ (4.4) can be rewritten to

$$\begin{aligned} \dot{E}_{kin}(\boldsymbol{\omega}) &= (\underline{\mathbf{I}} \boldsymbol{\omega})^T \underbrace{\underline{\mathbf{S}}(\boldsymbol{\omega}) \boldsymbol{\omega}}_0 + (\mathbf{N}_{dist}^T + \mathbf{N}_{ctrl}^T) \boldsymbol{\omega} \\ &= (\mathbf{N}_{dist}^T + \mathbf{N}_{ctrl}^T) \boldsymbol{\omega} \end{aligned} \quad (4.5)$$

By excluding the disturbance torque \mathbf{N}_{dist} , the time derivative of the kinetic energy is given by

$$\dot{E}_{kin}(\boldsymbol{\omega}) = \mathbf{N}_{ctrl}^T \boldsymbol{\omega} \quad (4.6)$$

For the controller to be asymptotically stable (defined in Chapter F), the change in kinetic energy should have a negative coefficient , i.e. (4.6) need to be negative, providing the following constrain

$$\mathbf{N}_{ctrl}^T \boldsymbol{\omega} < 0 \quad (4.7)$$

As described in Section 2.1.7 the control torque is given by

$$\mathbf{N}_{ctrl} = \mathbf{m} \times \mathbf{B} \quad (4.8)$$

where \mathbf{m} is the satellite magnetic dipole moment and \mathbf{B} is the geomagnetic B-field vector. By substituting (4.8) into (4.7) yields

$$\begin{aligned} (\mathbf{m} \times \mathbf{B})^T \boldsymbol{\omega} &< 0 \\ \Updownarrow \\ -\boldsymbol{\omega}^T (\mathbf{B} \times \mathbf{m}) &< 0 \\ \Updownarrow \\ \mathbf{m}^T (\boldsymbol{\omega} \times \mathbf{B}) &> 0 \end{aligned} \quad (4.9)$$

It is now easily seen that for any constant $C > 0$, (4.9) is solved by

$$\mathbf{m} = C(\boldsymbol{\omega} \times \mathbf{B}) \quad (4.10)$$

due to the fact that $(\boldsymbol{\omega} \times \mathbf{B})^T(\boldsymbol{\omega} \times \mathbf{B})$ always will be greater than zero, under the assumption that $\boldsymbol{\omega}$ and \mathbf{B} are not parallel, and that neither of them are zero vectors. In this case $\dot{E}_{kin}(\boldsymbol{\omega})$ will equal zero, which will make the system marginally stable. The constant C , determines how fast the energy will dissipate, and is thus limited by the saturation of the magnetorquers. The change of the B-field vector $\dot{\mathbf{B}}$ is affected by the inclination of the satellites orbit, the earths rotation, the satellite attitude and the satellite angular rate. For near polar orbit spacecrafts it is reasonable to assume that the change of geomagnetic field that is caused by the earth rotation and the satellite attitude can be neglected, such that the change of geomagnetic field only depends on the satellite angular rate [Wiśniewski 96, p. 143]. $\dot{\mathbf{B}}$ is thus given by

$$\dot{\mathbf{B}} = -\boldsymbol{\omega} \times \mathbf{B} \quad (4.11)$$

Now (4.11) can be substituted into (4.10) and a simple control law is obtained

$$\mathbf{m} = -C\dot{\mathbf{B}} \quad (4.12)$$

4.1.2 B-dot filter

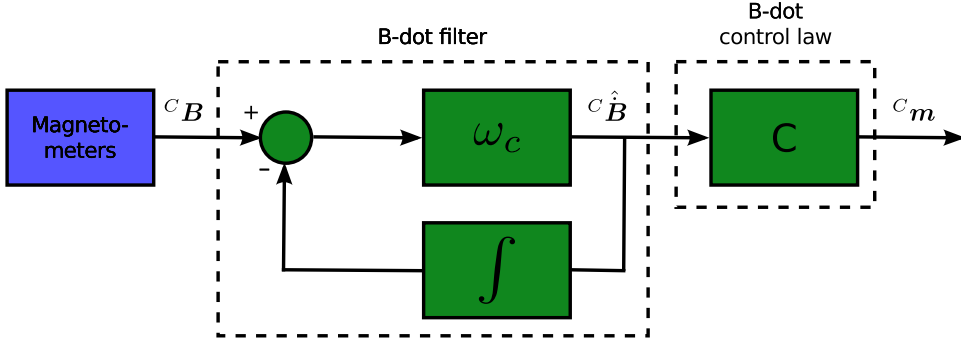
To make use of the control law in (4.12) the measured B-field vector from the magnetometers must be differentiated, which would give the simple transfer function in the frequency domain

$$G(s) = \frac{\dot{\mathbf{B}}(s)}{\mathbf{B}(s)} = s \quad (4.13)$$

To avoid high frequency noise from $\dot{\mathbf{B}}$, the differentiation is implemented with a band limited filter. To ensure stability, the filter requirement is studied: From (4.6), (4.8), (4.10), and (4.12) the change in kinetic energy is given by

$$\begin{aligned} \dot{E}_{kin}(\boldsymbol{\omega}) &= \mathbf{N}_{ctrl}^T \boldsymbol{\omega} \\ &= (\mathbf{m} \times \mathbf{B})^T \boldsymbol{\omega} \\ &= (-C\hat{\mathbf{B}} \times \mathbf{B})^T \boldsymbol{\omega} \\ &= -C(\hat{\mathbf{B}} \times \mathbf{B})^T \boldsymbol{\omega} \\ &= -C(\underline{\mathbf{S}}(\hat{\mathbf{B}})\mathbf{B})^T \boldsymbol{\omega} \\ &= C\hat{\mathbf{B}}^T \underline{\mathbf{S}}(\mathbf{B})^T \boldsymbol{\omega} \\ &= -C\hat{\mathbf{B}}^T (\mathbf{B} \times \boldsymbol{\omega}) \\ &= -C\hat{\mathbf{B}}^T \dot{\mathbf{B}} \end{aligned} \quad (4.14)$$

From (4.14) it is obvious that the phase of $\dot{\mathbf{B}}$ is not allowed to lead by 90° or more, wrt. $\hat{\mathbf{B}}$, as this will make the kinetic energy increase. For this reason the band limited filter should be of the first order, such that a 90° phase shift is only obtained at a frequency of infinity.

**Figure 4.1:** Band limiting differential filter

The transfer function for the band limiting differentiator, is inspired by [Graversen 02, p. 43]. In the frequency domain, the filter is given by

$$H(s) = \frac{\hat{B}(s)}{B(s)} = s \frac{\omega_c}{s + \omega_c} \quad (4.15)$$

In Fig. 4.1 the band limiting differential filter is illustrated. For the filter to operate as desired, some design approaches must be taken. As the filter should function as an estimated differentiator, the frequency characteristics of (4.15) should stay close to the frequency characteristics of (4.13) within the desired frequency range. This can be expressed as

$$\begin{aligned} s &\approx s \frac{\omega_c}{s + \omega_c} \\ &\Updownarrow \\ j\omega &\approx j\omega \frac{\omega_c}{j\omega + \omega_c} \\ &\approx j\omega \frac{\omega_c(\omega_c - j\omega)}{(j\omega + \omega_c)(\omega_c - j\omega)} \\ &\approx \frac{j\omega\omega_c^2 + \omega_c\omega^2}{\omega_c^2 + \omega^2} \\ &\approx j\omega \frac{\omega_c^2}{\omega_c^2 + \omega^2} + \frac{\omega_c\omega^2}{\omega_c^2 + \omega^2} \end{aligned} \quad (4.16)$$

By locating the filter cut-off frequency ω_c far above the frequencies of interest, that is $\omega \ll \omega_c$, ω^2 can be removed from the denominator. (4.16) can thus be rewritten to

$$\begin{aligned} j\omega &\approx j\omega \frac{\omega_c^2}{\omega_c^2} + \frac{\omega_c\omega^2}{\omega_c^2} \\ &\approx j\omega + \frac{\omega^2}{\omega_c} \end{aligned} \quad (4.17)$$

Now the approximation of (4.17) will be true for $\omega \ll \omega_c$. This means that a trade-off exist between suppressing high-frequency noise and having \hat{B} be a reasonable assumption in a given frequency range. It is assumed that the satellite will have a angular rate of no more than 0.1 rad/s when deployed from the P-POD[Green 06, p. 174]. For this reason the filter cut-off frequency is located at 1 rad/s . The gain and phase of $G(s)$ and $H(s)$

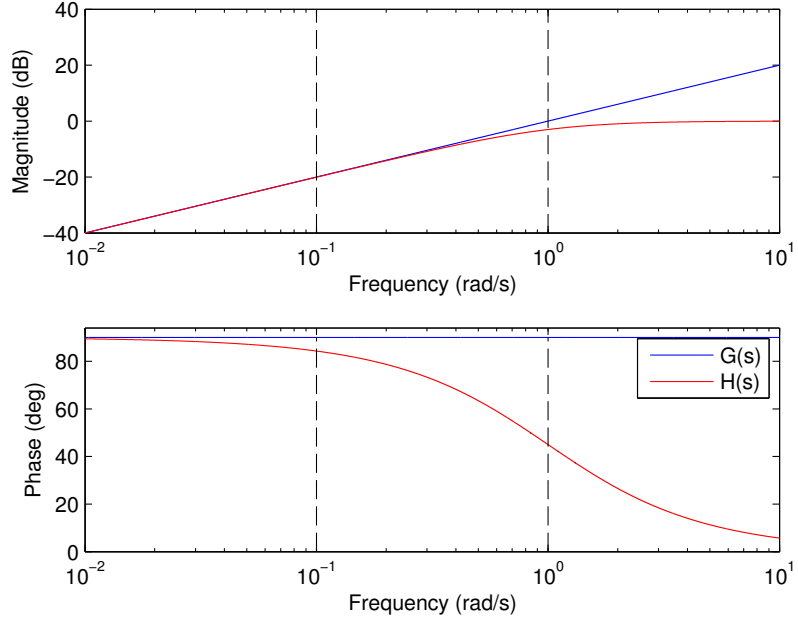


Figure 4.2: Bodeplot of regular differentiator ($G(s)$) and band limiting differential filter ($H(s)$)

are shown in Fig. 4.2. Here it is seen that for the expected tumbling rate (0.1 rad/s), the magnitude of $H(s)$ practically is the same as $G(s)$, while the phase shift between $G(s)$ and $H(s)$ is about 6° . For higher frequencies the controller will still be stable, but as these frequencies are damped the controller will underestimate the value of $\dot{\mathbf{B}}$ and thus make the controller react slower than if a real differentiator was used.

By empirical analysis the control law constant C is chosen to 10,000. The acceptance test of the B-dot controller is described in Section 7.1

4.2 Reference Frame Pointing Controllers

In this section, two reference frame controllers are designed, which makes use of the linearized models found in Chapter 3. The control theory in this section is based on periodic systems as the geomagnetic field seen from the satellite can be considered as periodic, which is assumed in order to design controllers and to check the stability of the system. The periodic magnetic field however causes some control limitations, which is also studied in this section.

Some methods exist for designing a linear reference controller, and the one used in this project is the constant gain controller. A constant gain controller is designed for both nadir reference pointing and for inertial reference pointing. For the nadir reference pointing, the ORF is used as the reference frame, that the CRF should coincide with and likewise for the inertial reference pointing the ECI is used.

As described in Section 2.1.6, the satellite is equipped with a permanent magnet, located in the Z-axis of the SBRF. It is assumed that the contribution from the permanent magnet can be easily canceled by generating an opposite constant dipole moment in the magnetorquers. Thus the contribution permanent magnet is neglected throughout

the design of the pointing controllers.

Control Limitations

As previously mentioned, the only actuators on the spacecraft are the three set of magnetorquers. This introduces some controllability limitations given that the produced torque is always perpendicular to the geomagnetic field. This implies that represented in ORF, the yaw (Z-axis) controllability is reduced when the spacecraft is parsing over the poles and the pitch (Y-axis) controllability is reduced when the spacecraft is parsing over equator. In spite of the periodic lack of controllability, during an orbit, it is possible to control all three axis.

Periodic Linear System

As seen in Section 3.2, the magnetic field represented in ORF and ECI can approximately be considered a periodic signal. This is because the earth magnetic field basically can be considered as a magnetic dipole with some abnormalities. By making this assumption, the time dependent input matrix can now be approximated as $\underline{B}(t + T) = \underline{B}(t)$. Deviation between the ideal periodic signal and the real periodic signal is considered as a disturbance.

In the region around an operation point, the system now is considered periodic and linear. Thus, theory for periodic linear systems can be applied.

For the further calculations, it is necessary to approximate an ideal periodic $\underline{B}_{ave}(t)$ for a orbit. This is obtained using (4.18).

$$\underline{B}_{ave}(t) = \frac{1}{N} \sum_{i=1}^N \underline{B}(t + Ocdot i) \quad (4.18)$$

Where O is the time of one orbit.

N is the number of orbits of $\underline{B}(t)$ used in the approximation (29 were used).

t is the time ($0 \leq t \leq O$).

The ideal periodic signal over one orbit is generated both for the nadir and inertial pointing controller.

The average B-field in ORF and ECI are shown in Fig. 4.3 and Fig. 4.4.

4.2.1 Constant Gain Controller

For periodic linear systems, different controller types can be applied. In [Wiśniewski 96] infinite- and finite horizon, and a constant gain periodic attitude controller is presented. The infinite horizon can be calculated offline for CPU saving but requires a large amount of memory. The finite horizon controller requires a large amount of CPU power in order to solve the time dependent Riccati equation while in flight. An alternative to the finite- and infinite horizon controllers, is the constant gain controller that requires a low amount of memory and for which the solution to the Riccati equation for a time invariant system can be computed offline.

Because the constant gain controller is the most simple controller, and requires least CPU power and memory, the constant gain controller is chosen.

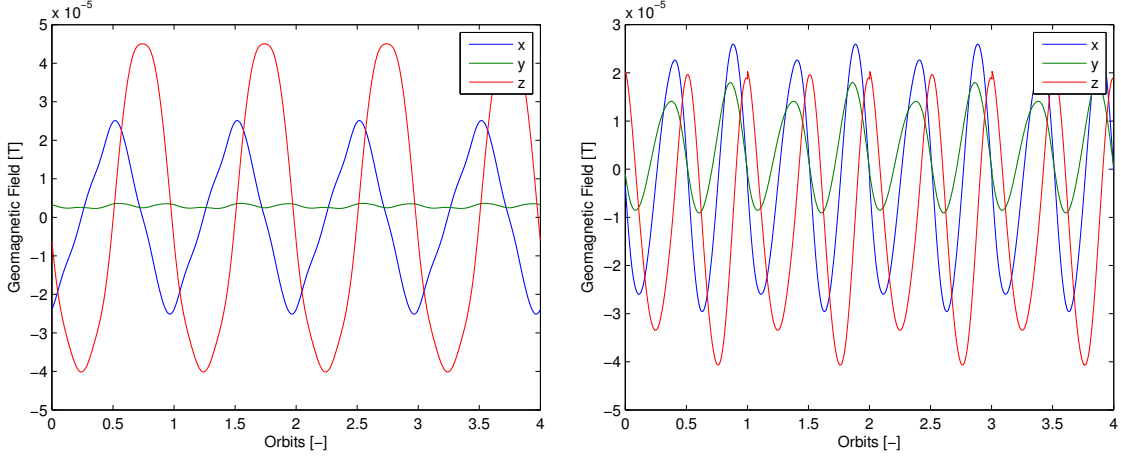


Figure 4.3: The averaged magnetic field in the ORF

Figure 4.4: The averaged magnetic field in the ECI

LQR Design

The design of the Linear Quadratic Regulator (LQR) concerns with an optimal selection for the feedback-matrix (\underline{L}) such that a given feedback, in addition to provide a stable system, also contains a certain degree of performance. In general, the values in the feedback-matrix determines how much the system should actuate due the behavior of a given state. This relationship between state behavior and system actuation defines the movement of the satellite and must be considered in order to economize on power consumption, while maintaining a desired performance.

The continuous time, linear, time-variant system is described by

$$\dot{\mathbf{x}}(t) = \underline{\mathbf{A}}(t)\mathbf{x}(t) + \underline{\mathbf{B}}(t)\mathbf{u}(t) \quad (4.19)$$

with the cost-function defined as

$$\mathcal{J} = \int_0^{\infty} (\mathbf{x}(t)^T \underline{\mathbf{Q}} \mathbf{x}(t) + \mathbf{u}(t)^T \underline{\mathbf{R}} \mathbf{u}(t)) dt. \quad (4.20)$$

In (4.20) the cost function is defined as the continuous sum of the squared control input and the squared state variables. The matrix $\underline{\mathbf{R}}$ weights the control effort, and thereby the control performance, while the matrix $\underline{\mathbf{Q}}$ weights the states variables and thereby the effort of the system actuators. Here $\underline{\mathbf{Q}}$ is a constant positive semi-definite matrix and $\underline{\mathbf{R}}$ is a constant positive definite matrix.

The control law that minimizes the cost-function in (4.20) is given by

$$\mathbf{u}(t) = \underline{\mathbf{L}}(t)\mathbf{x}(t) \quad (4.21)$$

Providing the following closed loop transfer

$$\begin{aligned} \dot{\mathbf{x}}(t) &= \underline{\mathbf{A}}(t)\mathbf{x}(t) + \underline{\mathbf{B}}(t)\underline{\mathbf{L}}\mathbf{x}(t) \\ &= (\underline{\mathbf{A}}(t) + \underline{\mathbf{B}}(t)\underline{\mathbf{L}}(t))\mathbf{x}(t) \\ &= \underline{\mathbf{A}}_{cl}(t)\mathbf{x}(t) \end{aligned} \quad (4.22)$$

The feedback matrix $\underline{\mathbf{L}}$ in (4.21), which provides the optimal control gain is found by

$$\underline{\mathbf{L}}(t) = -\underline{\mathbf{R}}^{-1} \underline{\mathbf{B}}(t)^T \underline{\mathbf{P}}(t) \quad (4.23)$$

Here $\underline{\mathbf{P}}$ is found by solving the algebraic Riccati equation given by

$$-\dot{\underline{\mathbf{P}}}(t) = \underline{\mathbf{Q}} + \underline{\mathbf{A}}(t)^T \underline{\mathbf{P}}(t) + \underline{\mathbf{P}}(t) \underline{\mathbf{A}}(t) - \underline{\mathbf{P}}(t) \underline{\mathbf{B}}(t) \underline{\mathbf{R}}^{-1} \underline{\mathbf{B}}(t)^T \underline{\mathbf{P}}(t) \quad (4.24)$$

The major disadvantages of a time dependent feedback matrix is as mentioned the amount of calculations which will need to be computed, as (4.23) and (4.24) should be computed (in discrete time) for each iteration, when implemented. In order to minimize this, the feedback matrix is approximated as time-independent. From (4.23) and (4.24) it can be seen that both the system matrix $\underline{\mathbf{A}}$ and $\underline{\mathbf{B}}$ should be time-independent. As $\underline{\mathbf{A}}(t)$ already is time independent ($\underline{\mathbf{A}}(t) = \hat{\underline{\mathbf{A}}} = \underline{\mathbf{A}}$), only $\underline{\mathbf{B}}(t)$ needs to be time-independent which is done by averaging $\underline{\mathbf{B}}(t)$ such that

$$\hat{\underline{\mathbf{B}}} = \frac{1}{T} \int_{t_0}^{t+T} \underline{\mathbf{B}}(t) dt \quad (4.25)$$

In this way the Riccati Equation from (4.24) is reduced to the stationary solution and the optimal control gain from (4.23) becomes time-independent. This can be written as

$$\underline{\mathbf{L}} = -\underline{\mathbf{R}}^{-1} \hat{\underline{\mathbf{B}}}^T \underline{\mathbf{P}} \quad (4.26)$$

where

$$\underline{\mathbf{Q}} + \hat{\underline{\mathbf{A}}}^T \underline{\mathbf{P}}(t) + \underline{\mathbf{P}} \hat{\underline{\mathbf{A}}} - \underline{\mathbf{P}} \hat{\underline{\mathbf{B}}} \underline{\mathbf{R}}^{-1} \hat{\underline{\mathbf{B}}}^T \underline{\mathbf{P}} = \underline{\mathbf{0}} \quad (4.27)$$

For the time-invariant system the feedback-matrix only becomes time-invariant by choosing an infinite horizon cost-function. Now (4.26) can be substituted into the control law (4.21), such that

$$\begin{aligned} u(t) &= -\underline{\mathbf{R}}^{-1} \hat{\underline{\mathbf{B}}}^T \underline{\mathbf{P}} \mathbf{x}(t) \\ &\Updownarrow \\ {}^C \tilde{\mathbf{m}} &= -\underline{\mathbf{R}}^{-1} \hat{\underline{\mathbf{B}}}^T \underline{\mathbf{P}} \begin{bmatrix} \tilde{\mathbf{q}}_{1:3} \\ \tilde{\boldsymbol{\omega}} \end{bmatrix} \end{aligned} \quad (4.28)$$

4.2.2 Stability for Periodic Linear System

Though the stationary solution for the Riccati Equation stabilizes the time invariant system, the solution does not necessary stabilize the time variant system. Therefore the stability of the periodic linear system must analyzed. This is addressed in Appendix E in which Floque theory is applied and the monodromy matrix is calculated in order to check for stability of a periodic linear system. When using the Floque theory, it assumed that the system is ideal periodic ($\underline{\mathbf{A}}_{cl}(t) = \underline{\mathbf{A}}_{cl}(t + T)$). Therefor, a periodic input matrix is generated using (4.18) inserted in (3.63). Together with the linearized $\underline{\mathbf{A}}$ from Appendix C and the generated optimal control gain matrix $\underline{\mathbf{L}}$, the monodromy matrix is calculated. By plotting the eigenvalues of the monodromy matrix it is possible to check whether the closed loop system is stable under the assumption that the system is ideal periodic.

Determining Weight Matrixes $\underline{\mathbf{R}}$ and $\underline{\mathbf{Q}}$

The control gain matrix $\underline{\mathbf{L}}$ is, as mentioned, derived using LQR design. In order to obtain a stable system and a reasonable performance that satisfy the requirements, it is necessary to choose the weighting matrixes for LQR with care. There are no given rules for determination of $\underline{\mathbf{R}}$ and $\underline{\mathbf{Q}}$, but a rule of thumb is Bryson's rule that can be used as a starting guess. Bryson's rule suggest that $\underline{\mathbf{R}}$ and $\underline{\mathbf{Q}}$ is diagonal matrixes with

$$\underline{\mathbf{Q}}_{ii} = \frac{1}{x_{i_{max}}^2} \text{ and } \underline{\mathbf{R}}_{jj} = \frac{1}{u_{j_{max}}^2} \quad (4.29)$$

Where $x_{i_{max}}$ and $u_{j_{max}}$ respectively is the maximal allowable values for state and input. Unfortunately, in this application, Brysons rule did not provide a stabilizing results in practice. In [Vedstesen 02] another method for determination of the weight matrixes is used. Here $\underline{\mathbf{R}}$ is defined as the identity matrix, and $\underline{\mathbf{Q}}$ is defined as

$$\underline{\mathbf{Q}} = \begin{bmatrix} qk_1\mathbf{1} & \mathbf{0} \\ \mathbf{0} & qk_2\mathbf{1} \end{bmatrix} \begin{bmatrix} \frac{1}{2}\mathbf{1} & \frac{1}{2}\mathbf{1} \\ \frac{1}{2}\mathbf{1} & \frac{1}{2}\mathbf{1} \end{bmatrix} \begin{bmatrix} qk_1\mathbf{1} & \mathbf{0} \\ \mathbf{0} & qk_2\mathbf{1} \end{bmatrix} \quad (4.30)$$

In which k_1 , k_2 and q are constants. q is used for sweeping, in order to find the most stabilizing solution.

4.2.3 Implementation and Simulation

In order to implement the constant gain controller, the following design procedure has been carried out and is followed for both the inertial and nadir controller:

1. Choose the weight constants $\underline{\mathbf{R}}$ and $\underline{\mathbf{Q}}$.
2. Solve the time invariant Riccati equation using MATLAB to obtain the feedback matrix $\underline{\mathbf{L}}$.
3. Calculate the monodromy matrix and check for stability.
4. Check performance by implementation in the simulation environment, which includes the time variant nonlinear system and environment disturbances.
5. If the current $\underline{\mathbf{L}}$ does not perform satisfactory, go to step 1.

Nadir Controller

By using the method described in Section 4.2.2a choice of the constants $k_1 = 0.001$ and $k_2 = 0.00001$ of the weighting matrices are obtained. The eigenvalues of the monodromy matrix are calculated, in a sweep of the gain constant q between 250 to 37500, which is depicted in Fig. 4.5.

By calculating the maximum length of the eigenvalues for each q , it is possible to determine which q produces the set with the maximum pole closest to origo. This is a method of expressing the stability of the system, in which the set with the maximum pole closest to origo, is considered the most stable solution. The length of the largest eigenvalue is depicted in Fig. 4.7 Also, the summarized eigenvalues sets are depicted in Fig. 4.6.

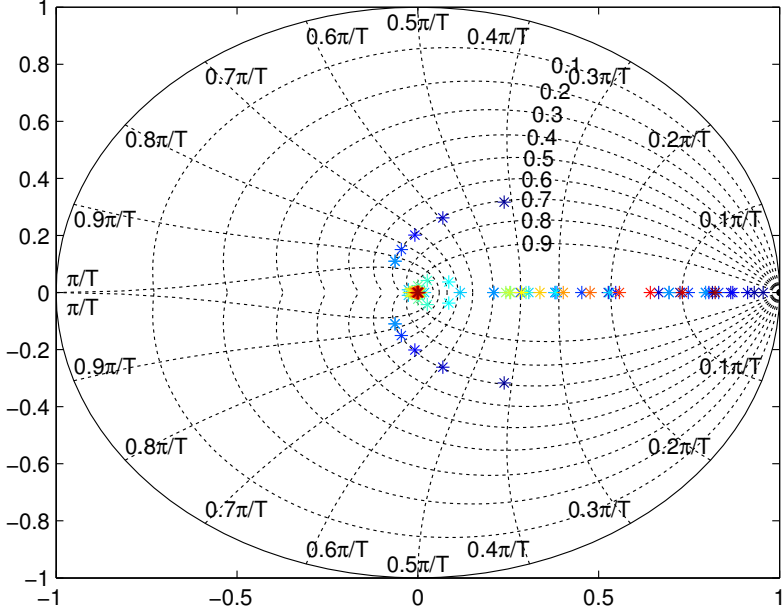


Figure 4.5: Eigenvalues of monodromy matrix. The color scale is used to illustrate the value of q where the lowest values is blue (cold) and goes towards red (warm) as the q increases

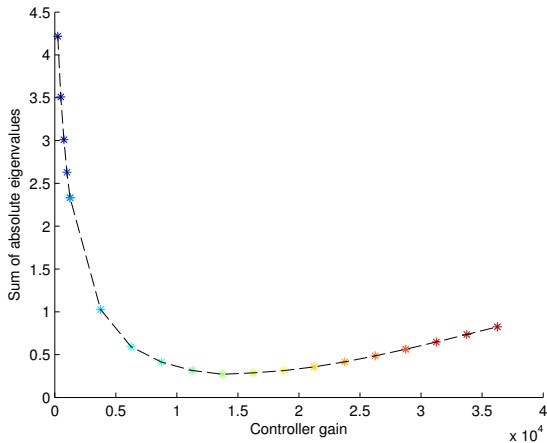


Figure 4.6: The summarized set of eigenvalue for each q . The color scale is used to illustrate the value of q , where the lowest values is blue (cold) and goes towards red (warm) as the q increases

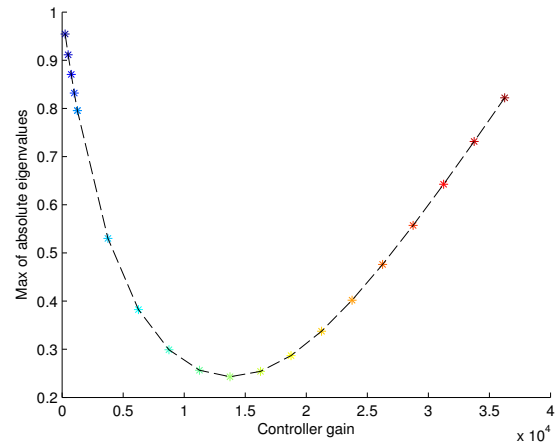


Figure 4.7: The maximum eigenvalue length for each q . The color scale is used to illustrate the value of q , where the lowest values is blue (cold) and goes towards red (warm) as the q increases

From Fig. 4.6 and Fig. 4.7, it is observed that the lowest point is located at a gain between 13000 and 14000. This gain is used as a start guess for the simulation. By empirical analyze, by means of simulation environment shown in Section 3.7, it is verified that the most stabilizing and best performance was obtained at $q = 16000$.

Inertial Controller

By following the same procedure as for the nadir controller, the weighting matrices for the inertial controller are found. Here the weight constants are also found to be $k_1 = 0.001$ and $k_2 = 0.00001$. By sweeping the gain constant q from 250 to 10500, the eigenvalues of the monodromy matrix are calculated, which is depicted in Fig. 4.8.

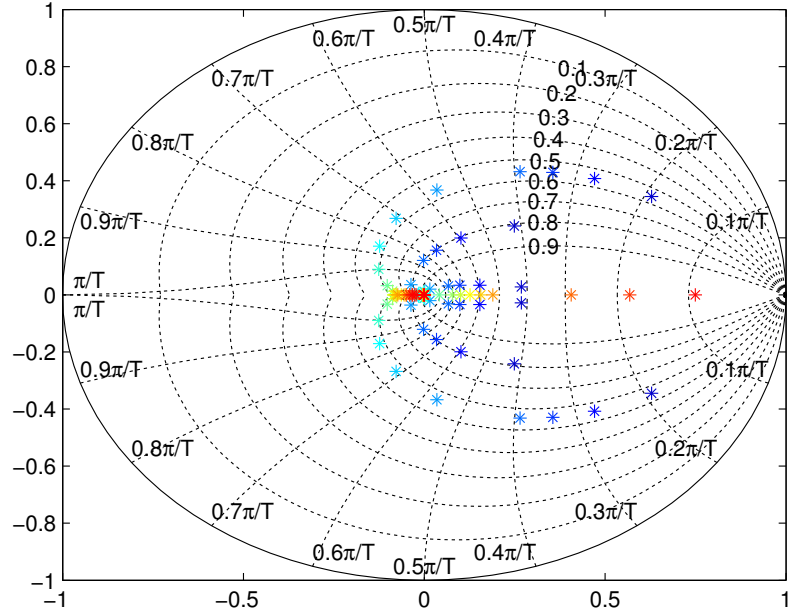


Figure 4.8: Eigenvalues of monodromy matrix. The color scale is used to illustrate the value of q where the lowest values is blue (cold) and goes towards red (warm) as the q increases

The length of the maximum eigenvalue is depicted in Fig. 4.10 to the corresponding controller gain q and likewise the summarized eigenvalues sets are depicted in Fig. 4.9.

From Fig. 4.9 and Fig. 4.10 it is seen that the lowest point is where the gain approximate is between 6000 and 7000. This gain is used as a start guess in the simulation. By empirical analyze, by means of simulation environment, it is verified that the most stabilizing and best performance was obtained at $q = 8000$.

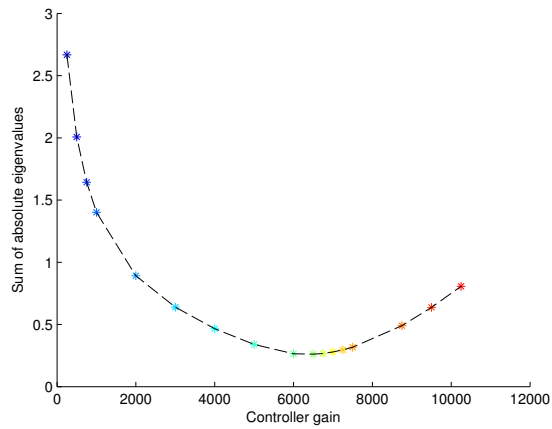


Figure 4.9: The summarized set of eigenvalue for each q . The color scale is used to illustrate the value of q , where the lowest values is blue (cold) and goes towards red (warm) as the q increases

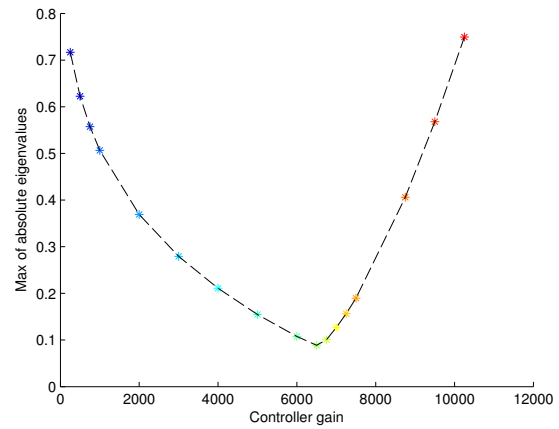


Figure 4.10: The maximum eigenvalue for each q . The color scale is used to illustrate the value of q , where the lowest values is blue (cold) and goes towards red (warm) as the q increases

Chapter 5

Fault Analysis

In this chapter, faults which possibly can occur in the system, is analysis through a Failure Mode and Effects Analysis (FMEA). Then a severity and occurrence (SO) analysis is conducted, which describes how likely a fault is to occur and how severe the effect is estimated to be if it occurs.

The fault analysis is performed for the gyroscopes, the ADS, the magnetorquers and the permanent magnet.

5.1 Failure Mode and Effects Analysis

In this section, an FMEA is conducted on the components used in the ADCS. The purpose of the FMEA is to enlist faults that can happen in each component and what effect these fault will lead to. The result of the FMEA, is a detailed description of the faults and their effect and the FMEA scheme in which it is illustrated how the fault propagate through out the system.

5.1.1 Gyroscopes

As described, the satellite is equipped with two analog gyroscopes; one measuring the x-axis and the y-axis and one measuring the z-axis. The faults are denoted with subscript 1 for x-axis, 2 for y-axis, and 3 for z-axis. The gyroscopes analog output are sampled by an ADC.

Fault Types

($f_{scg_{1-3}}$) **Short circuit to ground on one axis** One of the analog outputs of the gyroscope is short circuited to ground plane.

($f_{scsg_{1-3}}$) **Short circuit to supply on one axis** One of the analog outputs of the gyroscope is short circuited to the supply voltage.

(f_{mis_g}) **Misalignment of the sensor placement** Due to the difficulties of implementation and assembling of the satellite or complications during the launch, the gyroscope is misaligned. It is guesstimated that a misalignment of a gyroscope is considered a fault, if it exceed 5 °.

(f_{bias_g}) **Bias** due to the ambient temperature, the analog output of the gyroscope is biased. It is guesstimated that a bias of a gyroscope is considered a fault, if it exceeds 0.1 °/s.

For later reference, the boolean fault vector of the gyroscope is defined as (5.1):

$$\mathbf{f}_g = \begin{bmatrix} f_{scg_g} \\ f_{scs_g} \\ f_{mis_g} \\ f_{bias_g} \end{bmatrix} \quad (5.1)$$

Effects

The faults in the gyroscope can have the following effects on the measurement of the gyroscope:

(e_{high_g}) **Constant high** The gyroscope is constantly measuring the angular velocity as the highest value of the ADC.

(e_{low_g}) **Constant low** The gyroscope is constantly measuring the angular velocity as zero.

(e_{error_g}) **Error** The gyroscope measures a faulty angular velocity.

For later reference, the boolean effect vector of the gyroscope is defined as (5.2):

$$\mathbf{e}_g = \begin{bmatrix} e_{high_g} \\ e_{low_g} \\ e_{error_g} \end{bmatrix} \quad (5.2)$$

5.1.2 Attitude Determination System

As described in Section 2.2, the ADS system is seen as a gray box. Consequently, the different internal possible faults of ADS is not regarded.

Fault Types

$(f_{error_{ads}})$ **Internal fault** An internal fault has occurred in the ADS.

For later reference, the boolean fault vector of the ADS is defined as (5.3):

$$\mathbf{f}_{ads} = [f_{error_{ads}}] \quad (5.3)$$

Effects

$(e_{inst_{ads}})$ **Instantly faulty attitude estimate** The ADS output instantly starts to faulty estimate the spacecraft attitude. This is an instantly rotation of the real attitude.

$(e_{slow_{ads}})$ **Slowly faulty attitude estimate** The ADS output slowly perform a estimate of the spacecraft attitude which becomes incrementally more faulty. This is a increasing rotation of the real attitude.

For later reference, the boolean effect vector of the ADS is defined as (5.4):

$$\mathbf{e}_{ads} = \begin{bmatrix} e_{inst_{ads}} \\ e_{slow_{ads}} \end{bmatrix} \quad (5.4)$$

5.1.3 Magnetorquers

The different faults, occurring in the magnetorquers are explained here.

Fault Types

($f_{scg_{mt,1-3}}$) **Short circuit to ground** Magnetorquers are short circuited to ground.

($f_{scs_{mt,1-3}}$) **Short circuit to supply** Magnetorquers are short circuited to the supply.

($f_{isom_{mt,1-3}}$) **Isolation break** the isolation between the windings in the magnetorquers are piecewise broken. It is guesstimated that a isolation break is considered a fault, if the ratio on broken windings exceed 10 % of the totalt windings.

($f_{mis_{mt,1-3}}$) **Misalignment** Due to the difficulties of implementation and assembling of the satellite or complications during the launch, the magnetorques are misaligned. It is guesstimated that a misalignment of a magnetorque is considered a fault, if it exceeds a 5° i an arbitrary axis.

($f_{switch_{mt,1-3}}$) **Switched control and ground signals** The magnetorquers has been implemeted with the current running in opposite direction than planned.

($f_{supply_{mt,1-3}}$) **Supply voltage offset** The supply voltage is offset to a different level than the normal supply voltage. It is guesstimated that a supply voltage offset is considered a fault, if it exceeeds 0.5 v.

For later reference, the boolean fault vector of the magnetorquers is defined as (5.5):

$$\mathbf{f}_{mt} = \begin{bmatrix} f_{scg_{mt}} \\ f_{scs_{mt}} \\ f_{isom_{mt}} \\ f_{mis_{mt}} \\ f_{switch_{mt}} \\ f_{supply_{mt}} \end{bmatrix} \quad (5.5)$$

Effects

($e_{low_{mt}}$) **Low actuating** The actuating is lower than expected or no actuating.

($e_{high_{mt}}$) **High actuating** The actuating is higher than expected or constantly actuating with maximum power.

($e_{error_{mt}}$) **Error** The magnetorquers is actuating in a different axis of the SBRF frame than expected.

For later reference, the boolean effect vector of the magnetorquers is defined as (5.6):

$$\mathbf{e}_{mt} = \begin{bmatrix} e_{high_{mt}} \\ e_{low_{mt}} \\ e_{error_{mt}} \end{bmatrix} \quad (5.6)$$

5.1.4 Permanent magnet

The different faults, occurring in the permanent magnet is explained here.

Fault Types

$(f_{mis_{pm,1-3}})$ **Misalignment** Due to the difficulties of implementation and the assembling of the satellite or complications during the launch, the permanent magnet is misplaced. It is guesstimated that a misalignment of the permanent magnet is considered a fault, if it exceed 5 °.

For later reference, the boolean fault vector of the permanent magnet is defined as

$$\mathbf{f}_{pm} = [f_{mis_{pm}}] \quad (5.7)$$

Effects

$(e_{error_{pm}})$ **Error** The permanent magnet is actuating in a different axis of the spacecraft body frame than expected.

For later reference, the boolean effect vector of the magnetorquers is defined as (5.8):

$$\mathbf{e}_{pm} = [e_{error_{pm}}] \quad (5.8)$$

5.1.5 Satellite

No faults, which is not caused by a subsystem, is considered to occur in the satellite, but effects are described for later use.

Effects

$(e_{q_{sc}})$ **Faulty quaternion** The attitude of the satellite is altered or faulty measured.

$(e_{\omega_{sc}})$ **Faulty angular velocity** The angular velocity of the satellite is altered or faulty measured.

For later reference, the boolean effect vector of the spacecraft is defined as (5.9):

$$\mathbf{e}_{sc} = \begin{bmatrix} e_{q_{sat}} \\ e_{\omega_{sat}} \end{bmatrix} \quad (5.9)$$

5.1.6 Fault Propagation

The idea is to investigate the propagation of the faults through the system, and how the different faults affect the end effects. The FMEA scheme is illustrated in Fig. 5.1.

The calculations of the FMEA scheme, is shown in appendix G, in which it is concluded that the association between the faults (\mathbf{f}_{sys}) and spacecraft end effect (\mathbf{e}_{sc}), can be described as:

$$\mathbf{e}_{sc} = \underline{\mathbf{A}}_{f_{sys}} \otimes \mathbf{f}_{sys}^{\text{ }^1} \quad (5.10)$$

¹ \otimes is the inner product disjunction operator, which correspond to regular matrix multiplication, only using boolean values and logic. This can formally be written as $(AB)_{ij} = \sum_{r=1}^n A_{ir} \wedge B_{rj}$, where the summation is logical OR operations.

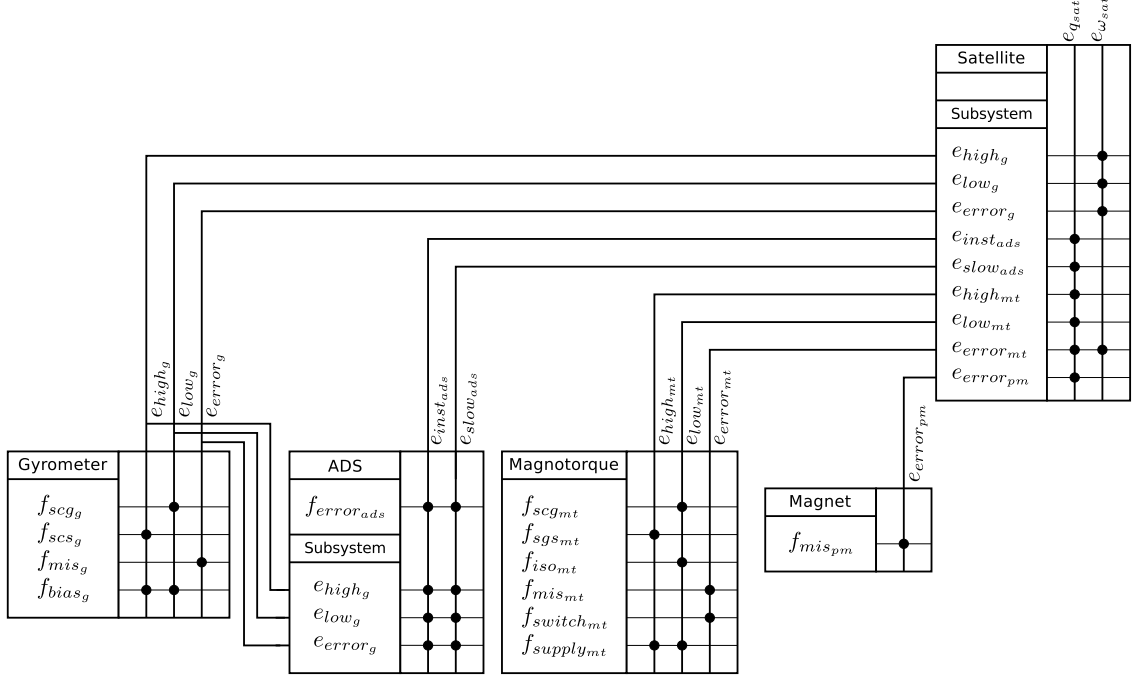


Figure 5.1: The FMEA scheme of the system

With the system fault vector (\mathbf{f}_{sys}) defined as :

$$\mathbf{f}_{sys} = \begin{bmatrix} \mathbf{f}_g \\ \mathbf{f}_{ads} \\ \mathbf{f}_{mt} \\ \mathbf{f}_{pm} \end{bmatrix} \quad (5.11)$$

The association matrix $\underline{\mathbf{A}}_{f_{sys}}$, is calculated in appendix G to be:

$$\underline{\mathbf{A}}_{f_{sys}} = \begin{bmatrix} 1 & 1 & 1 & 1 & 1 & 1 & 1 & 1 & 1 & 1 & 1 & 1 \\ 1 & 1 & 1 & 1 & 0 & 0 & 0 & 0 & 1 & 1 & 0 & 0 \end{bmatrix} \quad (5.12)$$

By observing (5.12), it is seen that all the faults in the system is expected to affect the quaternions, but only some faults directly affects the angular velocity.

5.2 Severity Occurrence Analysis

To identify the most critical faults that the FDI should detect and isolated, a Severity and Occurrence (SO) analysis is conducted on the faults described in the FMEA. This is done by assigning each fault with a severity index and an occurrence index. These two is then multiplied together to yield the SO index. The faults with the highest SO index is regarded the most critical. In the requirement specification in Section 2.4 it is stated that the FDI should be able to detect the five most critical faults, which are found by the SO-analysis.

The SO analysis is shown in Table 5.1. The SO analysis is based on the definition in [Schacht 09].

Gyroscope			
<i>Reference</i>	<i>Severity</i>	<i>Occurrence</i>	<i>SO Index</i>
f_{scg_g}	8	3	24
f_{scs_g}	8	2	12
f_{mis_g}	3	3	9
f_{bias_g}	4	5	20
Attitude Determination System			
<i>Reference</i>	<i>Severity</i>	<i>Occurrence</i>	<i>SO Index</i>
$f_{error_{ads}}$	8	6	48
Magnetorquer			
<i>Reference</i>	<i>Severity</i>	<i>Occurrence</i>	<i>SO Index</i>
$f_{scg_{mt}}$	6	4	24
$f_{scs_{mt}}$	8	3	24
$f_{iso_{mt}}$	3	4	12
$f_{mis_{mt}}$	2	3	6
$f_{switch_{mt}}$	8	2	16
$f_{supply_{mt}}$	2	6	12
Permanent Magnet			
<i>Reference</i>	<i>Severity</i>	<i>Occurrence</i>	<i>SO Index</i>
$f_{mis_{pm}}$	3	3	9

Table 5.1: Severity and Occurrence analysis of the gyroscope, ADS, magnetorquer, and permanent magnet

Fault Detection and Isolation

In this chapter, the design of the Fault Detection and Isolation (FDI) is described. The FDI system consist of two systems; the first one is based on simple methods in which the redundancy in the hardware, knowledge about the signals and general knowledge about the system is used to perform FDI. The other one is a model based FDI, based on Unknown Input Observers (UIO) and the CUSUM algorithm. Both the FDI systems reports to the supervisor, if a fault is detected. The supervisor then decides how to handle the detected fault. An system overview of the FDI systems is shown in Fig. 6.1.

The simple FDI methods, described in Section 6.1, can be used to detect faults in the magnetometers and magnetorquers and simple faults in other sensors. The model based FDI is used for detecting faults in the gyroscope, magnetorquers and the ADS. The general theory of UIOs is described in subsection 6.2. The description of the used UIO and CUSUM setup, is described in Section 6.3. The design of the supervisor is in Section 6.4.

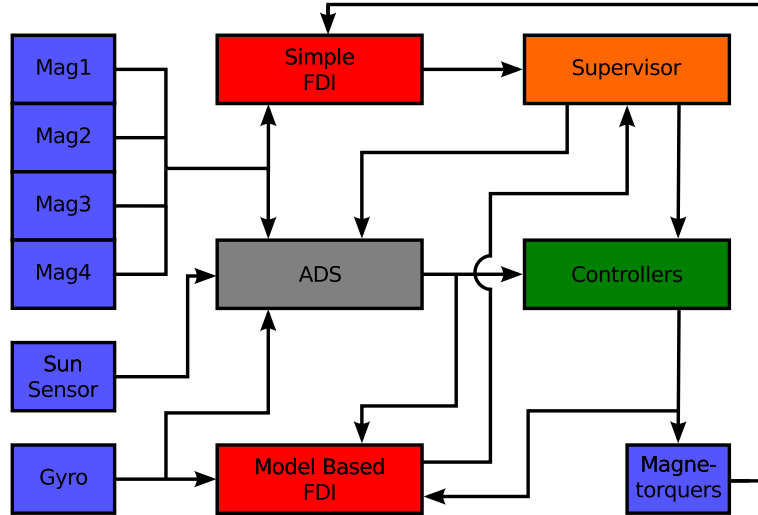


Figure 6.1: Full system overview with Sensors (Blue), FDI (Red), Supervisor (orange), ADS (Gray), and Controllers (Green)

6.1 Simple FDI Methods

The advantage of the simple FDI methods is that the theory and implementation is simple and the data processing requires a minimum of CPU power and thus can reduce the power consumption.

Though, the simple FDI methods possess beneficial properties, the methods are not suited for a project in the 8th semester. Therefore, the simple FDIs methods are only described and have not been implemented or tested.

6.1.1 FDI Based on Hardware Redundancy

If a system has multiple similar sensors measuring the same parameter, it is possible to take advantage of this redundancy for FDI using the voting method. The principle of voting is to have the similar sensors, perform the same measurements and then compare the output of the different sensors. If one of the sensors output differs significantly from the other sensors, a fault is assumed to have occurred in this sensor.

As described in Section 2.1, there is a total of four 3-axis magnetometers; two sets of two (one set connected to each micro controller). Generally, using voting, it is possible to detect and isolate one fault when three of the same sensors are available. Thus it should be possible to detect faults in the magnetometers of the satellite. To detect and isolate faults in the magnetometers, a combination of static and dynamic redundancy is used. The static redundancy is used to detect a fault. If e.g. ADCS1 is the running ADCS-subsystem, it is constantly comparing the measurements from Mag1 and Mag2. If they differs significantly, one of these two magnetometers are assumed to be faulty.

The dynamic redundancy is used to isolate faults, by communicating with ADCS2 and getting measurements from Mag3 and Mag4 to isolate the faults. Since ADCS2 might be turn off when ADCS1 is running, this is dynamic redundancy with cold standby.

Likewise, when ADCS2 is the running ADCS-subsystem, ADCS1 is turned on to isolate a fault.

An diagram of the hardware redundancy setup is shown in Fig. 6.2.

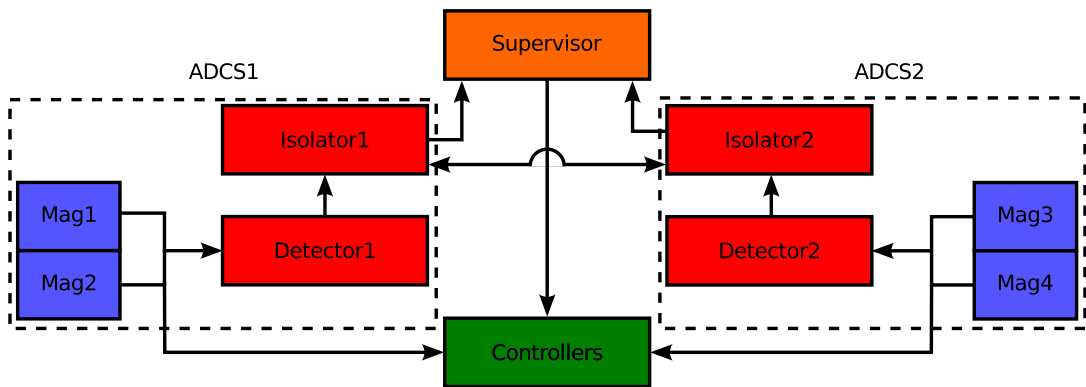


Figure 6.2: The different modules in the hardware redundancy FDI for the magnetometers

The detectors are used for the static redundancy, constantly comparing the two 3-axis magnetometers in ADCS1/ADCS2. If a detector detects a fault, it informs the isolator. The isolator then gets the measurements from the sensors connected to the other detector through the other isolator. When the isolator has all four measurements, it isolates the

fault by, first finding all the differences in the measurements:

$$\begin{aligned} M_{12} &= |M_1 - M_2| & M_{13} &= |M_1 - M_3| \\ M_{14} &= |M_1 - M_4| & M_{23} &= |M_2 - M_3| \\ M_{24} &= |M_2 - M_4| & M_{34} &= |M_3 - M_4| \end{aligned}$$

Where M_1 is the 3-axis measurement from Mag1, M_2 is the measurement from Mag2, etc. Then to isolate the fault, the following failure functions are calculated:

$$\begin{aligned} F_1 &= M_{12} \cdot M_{13} \cdot M_{14} & F_2 &= M_{12} \cdot M_{23} \cdot M_{24} \\ F_3 &= M_{13} \cdot M_{23} \cdot M_{34} & F_4 &= M_{14} \cdot M_{24} \cdot M_{34} \end{aligned}$$

If a fault occurs in Mag1, M_{12} , M_{13} and M_{14} is expected to increase, while the rest would be approximately zero. Consequently, F_1 will increase, because F_1 is the only F , which only consists of M_{12} , M_{13} and M_{14} .

So if F_1 has a significantly larger value than the rest, a fault is assumed in Mag1 and likewise for the others. To decide when a failure function is significantly larger, some test will have to be conducted on the magnetometers to decide a suitable threshold. Test of the magnetometers is out of the scope of this project and therefore not performed.

6.1.2 Signal Based FDI

When using signal based FDI, the signals from the different sensors is evaluated individually. The advantage of signal based FDIs are that they are simple, easy to implement and capable of finding many of the common faults. The signal based FDI on ADCS is conducted on the sensors before they go into the rest of the system.

Dead Signal

Dead signal method can be used to detect if a sensors output does not change, for instance if the output is short circuited to a DC voltage. It is done by differentiating the signal, and if the result is close to zero in some time, it is likely that a fault has occurred in the sensor. The implementation could be:

$$\sum_{k=1}^N |S_k - S_{k-1}| \approx 0 \Rightarrow \text{"dead signal"} \quad (6.1)$$

Range Check

This method simply checks if the sensors output is out of a certain range. The implementation could be as simple as one "if statement" that checks if the signal is higher or lower than predefined realistic boundaries, and then assume that the sensor is faulty.

Slew Rate

The Slew Rate method is used to detect if the signal changes unrealistically fast. The implementation could be:

$$x(k) = \frac{1}{T_d}(y(k) - \hat{y}(k)) \quad (6.2)$$

$$\hat{y}(k+1) = \hat{y}(k) + T_s x(k) \quad (6.3)$$

Where T_d indicates the dynamic of the system, that should be chosen large for slow systems and small for fast systems. T_s is the sample time.

RMS Check

RMS indicates the amount of the energy in the signal. A high RMS could indicate that the signal changes with a high amplitude, which could be the case for a badly/loose connected sensor which could be very noisy.

6.1.3 Simple FDI of the Magnetorques

In the satellite, it may be possible to detect and isolate faults in the actuators, since the output of the actuators can be measured by the magnetometers.

As described in Section 2.1, the magnetometers can not measure the magnetic field while the magnetorques are actuating, why the magnetorques only actuate 88% of the time with a period of 100 ms. This enable the possibility to use the magnetometer to check if the magnetorques are faulty, by measuring the combined magnetic field of the earth and the magnetorques while the magnetorques are actuating. By assuming that the magnetic field of the earth is equal to the last measurement of the magnetic field, the magnetic field of the magnetorques can be calculated. An expected output can be generated by use of the actuator input applied to the model of the magnetorquer. If the measured output, compared to the expected output differs significantly, a fault in the actuators are assumed.

If a fault in the actuators is detected, a procedure to isolate the fault could be initiated. This isolation is performed by applying a test input to each separate magnetorquer sequentially, while measuring the output.

In addition, a startup procedure could be the two micro-controllers checking each others PWM channels are working as expected. This is possible since the ARM7 and the AVR8 share the same actuators and have mutually PWM pins connecting them. The PWM-pins can be configured to either function as a PWM-pin or an input pin. The PWM-pin could be changed to input pins on one micro-controller and then check whether the other micro-controllers PWM-pins works and visa versa.

6.2 Unknown Input Observer

The research of UIOs started as early as 1975 and has been a study for many years to follow [Chen 99, 66].

The definition of a UIO is given as [Chen 99, 69]: *An observer is defined as an unknown input observer for the system described by (6.4) and (6.5), if its state estimation error vector e approaches zero asymptotically, regardless of the presence of the unknown input (disturbance) in the system.*

The system is described by the linear model:

$$\dot{\mathbf{x}} = \underline{\mathbf{A}}\mathbf{x} + \underline{\mathbf{B}}\mathbf{u} + \underline{\mathbf{E}}\mathbf{d} \quad (6.4)$$

$$\mathbf{y} = \underline{\mathbf{C}}\mathbf{x} \quad (6.5)$$

$\mathbf{x} \in \mathbb{R}^{n \times 1}$: The states of the system

$\mathbf{y} \in \mathbb{R}^{m \times 1}$: The measured outputs of the system

$\mathbf{u} \in \mathbb{R}^{r \times 1}$: The known inputs of the system

$\mathbf{d} \in \mathbb{R}^{q \times 1}$: The unknown disturbance input

$\underline{E} \in \mathbb{R}^{n \times q}$: The disturbance distribution matrix, which defines the subspace in which the unknown disturbance input enters the system.

The general idea of the UIO, is to use the information about in which subspace of the system, the disturbances is entering to construct an observer, which is geometrically decoupled from these disturbances. The approach is to consider a new state z , of the UIO. The state z should be a transform so the subspace, which is affected by the disturbances, is geometrically decoupled. From this, an disturbance free estimate of the system output (\hat{y}) can be derived, and residuals (r) can be derived as $r = y - \hat{y}$.

The diagram of the UIO states is shown in Fig. 6.3.

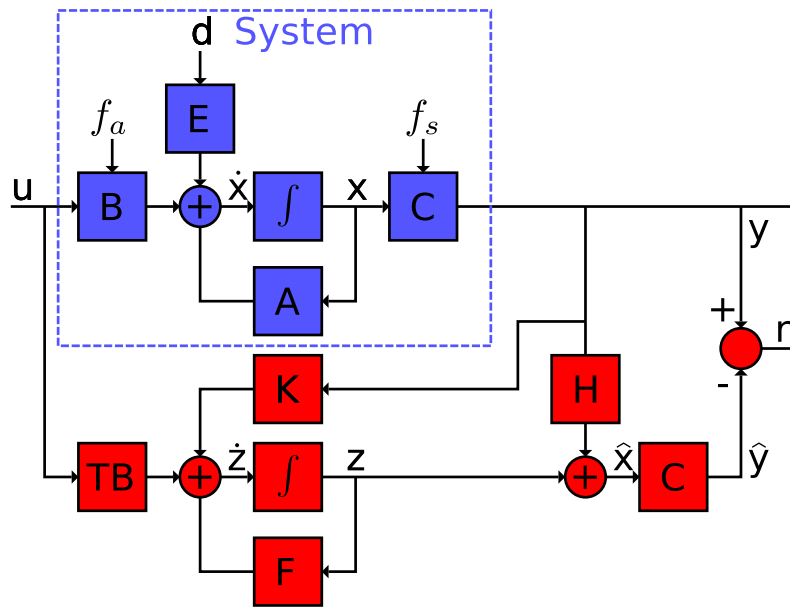


Figure 6.3: The general unknown input observer

The unknown input observer is described as:

$$\dot{z} = \underline{F}z + \underline{T}Bu + \underline{K}y \quad (6.6)$$

$$\hat{x} = z + \underline{H}y \quad (6.7)$$

\Downarrow

$$\dot{z} = \underline{F}(\hat{x} - \underline{H}y) + \underline{T}Bu + \underline{K}y \quad (6.8)$$

6.2.1 General UIO theory

The state error e is then described as:

$$\begin{aligned} e &= x - \hat{x} \\ &\Updownarrow \\ x &= e + \hat{x} \\ &= e + z + \underline{H}y \end{aligned} \quad (6.9)$$

By differentiating, the change in error is described as:

$$\begin{aligned}
 \dot{\epsilon} &= \dot{x} - \dot{\hat{x}} \\
 &= \dot{x} - (\dot{z} + \underline{H}\dot{y}) && \text{(differentiated (6.7) inserted)} \\
 &= \dot{x} - \dot{z} - \underline{H}(\underline{C}\dot{x}) && \text{(differentiated (6.5) inserted)} \\
 &= \dot{x} - (\underline{F}z + \underline{T}\underline{B}u + \underline{K}y) - \underline{H}(\underline{C}\dot{x}) && \text{((6.6) inserted)} \quad (6.10)
 \end{aligned}$$

For later convenience, \underline{K} from (6.10) is split into \underline{K}_1 and \underline{K}_2 , with $\underline{K} = \underline{K}_1 + \underline{K}_2$.

$$\begin{aligned}
 \dot{\epsilon} &= (\underline{1} - \underline{H}\underline{C})\dot{x} - \underline{F}z - \underline{T}\underline{B}u - \underline{K}_1y - \underline{K}_2y \\
 &= (\underline{1} - \underline{H}\underline{C})(\underline{A}x + \underline{B}u + \underline{E}d) - \underline{F}z - \underline{T}\underline{B}u - \underline{K}_1\underline{C}x - \underline{K}_2y \quad ((6.4) \text{ inserted}) \\
 &= (\underline{1} - \underline{H}\underline{C})\underline{A}x + (\underline{1} - \underline{H}\underline{C})\underline{B}u + (\underline{1} - \underline{H}\underline{C})\underline{E}d - \underline{F}z - \underline{T}\underline{B}u - \underline{K}_1\underline{C}x - \underline{K}_2y \\
 &= (\underline{A} - \underline{H}\underline{C}\underline{A} - \underline{K}_1\underline{C})x - \underline{F}z - \underline{K}_2y - [\underline{T} - (\underline{1} - \underline{H}\underline{C})]\underline{B}u + (\underline{1} - \underline{H}\underline{C})\underline{E}d \quad (6.11)
 \end{aligned}$$

The idea is to make $\dot{\epsilon}$ a stable state, and make it independent of the value of x , z , y , u , and d .

System state independence:

First, to eliminate the value of the system state x in the expression of $\dot{\epsilon}$, (6.9) is inserted which yield the rewritten expression as:

$$\begin{aligned}
 \dot{\epsilon} &= (\underline{A} - \underline{H}\underline{C}\underline{A} - \underline{K}_1\underline{C})e - \underbrace{[\underline{F} - (\underline{A} - \underline{H}\underline{C}\underline{A} - \underline{K}_1\underline{C})]z}_{(3)} \\
 &\quad - \underbrace{[\underline{K}_2 - (\underline{A} - \underline{H}\underline{C}\underline{A} - \underline{K}_1\underline{C})\underline{H}]y}_{(4)} - \underbrace{[\underline{T} - (\underline{1} - \underline{H}\underline{C})]\underline{B}u}_{(2)} - \underbrace{(\underline{1} - \underline{H}\underline{C})\underline{E}d}_{(1)} \quad (6.12)
 \end{aligned}$$

(1) Disturbance independence:

The second step is to design \underline{H} to make $\dot{\epsilon}$ independent of the disturbance d . \underline{H} must satisfy the following:

$$\begin{aligned}
 (\underline{H}\underline{C} - \underline{1})\underline{E} &= 0 \\
 \Updownarrow \\
 \underline{H}\underline{C}\underline{E} - \underline{E} &= 0 \\
 \Updownarrow \\
 (\underline{C}\underline{E})^T \underline{H}^T &= \underline{E}^T \\
 \Updownarrow \\
 \underline{H} &= \underline{E}(\underline{C}\underline{E})^{-1} \quad (6.13)
 \end{aligned}$$

Assuming \underline{E} has full column rank, (6.13) has a solution if and only if the following is satisfied [Chen 99, p. 72]:

$$\text{rank}(\underline{C}\underline{E}) = \text{rank}(\underline{E}) \quad (6.14)$$

This can be interpreted as the disturbances \underline{E} should be observable through \underline{C} or the disturbances should spanned in the subspace which is visible through C .

If $\underline{C}\underline{E}$ does not have full rank, the pseudoinverse can be used to find a special solution.

$$\underline{H} = \underline{E} \left(\left[(\underline{C}\underline{E})^T \underline{C}\underline{E} \right]^{-1} (\underline{C}\underline{E})^T \right) = \underline{E}\underline{C}\underline{E}^\dagger \quad (6.15)$$

(2) Input independence:

To remove the influence of the input \mathbf{u} from $\dot{\mathbf{e}}$, $\underline{\mathbf{T}}$ can be chosen as:

$$\begin{aligned} \underline{\mathbf{T}} - (\underline{\mathbf{1}} - \underline{\mathbf{H}}\underline{\mathbf{C}}) &= 0 \\ \Updownarrow \\ \underline{\mathbf{T}} &= \underline{\mathbf{1}} - \underline{\mathbf{H}}\underline{\mathbf{C}} \end{aligned} \quad (6.16)$$

(3) Observer state independence:

To remove the state of the observer \mathbf{z} from $\dot{\mathbf{e}}$, $\underline{\mathbf{F}}$ can be chosen to satisfy:

$$\begin{aligned} \underline{\mathbf{F}} - (\underline{\mathbf{A}} - \underline{\mathbf{H}}\underline{\mathbf{C}}\underline{\mathbf{A}} - \underline{\mathbf{K}}_1\underline{\mathbf{C}}) &= 0 \\ \Updownarrow \\ \underline{\mathbf{F}} &= \underline{\mathbf{A}} - \underline{\mathbf{H}}\underline{\mathbf{C}}\underline{\mathbf{A}} - \underline{\mathbf{K}}_1\underline{\mathbf{C}} \end{aligned} \quad (6.17)$$

In which $\underline{\mathbf{K}}_1$ can be chosen freely.

For later simplicity, it is convenient to introduce $\underline{\mathbf{A}}_1$ defined as:

$$\underline{\mathbf{A}}_1 = \underline{\mathbf{A}} - \underline{\mathbf{H}}\underline{\mathbf{C}}\underline{\mathbf{A}} \quad (6.18)$$

Yielding the rewriting of (6.17):

$$\underline{\mathbf{F}} = \underline{\mathbf{A}}_1 - \underline{\mathbf{K}}_1\underline{\mathbf{C}} \quad (6.19)$$

(4) Output independence:

Lastly, the following should be satisfied to remove the system output \mathbf{y} from $\dot{\mathbf{e}}$:

$$\begin{aligned} \underline{\mathbf{K}}_2 - (\underline{\mathbf{A}} - \underline{\mathbf{H}}\underline{\mathbf{C}}\underline{\mathbf{A}} - \underline{\mathbf{K}}_1\underline{\mathbf{C}})\underline{\mathbf{H}} &= 0 \\ \Updownarrow \\ \underline{\mathbf{K}}_2 - \underline{\mathbf{F}}\underline{\mathbf{H}} &= 0 \\ \Updownarrow \\ \underline{\mathbf{K}}_2 &= \underline{\mathbf{F}}\underline{\mathbf{H}} \end{aligned} \quad (6.20)$$

If the above independence criterias (1-4), is satisfied, the estimation error will be:

$$\dot{\mathbf{e}} = \underline{\mathbf{F}}\mathbf{e} \quad (6.21)$$

It is noted that (6.21) describes the dynamics of the error and that if $\underline{\mathbf{F}}$ only has negative eigenvalues, \mathbf{e} will converge asymptotically towards zero. Remembering that the design of $\underline{\mathbf{F}}$ included the freely chosen $\underline{\mathbf{K}}_1$, thus $\underline{\mathbf{K}}_1$ should be chosen so it stabilizes $\underline{\mathbf{F}}$ and provides satisfying dynamics.

6.2.2 Design Procedure of a UIO

This subsection is based on [Chen 99, 77], describing the design procedure of a UIO. When designing a UIO, the first thing to check whether (6.13) has a solution, by checking if (6.14) is satisfied. If this is not satisfied, a UIO does not exist.

Afterwards, $\underline{\mathbf{H}}$, $\underline{\mathbf{T}}$ and $\underline{\mathbf{A}}_1$ are calculated using respectively (6.13), (6.16) and (6.18).

To archive a desirable dynamic of the error, $\underline{\mathbf{K}}_1$ should be designed to place the poles of $\underline{\mathbf{F}}$ at desired locations. To be able to directly choose a satisfying $\underline{\mathbf{K}}_1$, $(\underline{\mathbf{A}}_1, \underline{\mathbf{C}})$ must be observable. If this holds, $\underline{\mathbf{K}}_1$ can be calculated to archive arbitrary pole placements of $\underline{\mathbf{F}}$, using a pole placement technique.

If $\underline{\mathbf{A}}_1$ is not observable through $\underline{\mathbf{C}}$, $\underline{\mathbf{K}}_1$ can not be calculated directly using pole placement. That $(\underline{\mathbf{A}}_1, \underline{\mathbf{C}})$ is not observable means that is not possible to observe all the states of \mathbf{e} through $\underline{\mathbf{C}}$.

The observable canonical decomposition can be used to archive a nonsingular transformation matrix $\underline{\mathbf{P}}$ which can be used for the similarity transformation:

$$\underline{\mathbf{P}} \underline{\mathbf{A}}_1 \underline{\mathbf{P}}^{-1} = \begin{bmatrix} \bar{\underline{\mathbf{A}}}_{1_{no}} & \bar{\underline{\mathbf{A}}}_{1_{12}} \\ \underline{\mathbf{0}} & \bar{\underline{\mathbf{A}}}_{1_o} \end{bmatrix} = \bar{\underline{\mathbf{A}}}_1 \quad (6.22)$$

$$\underline{\mathbf{C}} \underline{\mathbf{P}}^{-1} = \begin{bmatrix} \underline{\mathbf{0}} & \bar{\underline{\mathbf{C}}}_o \end{bmatrix} = \bar{\underline{\mathbf{C}}} \quad (6.23)$$

And introducing:

$$\begin{aligned} \bar{\mathbf{e}} &= \underline{\mathbf{P}} \mathbf{e} \\ &\Downarrow \\ \mathbf{e} &= \underline{\mathbf{P}}^{-1} \bar{\mathbf{e}} \end{aligned} \quad (6.24)$$

$\underline{\mathbf{A}}_{1_o} \in \mathbb{R}^{n_o \times n_o}$: The part of $\bar{\underline{\mathbf{A}}}_1$ which is observable through $\bar{\underline{\mathbf{C}}}$

$\underline{\mathbf{A}}_{1_{no}} \in \mathbb{R}^{n_{no} \times n_{no}}$ The part of $\bar{\underline{\mathbf{A}}}_1$ which is unobservable through $\bar{\underline{\mathbf{C}}}$.

It is possible to determine if the unobservable part of $\bar{\underline{\mathbf{A}}}_1$ is stable, by calculating the eigenvalues of $\bar{\underline{\mathbf{A}}}_{1_{no}}$. If these eigenvalues are positive it means that the unobservable states of $\bar{\mathbf{e}}$ will diverge and a UIO for the system does not exist. If the eigenvalues are negative, the unobservable states will converge towards zero. This states that $(\underline{\mathbf{A}}_1, \underline{\mathbf{C}})$ is detectable.

By applying (6.24), (6.21) can be rewritten as:

$$\begin{aligned} \dot{\mathbf{e}} &= \underline{\mathbf{F}} \mathbf{e} \\ &\Downarrow \\ \dot{\mathbf{e}} &= (\underline{\mathbf{A}}_1 - \underline{\mathbf{K}}_1 \underline{\mathbf{C}}) \mathbf{e} \\ &\Downarrow \\ \underline{\mathbf{P}}^{-1} \dot{\mathbf{e}} &= (\underline{\mathbf{A}}_1 - \underline{\mathbf{K}}_1 \underline{\mathbf{C}}) \underline{\mathbf{P}}^{-1} \bar{\mathbf{e}} \\ &\Downarrow \\ \dot{\mathbf{e}} &= (\underline{\mathbf{P}} \underline{\mathbf{A}}_1 \underline{\mathbf{P}}^{-1} - \underline{\mathbf{P}} \underline{\mathbf{K}}_1 \underline{\mathbf{C}} \underline{\mathbf{P}}^{-1}) \bar{\mathbf{e}} \\ &\Downarrow \\ \dot{\mathbf{e}} &= (\bar{\underline{\mathbf{A}}}_1 - \underline{\mathbf{P}} \underline{\mathbf{K}}_1 \bar{\underline{\mathbf{C}}}) \bar{\mathbf{e}} \end{aligned} \quad (6.25)$$

The behavior of this system is equal to the system:

$$\dot{\mathbf{e}} = (\bar{\underline{\mathbf{A}}}_{1_o} - \underline{\mathbf{K}}^* \bar{\underline{\mathbf{C}}}_o) \bar{\mathbf{e}} \quad (6.26)$$

It is then possible to assign n_o poles to the closed loop $\underline{\mathbf{A}}_{1_o} - \underline{\mathbf{K}}^* \bar{\underline{\mathbf{C}}}_o$, using pole placement.

The corresponding $\underline{\mathbf{K}}_1$ can then be found using

In which:

$$\underline{\mathbf{K}}_1 = \underline{\mathbf{P}}^{-1} \begin{bmatrix} \underline{\mathbf{K}}_*^T & \underline{\mathbf{K}}^{*T} \end{bmatrix}^T \quad (6.27)$$

In which $\underline{\mathbf{K}}_*$ can be chosen arbitrary, because the states affected by $\underline{\mathbf{K}}_*$ can not be observed through $\underline{\mathbf{C}}$. A good choose for $\underline{\mathbf{K}}_*$ could be zeros.

Now $\underline{\mathbf{F}}$ and $\underline{\mathbf{K}}_2$ can be calculated using (6.19) and (6.20). Lastly, $\underline{\mathbf{K}}$ is calculated as $\underline{\mathbf{K}} = \underline{\mathbf{K}}_1 + \underline{\mathbf{K}}_2$.

6.2.3 Disturbance Distribution Matrix

In the design of the UIO, $\underline{\mathbf{E}}$ is an important parameter. As mentioned, $\underline{\mathbf{E}}$ describes the subspace in which the unknown disturbances are entering the system.

In the linearized system equation (D.23), page 106, the disturbances are described as

$$\underline{\mathbf{E}}\underline{\mathbf{d}} = \begin{bmatrix} \mathbf{0}_{3 \times 3} \\ \underline{\mathbf{I}}^{-1} \end{bmatrix} \tilde{\mathbf{N}}_{dist} \quad (6.28)$$

(6.28) indicates that the disturbances is entering the same three dimensional state subspace, as the angular velocity (ω) states, which is also the same subspace as the actuators is entering.

This method of determining $\underline{\mathbf{E}}$ directly from the derived model is called the direct inspection method [Chen 99, 140].

6.3 Model Based FDI Overview

The general concept of the model based FDI, is to generate enough residuals to be able to determine if a fault has occurred and in which transducer. The most evident method would be to generate a residual which is sensitive to faults in one specific transducer and insensitive to other faults. This is however often difficult to archive and has others inconveniences [Chen 99, 79]. An used approach is instead to generate residuals which is sensitive to faults in all transducers except one.

An overview of the model based part of the FDI, is shown in Fig. 6.4. It consists of the

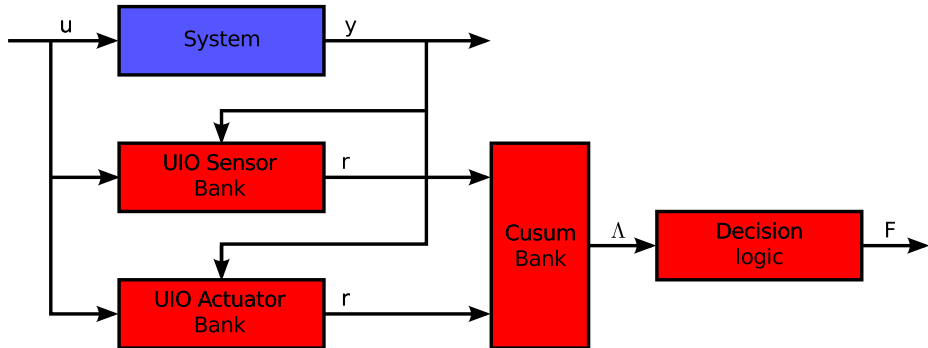


Figure 6.4: Overview of the model based FDI

four part: an UIO bank for sensor faults, an UIO bank for actuator faults, a CUSUM bank and decision logic.

The UIO bank for sensor faults consists of six UIOs, which are designed to generate residuals which are sensitive to all except one sensor fault.

The UIO bank for actuator faults consists of three UIOs, which are designed to generate residuals which are sensitive to all except one actuator fault.

The CUSUM bank is used to indicated whether the generated, individual residuals could indicate a fault in the system.

The decision logic determines if the combined fault indications of the CUSUM bank indicates a fault has occurred and in which sensor/actuator.

6.3.1 UIO Bank for Sensor Faults

The idea of the UIO bank for sensor fault, is to generate UIOs which would not be sensitive to one particular sensor fault.

Sensor faults can be modeled as a fault vector \mathbf{f}_s , in which an entry in the j^{th} component of \mathbf{f}_s indicates a fault in the j^{th} sensor.

This is inserted in the state space equation as:

$$\dot{\mathbf{x}} = \underline{\mathbf{A}}\mathbf{x} + \underline{\mathbf{B}}\mathbf{u} + \underline{\mathbf{E}}\mathbf{d} \quad (6.29)$$

$$\mathbf{y} = \underline{\mathbf{C}}\mathbf{x} + \mathbf{f}_s \quad (6.30)$$

To be able to create residuals, which are sensitive to all faults except one, a scheme is performed, which (6.30) is divided into:

$$\mathbf{y}^j = \underline{\mathbf{C}}^j \mathbf{x}^j + \mathbf{f}_s^j \quad (6.31)$$

$$\mathbf{y}_j = \underline{\mathbf{c}}_j \mathbf{x}_j + \mathbf{f}_{s_j} \quad (6.32)$$

$\mathbf{c}_j \in \mathbb{R}^{1 \times n}$: The j^{th} row of $\underline{\mathbf{C}}$

$\underline{\mathbf{C}}^j \in \mathbb{R}^{m-1 \times n}$: The remaining part of $\underline{\mathbf{C}}$ when \mathbf{c}_j has been removed.

$\mathbf{y}_j \in \mathbb{R}^{1 \times 1}$: The j^{th} component of \mathbf{y}

$\mathbf{y}^j \in \mathbb{R}^{(m-1) \times 1}$: The remaining part of \mathbf{y} , when y_j has been removed.

$f_{s_j} \in \mathbb{R}^{1 \times 1}$: The j^{th} component of \mathbf{f}_s

$\mathbf{f}_s^j \in \mathbb{R}^{(m-1) \times 1}$: The remaining part of \mathbf{f}_s , when f_{s_j} has been removed.

By constructing the UIO, using (6.31) in the design procedure, residuals which is insensitive to faults in f_{s_j} , but sensitive to all other sensor faults, can be generated.

In the implementation, only y^j instead of y should be inputted into the UIO. An illustration of the setup of the UIO bank for sensor faults is shown in Fig. 6.5

It is noted, that when designing UIO for sensor faults in the gyroscopes using the $\underline{\mathbf{E}}$, described in (6.28) on page 66, the requirement (6.14) in page 63 can not be satisfied. This is because, according to (6.28), the disturbances is entering the same state subspace as the angular velocity (ω) states.

For example:

For an UIO to be able to decouple the disturbances entering in the ω_1 subspace, it has to observe this subspace through $\underline{\mathbf{C}}$. But when designing an UIO to be insensitive for f_{s_4}

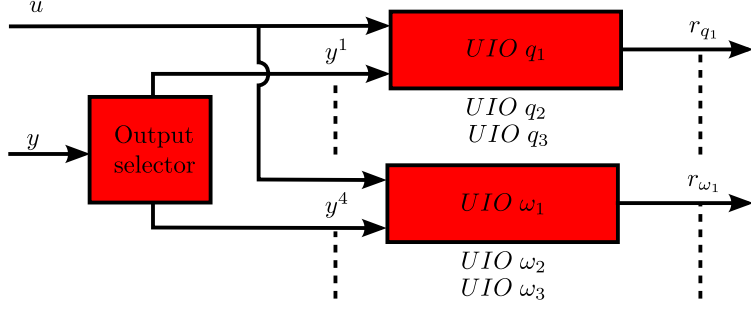


Figure 6.5: The UIO bank for sensor faults

(faults in gyroscope in 1st axis), this row of \underline{C} is removed, thus making it impossible to decouple the disturbances in this subspace.

To be able to design UIOs insensitive to the gyroscope faults, an reduction of robustness has to be made. This is that the j^{th} row of \underline{E} is neglected when designing these UIOs, thus not decoupling the disturbances in this subspace.

6.3.2 Actuator Fault Isolation

The idea of the UIO bank for actuator fault, is to generate UIOs which would not be sensitive to one particular actuator fault. Actuator faults can be modeled as a fault vector \mathbf{f}_a in which an entry in the j^{th} component of \mathbf{f}_a indicates a fault in the j^{th} actuator. This is inserted in the state space equation as:

$$\dot{x} = \underline{A}x + \underline{B}u + \underline{E}d + \underline{B}\mathbf{f}_a \quad (6.33)$$

$$y = \underline{C}x \quad (6.34)$$

Likewise, the design of the UIOs for sensor fault in Section 6.3.1, the objective is to make the UIOs sensitive to all faults except one specific fault in \mathbf{f}_a . To be able to create residuals, which are sensitive to all faults except one, a scheme is performed in which (6.33) is divided into:

$$\begin{aligned} \dot{x} &= \underline{A}x + \underline{B}^i u^i + \underline{B}^i \mathbf{f}_a^i + \mathbf{b}_i(u_i + f_{a_i}) + \underline{E}d \\ &= \underline{A}x + \underline{B}^i u^i + \underline{B}^i \mathbf{f}_a^i + \underline{E}^i d^i \end{aligned} \quad (6.35)$$

$$\text{in which } \underline{E}^i = \begin{bmatrix} \underline{E} & \mathbf{b}^i \end{bmatrix}$$

$$\mathbf{d}^i = \begin{bmatrix} \mathbf{d} \\ u_i + f_{a_i} \end{bmatrix}$$

$\mathbf{b}_i \in \mathbb{R}^{n \times 1}$: The i^{th} column of B

$\underline{B}^i \in \mathbb{R}^{n \times r-1}$: The remaining part of B , when \mathbf{b}_i has been removed.

$u_i \in \mathbb{R}^{1 \times 1}$: The i^{th} component of \mathbf{u}

$\mathbf{u}^i \in \mathbb{R}^{(r-1) \times 1}$: The remaining part of \mathbf{u} , when u_i has been removed.

$f_{a_i} \in \mathbb{R}^{1 \times 1}$: The i^{th} component of \mathbf{f}_a

$\mathbf{f}_a^i \in \mathbb{R}^{(n-1) \times 1}$: The remaining part of \mathbf{f}_a , when f_{a_i} has been removed.

By constructing the UIO, using (6.35) in the design procedure, residuals which is insensitive to faults in f_{ai} , but sensitive to all other actuator faults, can be generated. In the implementation, only u^i instead of u should be inputted into the UIO. An illustration of the setup of the UIO bank for actuator faults is shown in Fig. 6.6. It is noted that when

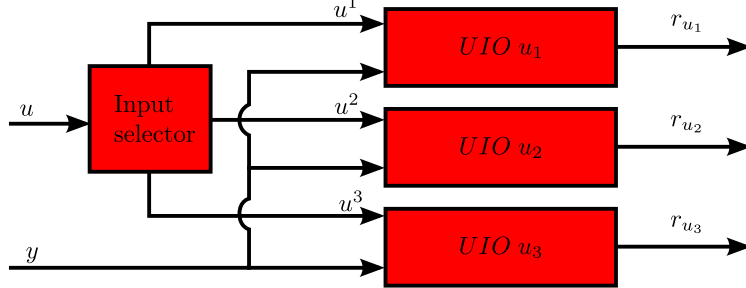


Figure 6.6: The unknown input observer setup for actuator faults

designing UIO for actuator faults, using the \underline{E} , described in (6.28), 66, the disturbances enters the same subspace as the actuators. To be able to detect faults in the actuators, an reduction of robustness been made, which is to neglect the entries in \underline{E} , not decoupling any disturbances except the column vector \mathbf{b}_i .

Selection of used \underline{B}

The satellite is considered a linear time varying system, with a $\underline{B}(t)$ as the time varying parameter. For the actuator fault UIOs, two different approaches of determine an appropriate \underline{B} has been considered.

The first approach is to use the approximated constant \underline{B}_C found in (4.25) in page 47 and design one UIO for each actuator.

The second approach is to use the approximated periodic $\underline{B}_p(t)$, found in (4.18) in page 45. As $\underline{B}_p(t)$ also is time varying, it could be divided into several constants \underline{B}_k for $k = 1..N$, approximating $\underline{B}(t)$ at different positions in the orbit. As the position of the satellite is known through the SPG4, a suitable \underline{B}_k , could be chosen to yield a better approximation of $\underline{B}(t)$, then when using \underline{B}_C and thus achieving better fault detection.

It has been chosen the latter choose, thus using \underline{B}_k in the design of the UIOs.

6.3.3 CUSUM

This section is based on [Blanke 06].

As the residuals has been generated by the UIO bank, it is necessary to evaluate whether a fault has occurred. For this purpose some kind of decision rule need to be applied. This could be done by comparing the residual with a fixed threshold and state that a fault has occurred if a given threshold is exceeded. As the residual signal is contaminated with noise, it is preferred to use a stochastic method to determine whether the residual is faulty.

It is chosen to use the CUSUM algorithm, which stands for CUMulative SUM. The CUSUM algorithm is based on hypothesis testing, testing the hypotheses:

\mathcal{H}_0 : The process is a normal operation (non faulty)

\mathcal{H}_1 : The process is a faulty operation

It is assumed that the signal $z(i)$ is a stochastic independent sequence with a Gaussian distribution, with mean μ and variance σ^2 ($\mathcal{N}(\mu, \sigma)$). The idea is to detect if the mean value of $z(i)$ has changed from the mean value of the normal process (μ_0), to a mean value of a faulty process (μ_1), while assuming that the variance (σ^2) is unchanged. The CUSUM algorithm uses a decision function $g(k)$ and a threshold h to decide which hypothesis to accept. The decision rule $g(k)$ is stated as

$$\begin{aligned} \text{if } g(k) \leq h & \text{ accept } \mathcal{H}_0 \\ \text{if } g(k) > h & \text{ accept } \mathcal{H}_1 \end{aligned} \quad (6.36)$$

The decision function $g(k)$ is based on the cumulative sum of the log-likelihood-ratio of the probability density functions for μ_0 and μ_1 . Furthermore $g(k)$ is biased in order to obtain a constant positive threshold (see (H.4) and (H.5)).

The CUSUM Algorithm in Recursive Form

For the implementation of the decision function it is advantageous to include the decision function in recursive form. As the minimum value for $g(k)$ is zero (see (H.5) and (H.6)), the recursive form becomes:

$$g(k) = \max(0, g(k-1) + s(z(k))) \quad (6.37)$$

substituting (6.37) by (H.3) yields

$$g(k) = \max \left(0, g(k-1) + \frac{\mu_1 - \mu_0}{2} \left(z(k) - \frac{\mu_0 + \mu_1}{2} \right) \right) \quad (6.38)$$

To be able to detect a change in the mean-value both above and below the mean of the normal process, a two sided CUSUM algorithm is applied and is given by

$$\begin{aligned} g^+(k) &= \max \left(0, g^+(k-1) + \underbrace{\frac{\mu_1 - \mu_0}{2} \left(z(k) - \mu_0 - \frac{\beta}{2} \right)}_{s^+(k)} \right) \\ g^-(k) &= \max \left(0, g^-(k-1) - \underbrace{\frac{\mu_1 - \mu_0}{2} \left(z(k) - \mu_0 - \frac{\beta}{2} \right)}_{s^-(k)} \right) \end{aligned} \quad (6.39)$$

β : The magnitude of the change of mean, i.e. $\beta = |\mu_1 - \mu_0|$

The implementation of the two-sided CUSUM-algorithm is seen in Fig. 6.7. And contains beside the decision functions, a function selector (a maximum box) and a threshold logic box.

Determining Stochastic Parameters and Threshold

The estimated mean of the normal process ($\hat{\mu}_0$) and the estimated process variance ($\hat{\sigma}^2$) are found by running a fault free simulation and afterwards numerically calculating the

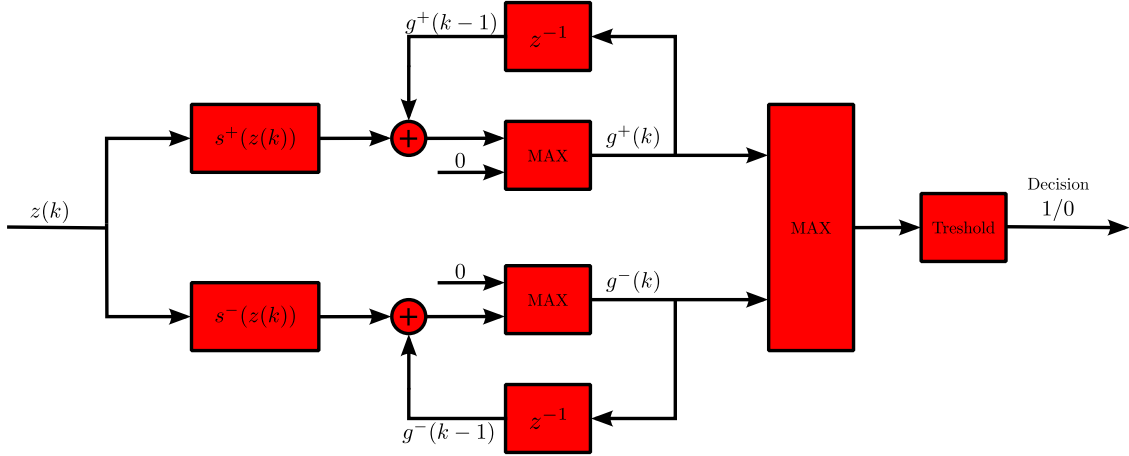


Figure 6.7: Block diagram of the two-sided CUSUM algorithm

mean and variance. The estimated mean value of the faulty process is unknown and is suggested estimated as [Blanke 06]:

$$\hat{\mu}_1 = \hat{\mu}_0 + 2\beta_{min} \quad (6.40)$$

where β_{min} is the minimum signal change value wanted to be detected.

Finding the threshold h is, as described in Appendix H, a compromise between the mean detection time T_d and the mean time between false alarms T_{fa} . These times is calculated by (H.10) and (H.11) and h can thus be chosen as a compromise between the two. In Section 2.4.4, it is stated that the fault should be detected within 500 s. T_d is selected to be 300 s to which is considered to be suitable.

An example of selecting of h , when considering T_d and T_{fa} is seen in Fig. 6.8. In Fig. 6.8 the selected average time for detecting a fault based on the residual q_3 from UIO q_2 is 300 s, while it is seen that the mean time between false alarms is calculated to be $7 \cdot 10^{65}$ s, which is practically infinity. This number could indicate that a lower value than the obtained 7.54 for h should be selected. However, as the process is not completely Gaussian distributed, the method applied for Fig. 6.8 is used as an initial guess, while h afterwards has been fitted empirically to obtain a satisfactory result.

In Fig. 6.9, an example in which the mean value of the non-faulty operation is altered at time 1000 s, is illustrated. This causes the decision function for $g^+(k)$ to rise and reach the threshold at 1099 s, as seen in Fig. 6.10, and will trigger the decision to a boolean "1".

As both $g^-(k)$ and $g^+(k)$ is affected by noise a simple threshold logic will cause the alarm to go "on and off" doing the period when the function is crossing the threshold value. To avoid this a hysteresis, with a lower threshold (h_{low}), has been added to the threshold logic in Fig. 6.7. The lower threshold is given as $h_{low} = h/2$. The low threshold insures that a shift from boolean "1" to "0" is not done before the decision function is below the value of h_{low} .

CUSUM Bank

In Fig. 6.11, the layout of the CUSUM bank is illustrated.

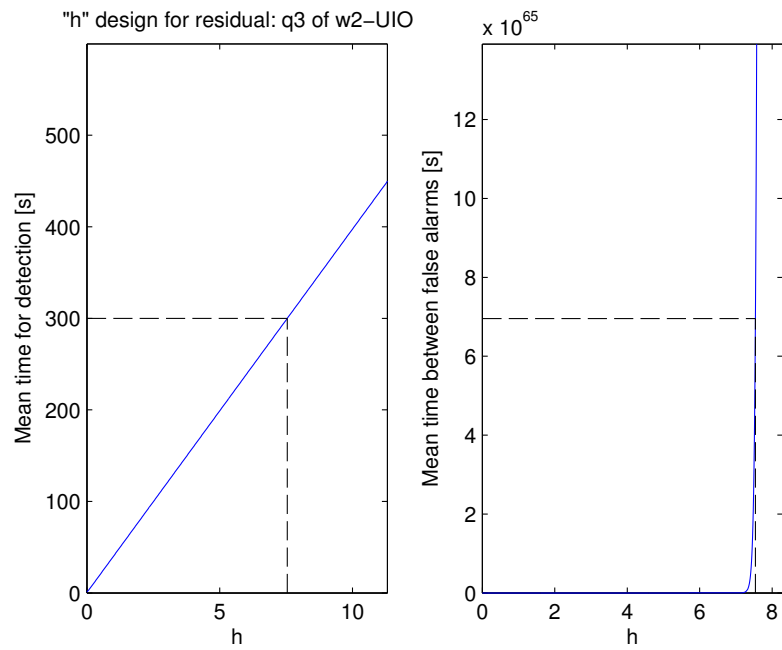


Figure 6.8: The threshold h selected to 7.54, considering the mean time of detection T_d and the mean time for a false alarm T_{fa}

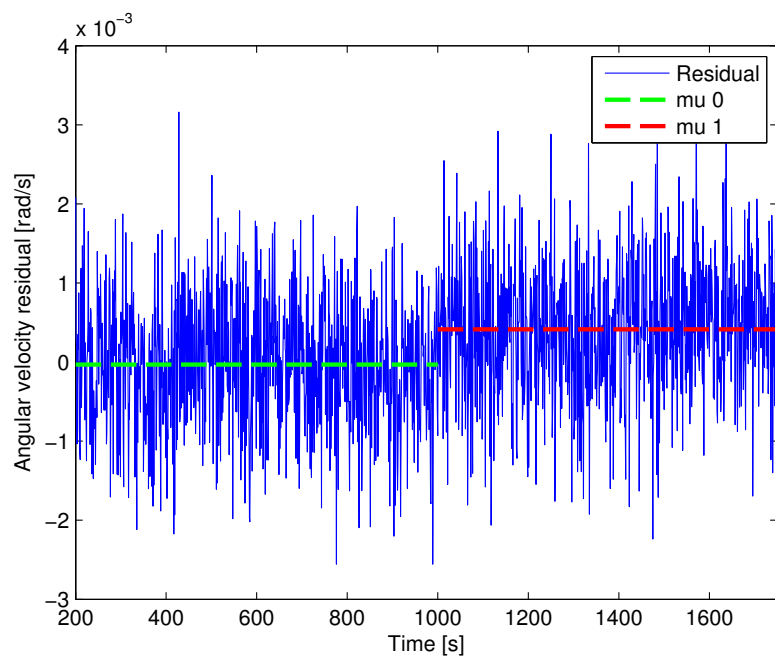


Figure 6.9: The residual, with fault occurring in 1000 s

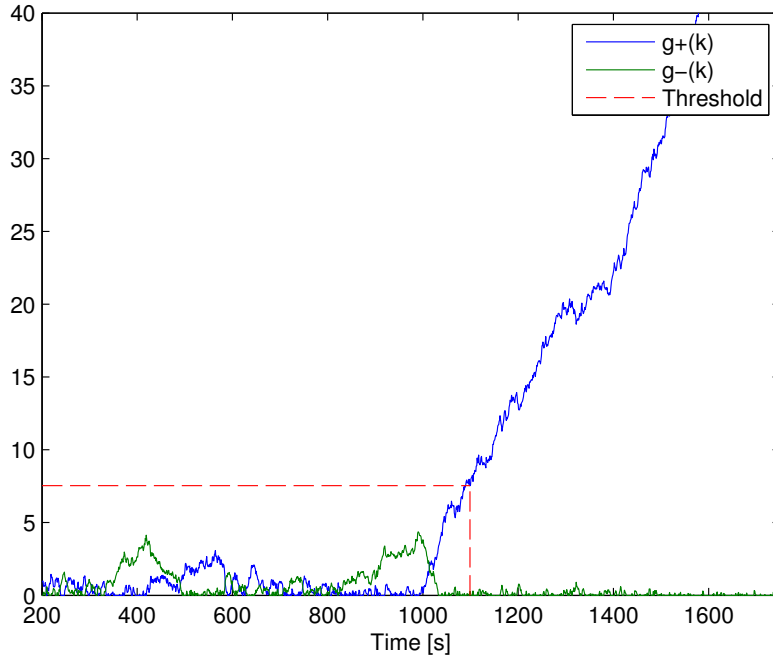


Figure 6.10: The decision function, with fault occurring in 1000 s

The residuals from the UIOs is sent into separate CUSUM boxes and the CUSUM outputs from each sensor/actuator is logical OR'ed together to indicate if one of these indicate a fault some where in the system

Additionally, the output of the OR'boxes of the quaternion CUSUM is OR'ed as it is unimportant if one or multiple quaternions are faulty, as they would all indicate a fault in the gray boxed ADS. It is noted that the not all the residuals generated in the UIO is forwarded into the CUSUM bank. This is because some states in these residuals is spanned in the subspace of \underline{E} and therefore are constantly zero, because of the geometric decoupling.

6.3.4 Decision Logic

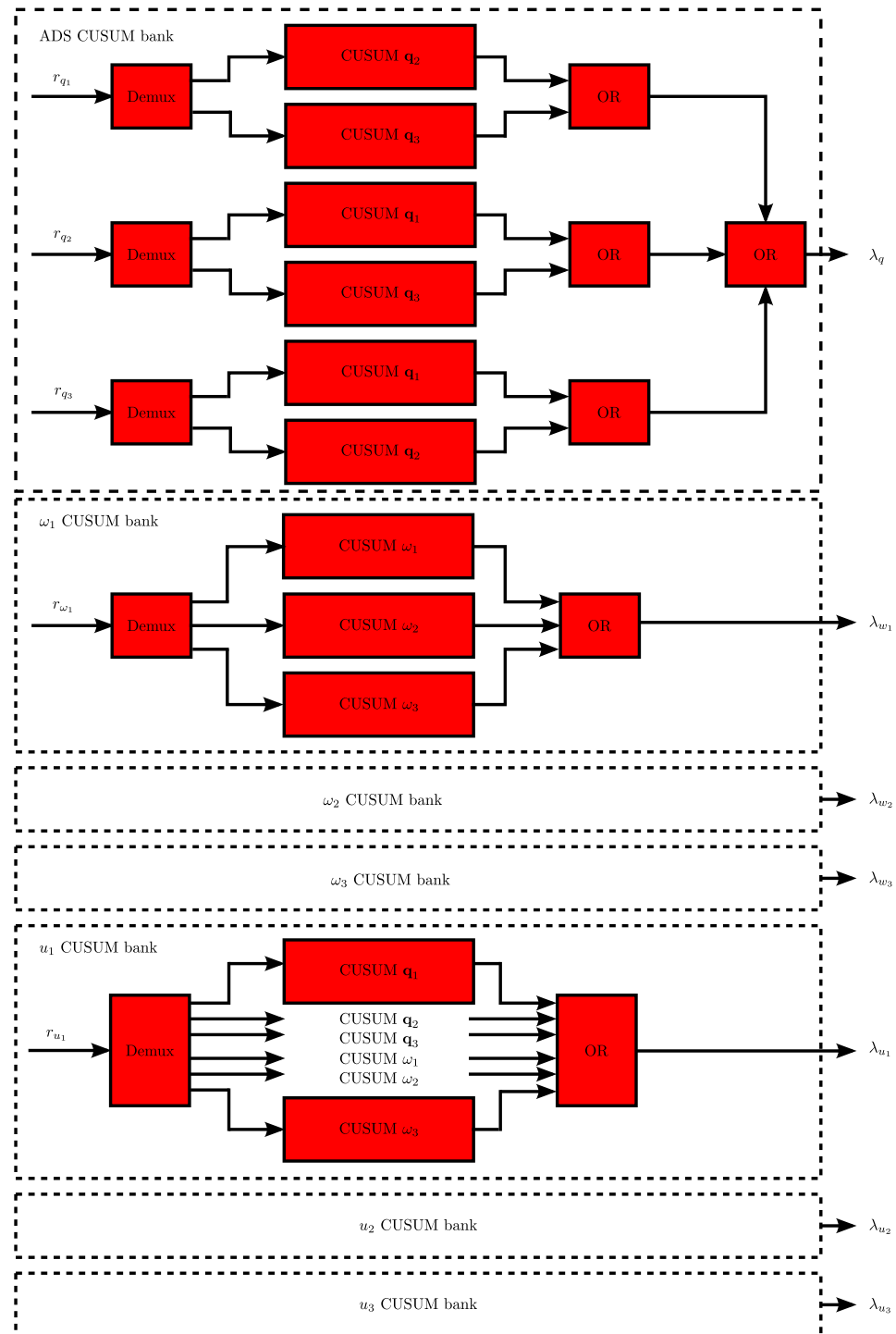
The decision logic should be able to determine if the combined boolean fault indications (λ) of the CUSUM bank, indicates a fault has occurred and in which sensor/actuator the fault has occurred.

The output of the CUSUM bank is:

λ_q : Indicates that one of the UIO is insensitive to faults in the ADS has reacted.

λ_{w_k} : Indicates that the UIO is insensitive to faults in the gyroscope in the k^{th} axis has reacted.

λ_{u_k} : Indicates that the UIO is insensitive to faults in the k^{th} actuator has reacted.

**Figure 6.11:** Overview of the CUSUM bank

Two vectors are defined as:

$$\boldsymbol{\Lambda}_s = \begin{bmatrix} \lambda_q \\ \lambda_{w_1} \\ \lambda_{w_2} \\ \lambda_{w_3} \end{bmatrix} \quad (6.41)$$

and

$$\boldsymbol{\Lambda}_a = \begin{bmatrix} \lambda_{u_1} \\ \lambda_{u_2} \\ \lambda_{u_3} \end{bmatrix} \quad (6.42)$$

The decision logic is divided into two parts; a decision logic to detect sensor faults and one to detect actuator faults. As explained, all the sensor fault UIOs are designed to be insensitive to one specific sensor fault, which yield the following determination and isolation logic:

$$\mathbf{Z}_s = \begin{bmatrix} 0 & 1 & 1 & 1 \\ 1 & 0 & 1 & 1 \\ 1 & 1 & 0 & 1 \\ 1 & 1 & 1 & 0 \end{bmatrix} \boldsymbol{\Lambda}_s \quad (6.43)$$

If only the k^{th} component of \mathbf{Z}_s reaches a value of 3, it means that all the boolean components in $\boldsymbol{\Lambda}_s$, except the k^{th} , indicates a fault. Because of the structured UIO design, this mean that a fault has occurred in k^{th} sensor component of $\boldsymbol{\Lambda}_s$.

In practice, if a significant fault occurs in the system, eventually all the components of $\boldsymbol{\Lambda}_s$ will indicate faults. So the component of \mathbf{Z}_s which reaches a value of 3 first is considered to be the faulty sensor. Likewise, the decision logic of the actuator faults is given as:

$$\mathbf{Z}_a = \begin{bmatrix} 0 & 1 & 1 \\ 1 & 0 & 1 \\ 1 & 1 & 0 \end{bmatrix} \boldsymbol{\Lambda}_a \quad (6.44)$$

With \mathbf{Z}_a having similar properties for actuator fault, as the described properties \mathbf{Z}_s has for sensor faults.

Known Issue

It is noted that the residuals used for \mathbf{Z}_a is both sensitive to faults in the actuators and the sensors, which could cause a sensor fault to be isolated as an actuator fault. Due to lack of time, this issue has not been solved in the project and has been left for future research.

6.4 Autonomous Supervisor

When a fault is detected and isolated by either the model based FDI or the simple FDI, it informs the autonomous supervisor about the fault. The supervisor is then responsible for the reconfiguration of the controllers, the switching between controller or in case of a fatal system failure; shutdown the ADCS. The different parts are of the supervisor is shown in Fig. 6.12, which is based on the modular architecture described in [Izadi-Zamanabadi 06].

The different parts are briefly described here:

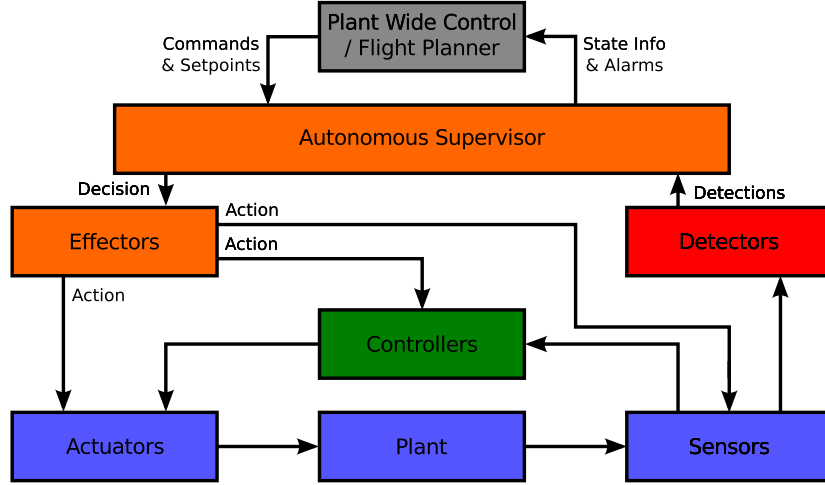


Figure 6.12: Overview of the different parts of the fault tolerant control system for the satellite

- Plant Wide Control: The overall control and state of the satellite, issues different commands to the Autonomous Supervisor. For instance that the available amount of power is limited.
- Autonomous Supervisor: Based on which faults is detected (from the detection part) and the commands from the Plant Wide Controller, the Autonomous Supervisor decides which controllers, actuators, and sensors to use.
- Effectors: Take action based on the decision from the supervisor. The actions can be to change actuator set, change controller or select which sensors to use.
- Detectors: Consists of both the model based and the simple FDI to detect faults and inform the supervisor when they are detected and isolated.
- Controllers: The different controllers, described in chapter 4.
- Satellite: Actuators, plant and sensors, controlled by the selected controller.

The states for the ADCS is described in Chapter 2, in which the three main states for ADCS is idle, detumbling, and pointing modes.

6.4.1 Supervisor for Detumbling

Since the detumbling of the satellite is the most mission critical (supervisor) state, only the supervisor logic for this state is described. Supervisors for the other states are not considered in this project, though the supervisor can easily be expanded to include them.

The components, which can be used when the satellite is in detumble mode, is listed Table 6.1. As seen in the table, components are both defined as sensor, actuators and microcontrollers. In the table, the health condition for each component is also listed. The health condition is a boolean value, indicating whether the component is enable for use. The health condition is used for constructing the decision logic for the supervisor through a component based approach, using the supervisor language defined in [Izadi-Zamanabadi 99, p. 45 - 55]

System	Component	Health Condition
Magnetometers	Mag1	HC_{M1}
	Mag2	HC_{M2}
	Mag3	HC_{M3}
	Mag4	HC_{M4}
Micro-controller	AVR8	HC_{AVR8}
	ARM7	HC_{ARM7}
Magnetorquer	mt1,x	$HC_{mt1,x}$
	mt2,x	$HC_{mt2,x}$
	mt1,y	$HC_{mt1,y}$
	mt2,y	$HC_{mt2,y}$
	mt1,z	$HC_{mt1,z}$
	mt2,z	$HC_{mt2,z}$

Table 6.1: List of components useable for detumbling and their health condition

Based on the health conditions, a logical term describing the detumbling mode is written as:

$$D_L = S_{mt} \cdot S_M \quad (6.45)$$

In which S_{mt} represents the supervisor language for the magnetorquers and S_M the supervisor language for the magnetometers. The dot (\cdot) is logic AND. This means that if a set of magnetorquers ($S_{mt} = \text{true}$) and a set of magnetometers ($S_M = \text{true}$) are working, then D_L is true (one), and the detumbling controller is able to run.

S_{mt} contains the different combinations of possible sets of magnetorquers which can be used to detumble the satellite and is given by the list in (6.46). To have a working set of magnetorquers the health condition of each magnetorquer in the set (the given row of (6.46).) should be healthy (true/one). The value of S_{mt} is given by the row number of the first set of magnetorquers which is healthy. If there are no healthy set of magnetorquers then $S_{mt} = \emptyset$. Thus the ADCS can not be configured such that it can detumble and should therefore go to idle mode or shutdown.

$$S_{mt} = \left\{ \begin{array}{l} HC_{mt1,x} \cdot HC_{mt1,y} \cdot HC_{mt1,z} \\ HC_{mt1,x} \cdot HC_{mt1,y} \cdot HC_{mt2,z} \\ HC_{mt1,x} \cdot HC_{mt2,y} \cdot HC_{mt1,z} \\ HC_{mt1,x} \cdot HC_{mt2,y} \cdot HC_{mt2,z} \\ HC_{mt2,x} \cdot HC_{mt1,y} \cdot HC_{mt1,z} \\ HC_{mt2,x} \cdot HC_{mt1,y} \cdot HC_{mt2,z} \\ HC_{mt2,x} \cdot HC_{mt2,y} \cdot HC_{mt1,z} \\ HC_{mt2,x} \cdot HC_{mt2,y} \cdot HC_{mt2,z} \\ HC_{mt1,x} \cdot HC_{mt1,y} \\ HC_{mt1,x} \cdot HC_{mt1,z} \\ HC_{mt1,y} \cdot HC_{mt1,z} \\ HC_{mt1,x} \cdot HC_{mt2,y} \\ HC_{mt1,x} \cdot HC_{mt2,z} \\ HC_{mt1,y} \cdot HC_{mt2,z} \\ HC_{mt1,z} \cdot HC_{mt2,x} \\ HC_{mt1,z} \cdot HC_{mt2,y} \\ HC_{mt2,x} \cdot HC_{mt2,y} \\ HC_{mt2,x} \cdot HC_{mt2,z} \\ HC_{mt2,y} \cdot HC_{mt2,z} \end{array} \right\} \quad (6.46)$$

The order of the sets in S_{mt} defines the priority of the different sets of magnetorquers. In (6.46) it is seen that mt1 is selected prior to mt2, and that it is preferred to have magnetorquers in all three directions over only two directions.

S_M contains the different combinations of possible sets of the magnetometers and their microcontroller. This is due to the fact that two of the magnetometers are connected to the AVR8, and two to the ARM7. The health condition for the microcontrollers should therefore also be taking into account when looking for a healthy magnetometer. S_M will then be the first set containing a healthy magnetometer and a healthy microcontroller. This set will then be used for detumbling the satellite. The sets in S_M is shown in (6.47).

$$S_M = \left\{ \begin{array}{l} HC_{M1} \cdot HC_{AVR8} \\ HC_{M2} \cdot HC_{AVR8} \\ HC_{M3} \cdot HC_{ARM7} \\ HC_{M4} \cdot HC_{ARM7} \end{array} \right\} \quad (6.47)$$

The decision made by the supervisor is defined to use the components set to be healthy by S_{mt} and S_M . If one of the set is empty the ADCS can not start detumble. The effectors should then select the components defined by the two sets S_{mt} and S_M and start detumbling the satellite.

6.4.2 Example of the Supervisor

An example of the supervisor logic is shown in this section. It is assumed that $mt1, x$ and the ARM7 is faulty and that the rest of the components ate healthy. The supervisor logic for S_{mt} and S_M is shown in (6.48) and (6.49) respectively. In the set an extra column is shown, which indicates if the set on the row is usable (all the components in the set are healthy). This means that all the sets containing $mt1, x$, in (6.48), will be zero while the remaining sets will be one. The same is done in (6.49) just with respect to the ARM7.

The supervisor logic then go through the S_{mt} and S_M list to find the first set with the value one. The components from this set is then set active by the effectors.

$$S_{mt} = \left\{ \begin{array}{l|lll} 0 & HC_{mt1,x} & \cdot & HC_{mt1,y} & \cdot & HC_{mt1,z} \\ 0 & HC_{mt1,x} & \cdot & HC_{mt1,y} & \cdot & HC_{mt2,z} \\ 0 & HC_{mt1,x} & \cdot & HC_{mt2,y} & \cdot & HC_{mt1,z} \\ 0 & HC_{mt1,x} & \cdot & HC_{mt2,y} & \cdot & HC_{mt2,z} \\ 1 & HC_{mt2,x} & \cdot & HC_{mt1,y} & \cdot & HC_{mt1,z} \\ 1 & HC_{mt2,x} & \cdot & HC_{mt1,y} & \cdot & HC_{mt2,z} \\ 1 & HC_{mt2,x} & \cdot & HC_{mt2,y} & \cdot & HC_{mt1,z} \\ 1 & HC_{mt2,x} & \cdot & HC_{mt2,y} & \cdot & HC_{mt2,z} \\ 0 & HC_{mt1,x} & \cdot & HC_{mt1,y} & & \\ 0 & HC_{mt1,x} & \cdot & HC_{mt1,z} & & \\ 1 & HC_{mt1,y} & \cdot & HC_{mt1,z} & & \\ 0 & HC_{mt1,x} & \cdot & HC_{mt2,y} & & \\ 0 & HC_{mt1,x} & \cdot & HC_{mt2,z} & & \\ 1 & HC_{mt1,y} & \cdot & HC_{mt2,x} & & \\ 1 & HC_{mt1,y} & \cdot & HC_{mt2,z} & & \\ 1 & HC_{mt1,z} & \cdot & HC_{mt2,x} & & \\ 1 & HC_{mt1,z} & \cdot & HC_{mt2,y} & & \\ 1 & HC_{mt2,x} & \cdot & HC_{mt2,y} & & \\ 1 & HC_{mt2,x} & \cdot & HC_{mt2,z} & & \\ 1 & HC_{mt2,y} & \cdot & HC_{mt2,z} & & \end{array} \right\} \quad (6.48)$$

$$S_M = \left\{ \begin{array}{l|l} 1 & HC_{M1} \cdot HC_{AVR8} \\ 1 & HC_{M2} \cdot HC_{AVR8} \\ 0 & HC_{M3} \cdot HC_{ARM7} \\ 0 & HC_{M4} \cdot HC_{ARM7} \end{array} \right\} \quad (6.49)$$

In the example in which $mt1, x$ and $ARM7$ is faulty, the detumbling controller will use $mt2, x$, $mt1, y$ and $mt1, z$ as actuators and $M1$ as the sensor, while running on the AVR8.

Chapter 7

Acceptance Test

This chapter include all the test performed both on the FDI system and the test of the different controllers. When referring to a MATLAB scripts used in the test it can be found in Appendix J.

7.1 Test of the B-dot Controller

According to the requirement specification in Section 2.4.1, the B-dot controller should be able to lower the angular rate from 0.1 rad/s to 0.0026 rad/s relative to the ECI. This requirement is tested in the simulation environment discussed in Section 3.7 with all the mentioned disturbances and the permanent magnet enabled.

The test of the B-dot controller is conducted and the velocity is shown in Fig. 7.1

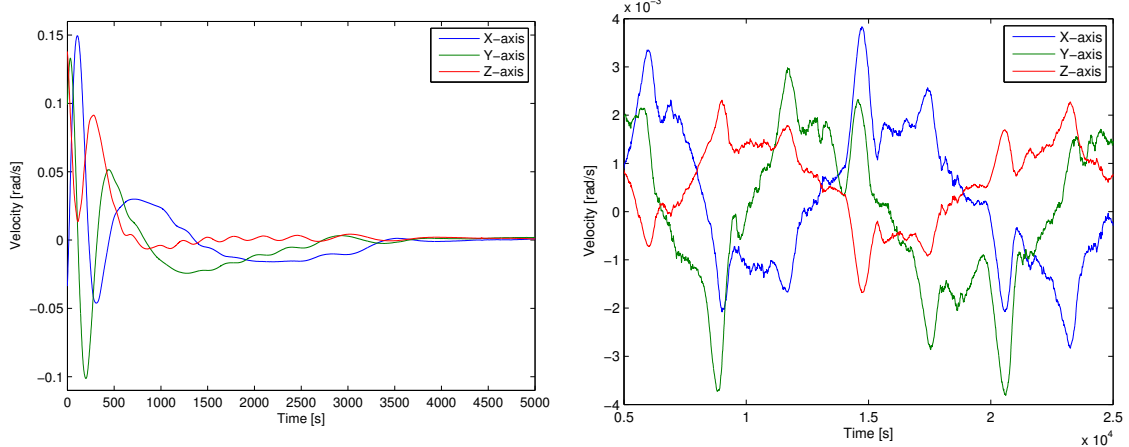


Figure 7.1: Angular velocity of the satellite seen from the CRF

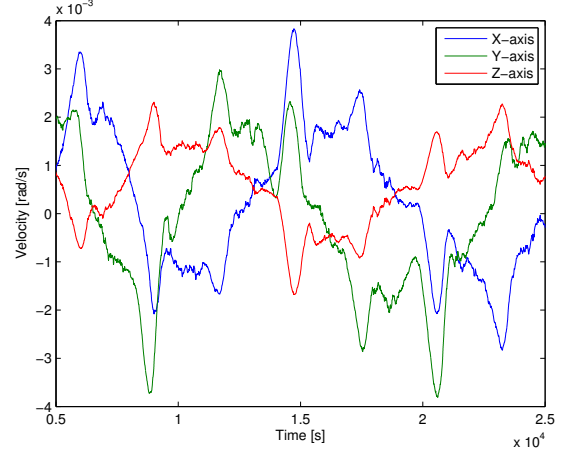


Figure 7.2: A zoom of the angular velocity of the satellite seen from the CRF

It is shown that the B-dot controller lowers the velocity as expected. After 5000 seconds, which approximately corresponds to one orbit, the velocity is lowered to a maximum velocity of $\pm 0.0040 \text{ rad/s}$, which is seen in Fig. 7.2. In bdot/statistic.m it is calculated that the angular velocity in all three axis is below 0.0026 rad/s 92.3% of the time. The statistics is conducted in the time interval from 5000 to 25000 s. It can be concluded that the B-dot controller satisfies the requirements from Section 2.4.1. Additionally it is noticed that

the total power consumption for detumbling the satellite during the first 5000 seconds is found to 1.03 J (calculated in `bdt/power_use.m`) , with a peak power of 0.07 W which is considered acceptable.

7.2 Test of Constant Gain Controller

In this section the acceptance tests for the constant gain controllers are described which includes a controller for nadir pointing that is based on the model described in Section 3.4.2 and another that is based on the model described in Section 3.4.3. Additionally a constant gain controller for the inertial pointing is tested. (Found in `constant_gain/nadir_controller.mdl` and `constant_gain/inertial_controller.mdl`)

7.2.1 Nadir Pointing Controller

This acceptance test is based on the controller designed wrt. the model conducted in Section 3.4.2. According to the requirement specification in Section 2.4.2, the nadir pointing controller should be able to satisfy the following demand:

- The eigenvector angle between ORF and CRF should be within 50° within four orbits in at least 90% of the time, for the simulation that includes environment disturbances and sensor dynamics.

The starting attitude is an 180° angle between ORF and CRF around an eigenvector, which is defined as $\left[\frac{1}{\sqrt{3}} \frac{1}{\sqrt{3}} \frac{1}{\sqrt{3}}\right]$. The starting angular velocity of the satellite is defined as the worst case detumbling rate which in Section 7.1 is found to be 0.004 rad/s . The simulation of the angle between ORF and CRF, represented as eigenaxis rotation angle and as quaternion is plotted in Fig. 7.3 and Fig. 7.4. It is shown that even with a large starting angle, the system regulates to the correct operating point with time.

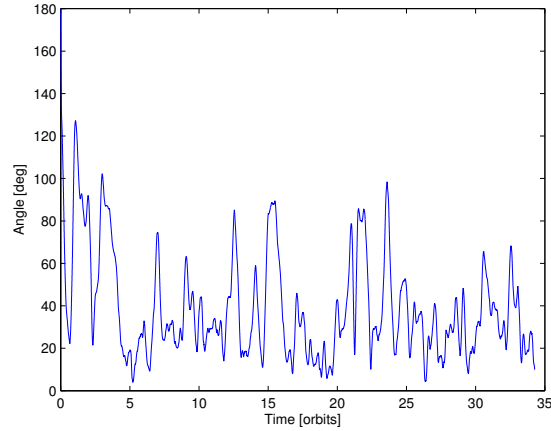


Figure 7.3: The rotation between ORF and CRF represented by an eigenaxis rotation

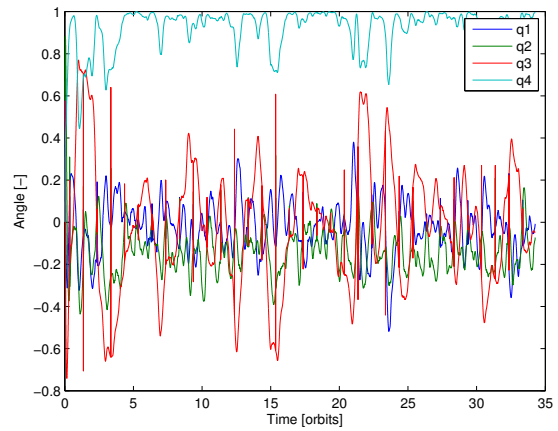


Figure 7.4: The rotation between ORF and CRF represented by a quaternion

In Fig. 7.3 it is seen that the eigenaxis rotation angle varies between approximately 0 and 100° . From the 4th to the 35th orbit, the angle is below 50° 83% (`constant_gain/statistic.m`) of the time, which is not sufficient to satisfy the requirement, that should be at least 90%.

7.2.2 Nadir Pointing Controller

This acceptance test is based on the controller designed wrt. the model conducted in Section 3.4.3. According to the requirement specification in Section 2.4, the nadir pointing controller should be able to comply with the following demand:

- The eigenvector angle between ORF and CRF should be within 50° within four orbits in at least 90% of the time, for the simulation that includes environment disturbances and sensor dynamics.

The starting attitude is an 180° angle between ORF and CRF around an eigenvector, which is defined as $\left[\frac{1}{\sqrt{3}} \frac{1}{\sqrt{3}} \frac{1}{\sqrt{3}}\right]$. The starting angular velocity of the satellite is defined as the worst case detumbling rate which in Section 7.1 is found to be 0.004 rad/s . The simulation of the angle between ORF and CRF, represented as eigenaxis rotation angle and as quaternion is plotted in Fig. 7.5 and Fig. 7.6. It is shown that even with a large starting angle, the system regulates to the correct operating point with time.

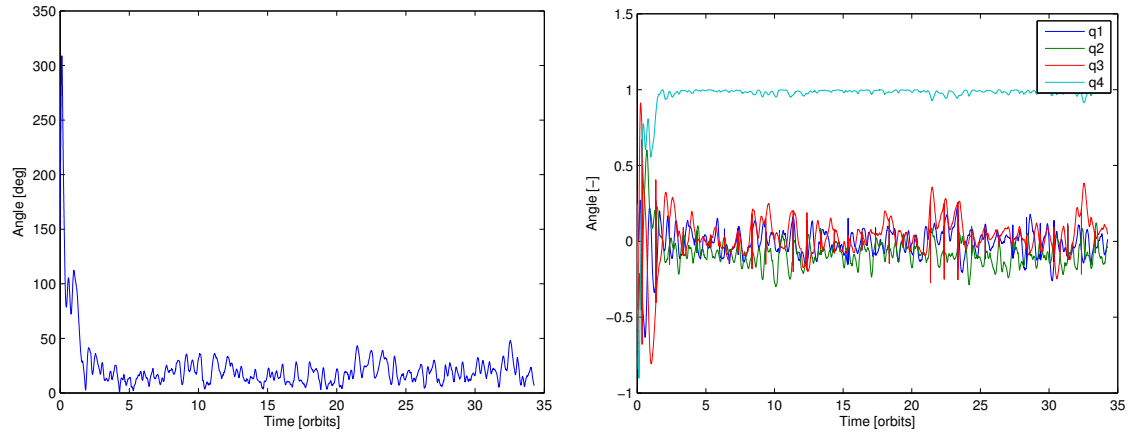


Figure 7.5: The rotation between ORF and CRF represented as an eigenaxis rotation angle

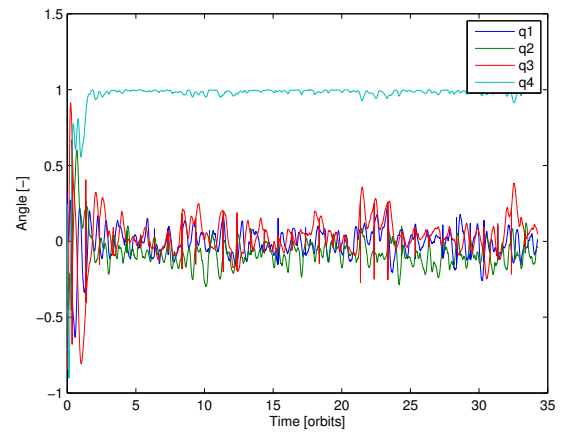


Figure 7.6: The rotation between ORF and CRF represented as a quaternion

In Fig. 7.5 it is seen that the eigenaxis angle varies between approximately 0 to 50° . From the 4th to the 35th orbit, the angle is below 50° 99.9% (*constant_gain/statistic.m*) of the time, which satisfy the requirement. Actually the eigenaxis angle is below 30° for 90% of the time.

The velocity between ORF and CRF seen from CRF is as expected close to 0 rad/s , for all three axis. The power consumption which is plotted in Fig. 7.8 is in average 557 nW based on 35 orbits, which seems reasonable.

7.2.3 Inertial Pointing Controller

According to the requirement specification in Section 2.4.3, the inertial pointing controller should be able to fulfill the following demands:

- The eigenvector angle between ECI and CRF should be within 50° within four orbits in at least 90% of the time, for the simulation that includes environment disturbances and sensor dynamics.

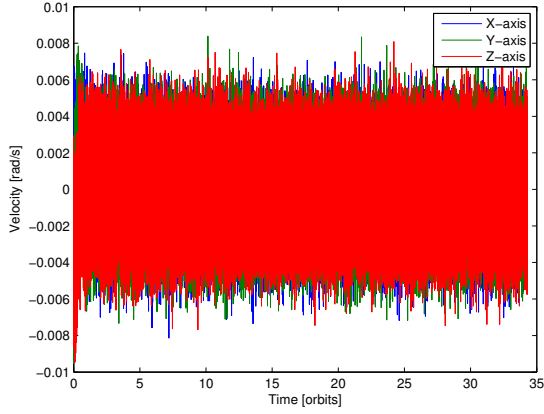


Figure 7.7: The velocity between ORF and CRF seen from the CRF

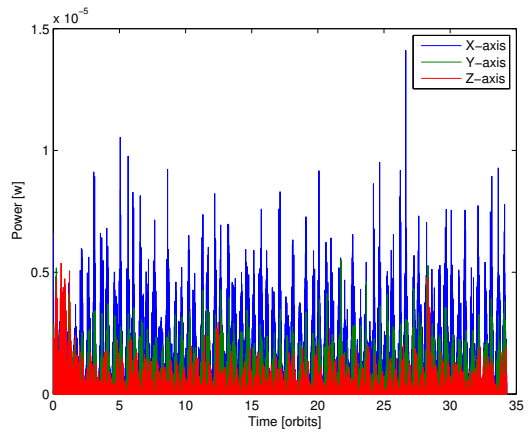


Figure 7.8: The power consumption for the nadir controller

The starting attitude is an 180° angle between ORF and CRF around an eigenvector, which is defined as $\left[\frac{1}{\sqrt{3}} \frac{1}{\sqrt{3}} \frac{1}{\sqrt{3}}\right]$. The starting angular velocity of the satellite is defined as the worst case detumbling rate which in Section 7.1 is found to be 0.004 rad/s . The simulation of the angle between ORF and CRF, represented as eigenaxis rotation angle and as quaternion is plotted in Fig. 7.9 and Fig. 7.10. It is shown that even with a large starting angle, the system regulates to the correct operating point with time.

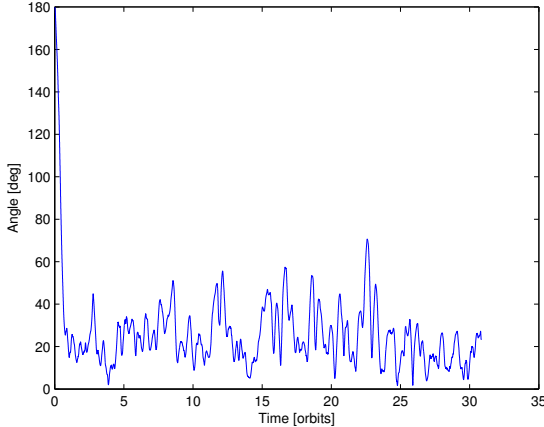


Figure 7.9: The rotation between ECI and CRF represented by an eigenaxis angle

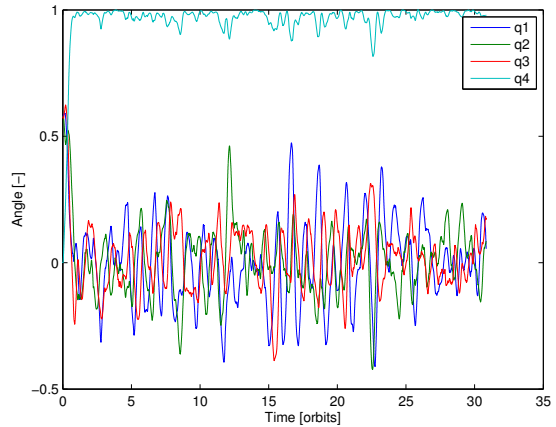


Figure 7.10: The rotation between ECI and CRF represented as a quaternion

In Fig. 7.9 it is seen that the eigenaxis angle varies between approximately 0 and 70° . From the 4th to the 35th orbit, the angle is below 50° 96% of the time (*constant_gain/statistic.m*), which satisfies the acceptance test. The angular velocity between ECI and CRF seen from the CRF is as expected close to 0 rad/s , though noisy due to sensor noise disturbance included in the simulation. The power consumption which is shown in Fig. 7.12 is in average 372nW , based on 32 orbits, which seems reasonable.

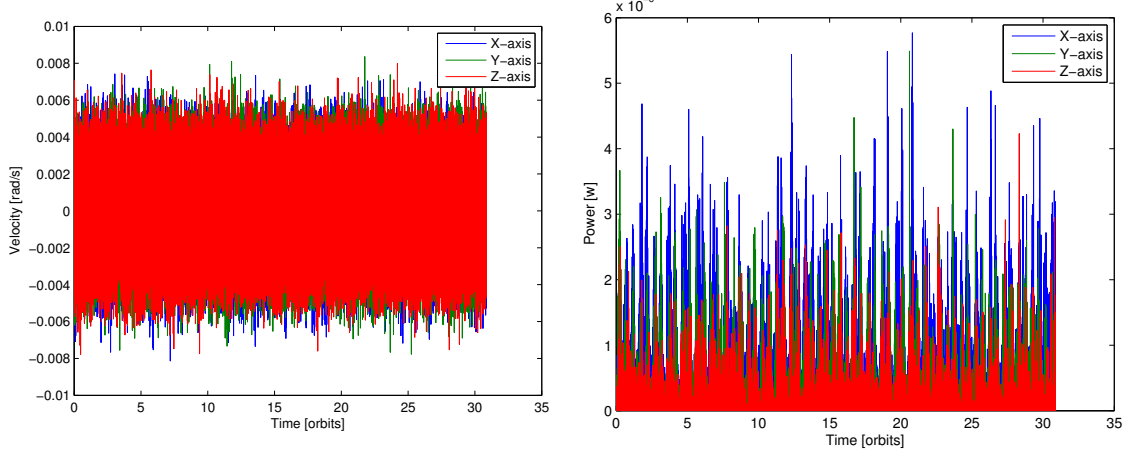


Figure 7.11: The angular velocity between ORF and CRF seen from the CRF

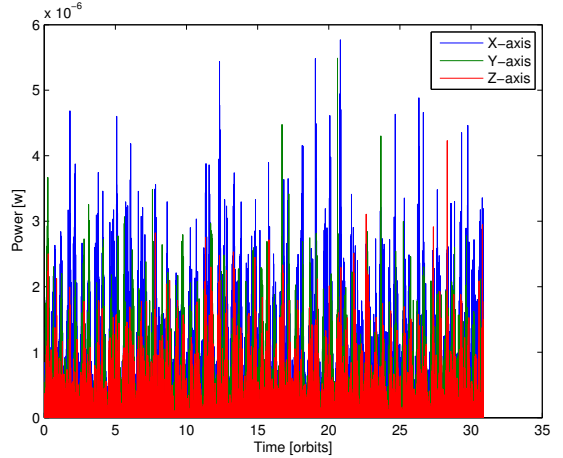


Figure 7.12: The power consumption for the inertial controller while pointing

7.3 Test of FDI system

To be able to evaluate whether the requirements for the fault detection, stated in Section 2.4.4, has been satisfied, tests of the FDI has been conducted. The main requirement is that the five faults with the highest SO index should be detected and isolated within 500 s. The tests consist of simulations of faults in the simulation environment, described in Section 3.7.

All the fault has been simulated with a starting time at 15000 s, to make sure that the controller has settled close to its working point, as the FDI has been design from a model which is linear close to this point. As described in subsection 6.3.2, it is chosen to use a time varying approximation of $\underline{\mathbf{B}}$. For the test, the input matrix used for the UIO design is the $\underline{\mathbf{B}}_k$ from the periodic approximation, for the time at 14900 s. The FDI has only been implemented and tested on the model and controller for the nadir pointing controller.

In each test, a plot of the components of \mathbf{Z}_s and \mathbf{Z}_a is shown. As described in section 6.3.4, a value of 3 in the k^{th} component of \mathbf{Z}_s , would lead to a conclusion of a fault in the k^{th} sensor. Likewise, a value of 2 in the k^{th} component of \mathbf{Z}_a , would lead to a conclusion of a fault in the k^{th} actuator.

It would be inconvenient to plot all the residuals, decision functions and decision logic in the CUSUM bank for each test. Consequently only a plot of a selected representing residual with corresponding decision functions and decision logic is shown for each test.

As described in Section 6.3.4, the decision logic has the unsolved problem that sensor faults, (faulty) can trigger the decision logic for actuator faults. This problem has been scoped for future work and thus will not be commented on further. Thus, if a sensor fault is first detected as an actuator fault, the requirement for the FDI is satisfying as long as the fault is afterwards isolated and occurs in the correct sensor. According to the requirement specification in Section 2.4.4 the FDI should comply with the demands decribed in the following sections.

7.3.1 Detection of Instantly Faulty ADS

The FDI should detect if the ADS instantly outputs a faulty estimate of the satellite attitude which is a 0.5° rotation of the real attitude, rotated around the unit eigenvector $\begin{bmatrix} \frac{1}{\sqrt{3}} & \frac{1}{\sqrt{3}} & \frac{1}{\sqrt{3}} \end{bmatrix}$.

In Fig. 7.13, a plot of the components of Z_s and Z_a is shown.

A plot of a residual and corresponding decision functions and decision logic is shown in Fig. 7.14.

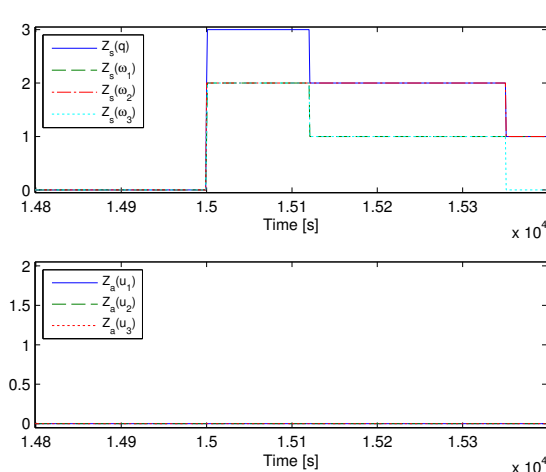


Figure 7.13: Simulation of a slowly instant fault in the ADS, for the components of Z_s and Z_a .

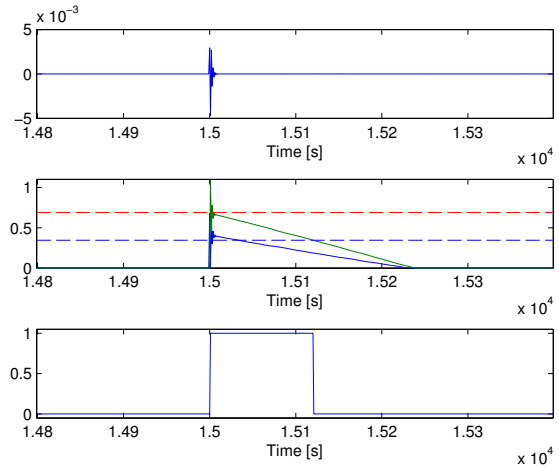


Figure 7.14: Simulation of an instant fault in the ADS. Selected residual, with corresponding decision function and decision logic

The fault logic, detects and isolate the fault to be in the quaternion sensor (the ADS) within a few seconds. No faults in the actuators are detected.

Is seen in Fig. 7.14 that the residual reacts significantly (both negative and positive) when the fault occurs, and that both decision functions exceed their thresholds, which trigs a decision of a fault.

Test Conclusion

As the FDI detected and isolated the fault to be in the ADS within the time limit, the requirement is satisfied.

However, it should be noted that, as described in section 2.2.3 in Fig. 2.7, when the satellite exits eclipse, the estimated quaternion jump suddenly. This would surely be detected as a fault, why the decision of the FDI should not be regarded in the period when exiting eclipse.

7.3.2 Detection of Slowly Increasingly Faulty ADS

The FDI should detect and isolate if the ADS slowly outputs an increasingly faulty estimate of the satellite attitude. If the attitude is increasing by $0.01^\circ/\text{s}$ wrt. the real attitude, rotated around the unit eigenvector $\begin{bmatrix} \frac{1}{\sqrt{3}} & \frac{1}{\sqrt{3}} & \frac{1}{\sqrt{3}} \end{bmatrix}$, an alarm should be triggered.

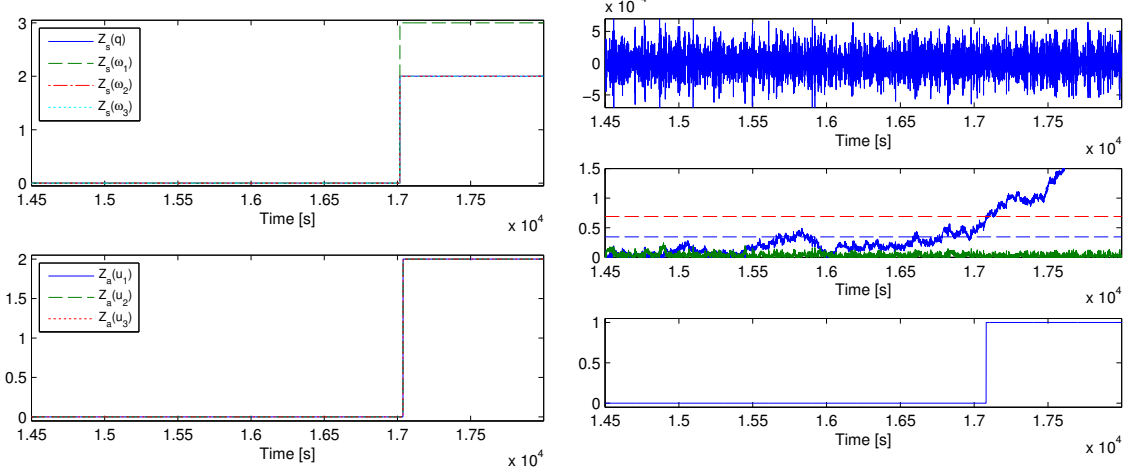


Figure 7.15: Simulation of a slowly increasing fault in the ADS, for the components of Z_s and Z_a

Figure 7.16: Simulation of a slowly increasing fault in the ADS. Selected residual, with corresponding decision function and decision logic

In Fig. 7.15, a fault is detected 17018 s after the fault has occurred and the fault is incorrectly isolated to have happened in the gyroscope of the 1st axis. 22 s after, the fault is also isolated to be an actuator fault.

As the fault enters the system, the residual does not make a notable change, but the decision function slowly grows until it exceeds the threshold and triggers a decision of a fault.

It is obvious, that this fault would not have been detected this early if the residuals had not been evaluated through the CUSUM algorithm.

Test Conclusion

As the FDI was too slow to detect the fault and isolated the fault incorrectly, the FDI did not satisfy this requirement. However, though slowly, it detected a fault in the system.

It should be noted that, as described in subsection 2.2.3 in Fig. 2.7, when the satellite enters eclipse, the estimated quaternion slowly diverges. This could be detected as a fault, why the decision from the FDI should not be regarded in the period when the satellite is in eclipse.

7.3.3 Detection of Grounded Gyroscope

The FDI should detect and isolate, if the gyroscope in one axis is instantly short circuited to ground. A simulation in which the gyroscope in the 1st axis has been instantly short circuited to ground.

It is seen in Fig. 7.17, that a fault is detected approximately 128 s after the fault has occurred and the fault is incorrectly isolated to have happened in the gyroscope of the 2nd axis. The fault is also isolated to be an actuator fault 112 s after the fault has occurred.

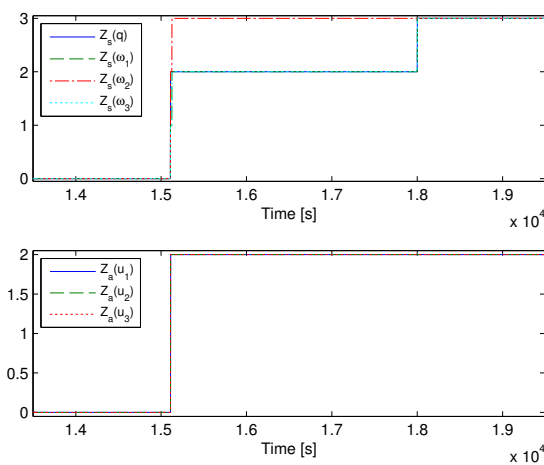


Figure 7.17: Simulation of a ground short circuit of gyroscope in SBRF x-axis, for the components of Z_s and Z_a

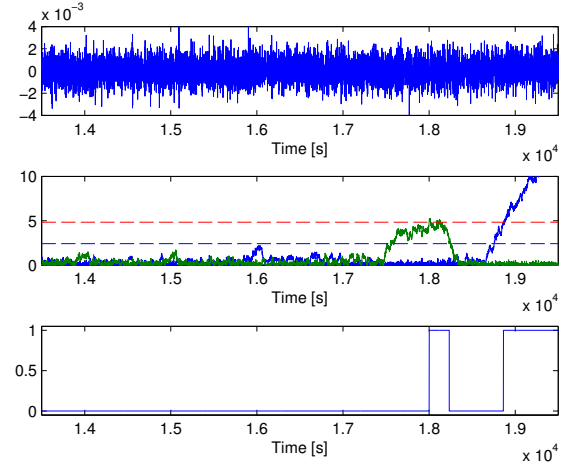


Figure 7.18: Simulation of a ground short circuit of gyroscope in SBRF x-axis. Selected residual, with corresponding decision function and decision boolean

The residual shown in Fig. 7.18, is from the estimation of q_1 from ω_2 -UIO. This UIO should be sensitive to faults in the 1st axis gyroscope, but this decision function is very slow to react.

Test Conclusion

As the FDI detected a fault within the time requirement, but failed to isolate the fault correctly the requirement is only partly satisfied.

The incorrect isolation has been found to be caused by a design flaw. In the design of the UIOs, which are insensitive to gyroscope faults, it is assumed that the gyroscopes are measuring the angular velocity in the CRF frame, but in reality, the gyroscopes are measuring in the SBRF frame. This means that a short circuit to ground, in the SBRF frame, will cause altered angular velocities in multiple axis in the CRF frame.

Detection of Gyroscope Fault in CRF

To test whether the above mentioned design flaw could cause the faulty isolation, a test has been conducted in which only the angular velocity represented in CRF, has been short circuited to ground in the 1st axis.

As seen in Fig. 7.19, the fault is detected and isolated correctly as a gyroscope fault in the 1st axis, 642 s after the fault has occurred.

As in Fig. 7.18, Fig. 7.20 is also from the estimation of q_1 in ω_2 -UIO, which should be sensitive to faults in the 1st axis gyroscope. It is noted in Fig. 7.20, that the noise of the residual disappears when the fault occurs and the decision function starts climbing after approximately 500 s and triggers a decision of a fault.

Through the requirement of detection and isolation within 500 s was not met, it succeeded in isolating the fault.

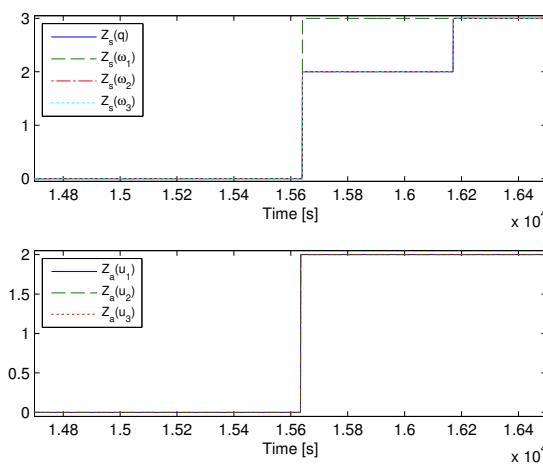


Figure 7.19: Simulation of a ground short circuit of gyroscope in CRF x-axis. Components of Z_s and Z_a

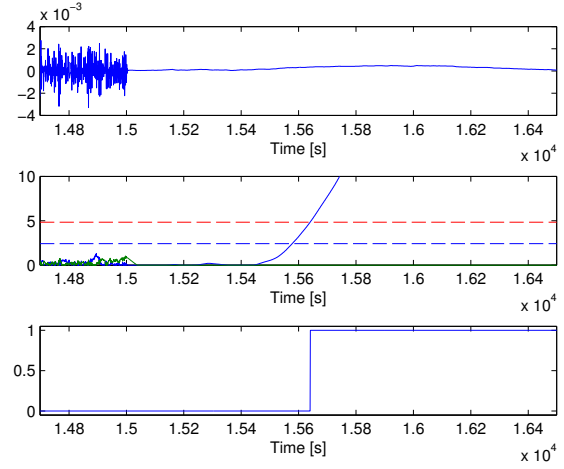


Figure 7.20: Simulation of a ground short circuit of gyroscope in CRF x-axis. Selected residual, with corresponding decision function and decision boolean

7.3.4 Detection of Biased Gyroscope

The FDI should detect and isolate if the gyroscope in one axis is instantly biased with $0.1 \text{ } ^\circ/\text{s}$.

A simulation in which the gyroscope in the 2nd axis has been instantly biased with $+0.1 \text{ } ^\circ/\text{s}$, is seen in Fig. 7.21 and Fig. 7.22.

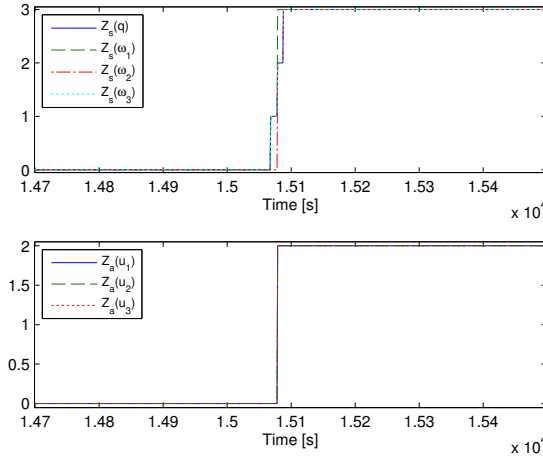


Figure 7.21: Simulation of an instant bias of the gyroscope in SBRF y-axis, for components of Z_s and Z_a

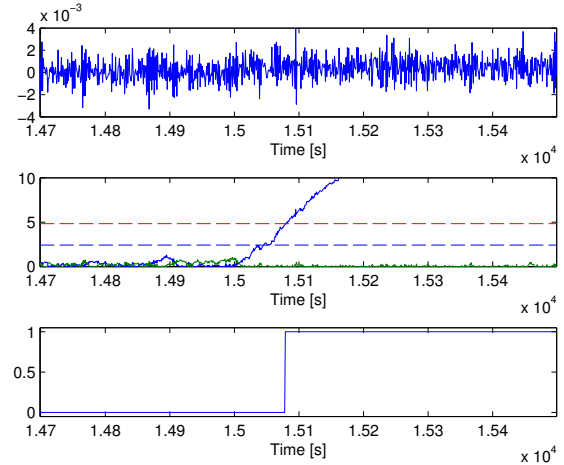


Figure 7.22: Simulation of an instant bias of the gyroscope in SBRF y-axis. Selected residual, with corresponding decision function and decision boolean

It is seen in Fig. 7.21 that the fault is detected 80 s after the fault occurs. However, the fault was incorrectly isolated to occur in the 1st axis, even though the fault occurred in the 2nd axis.

In Fig. 7.22, a slight offset of the residual can be spotted when the fault occurs, and

the decision function quickly exceeds its threshold triggering a decision of a fault.

Test Conclusion

As the FDI detected but isolated the fault incorrectly, within 500 s. The requirement is only partly satisfied.

7.3.5 Detection of Grounded Magnetorque

The FDI should detect and isolate if the magnetorquers dipole moment, in one plane of the satellite, is instantly reduced to zero.

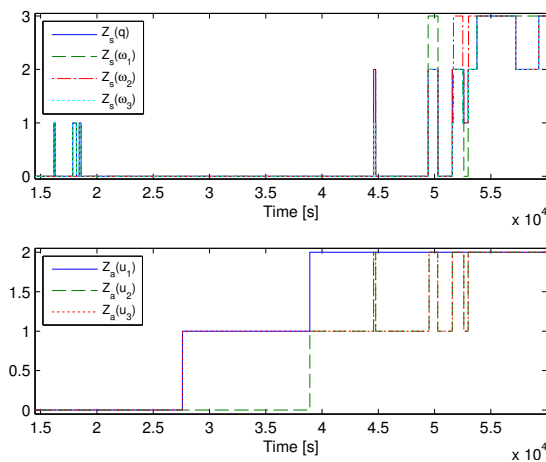


Figure 7.23: Simulation of the magnetorquers in SBRF xy-plane short circuited to ground for components of Z_s and Z_a

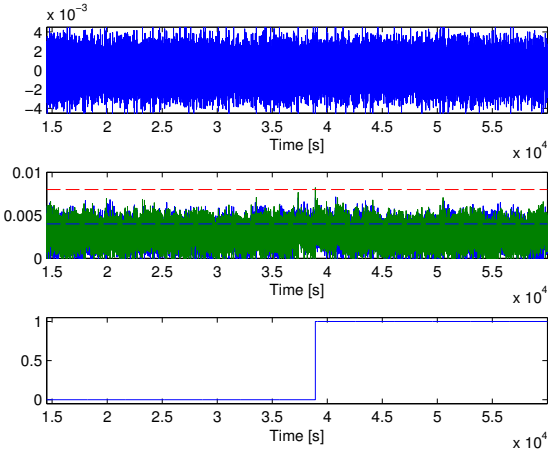


Figure 7.24: Simulation of the magnetorquers in SBRF xy-plane short circuited to ground. Selected residual, with corresponding decision function and decision logic

It is seen in Fig. 7.23, that a fault is not detected until 23913 s after the fault occurred. The fault is isolated to occur in the xy-axis.

In Fig. 7.24, it is noted that the decision function begins to have small oscillations and only an outlying noisy peak exceeds the upper threshold and triggers a decision of a occurred fault.

Test Conclusion

The FDI was very slow to detect the fault. When the fault eventually was detected, it was correctly isolated, but the observations of Fig. 7.24 could indicate that this may have been a random decision, and the results insinuate that the requirement has not been satisfied. Though slowly, it should be noted that a fault was eventually detected.

7.3.6 Detection of Supplied Magnetorquer

The FDI should detect and isolate if the magnetorquers dipole moment, in one plan of the satellite, is instantly increased to its maximum level.

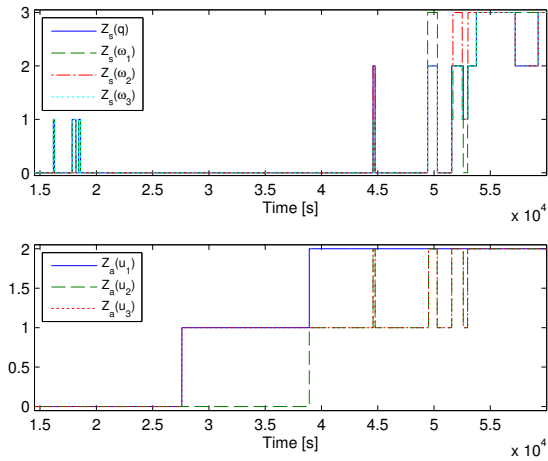


Figure 7.25: Simulation of the magnetorques in SBRF xy-plane short circuited to supply for the components Z_s and Z_a

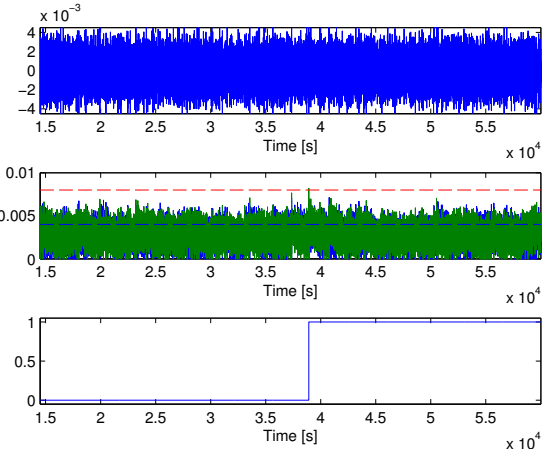


Figure 7.26: Simulation of the magnetorques in SBRF xy-plane short circuited to supply. Selected residual, with corresponding decision function and decision logic

It is seen in Fig. 7.21 that the fault is detected a few seconds after the fault has occurred. But the FDI is not able to detect which actuator is faulty. Also, the sensor fault decision function detect it as a fault shortly after.

Test Conclusion

As the FDI detected the fault within 500 s, but could not isolate it, the requirement is only partly satisfied.

Chapter 8

Closure

Roughly, the study handled out in this report is based on two main parts: one handling the attitude and angular velocity control system and one concerning with the detection of occurring transducer faults in the control system.

For the attitude control, three controllers are studied. One which lowers the angular rate (detumbling controller) and two which objective is to align with a given reference frame. The detumbling controller make use of the measured rate of the B-field vector (B-dot controller). Its primarily purpose will be to lower the rate after the satellite has been deployed from the P-POD, but is also the only controller which is able to run on the AVR8 introducing minimal power consumption. The reference frame controllers are designed to be able to align the satellite with both the ECI-frame (Inertial pointing) and the ORF-frame (Nadir pointing). Two different models, describing the kinematics and dynamics, of the satellite have been studied. One having an operating point in the ECI-frame and one in the ORF-frame. The model is simplified to describe an LTI-system (by averaging the approximated input matrix). The inertial and nadir pointing controllers are thus LTI-controllers, why the applied LQR-design is based on a stationary solution to the Riccati Equation. To test the stability of the found controllers, Floque theory for linear periodic system has been applied.

The detection of faults has been divided into two sub studies: a fault analysis and fault detection and isolation. In the analysis, the different fault types are described, along with the expected effects of them, and the propagation of faults is studied by a Failure Mode and Effect Analysis (FMEA). These fault scenarios have been narrowed down to the five most critical, by using severity and occurrence (SO) analysis.
The detection of faults is handled by Unknown Input Observers, generating model residuals to detect and isolate faults in the systems magnetorquers, gyroscopes and Attitude Determination System. The fault isolation has been conducted using the CUSUM-algorithm and decision logics.

8.1 Conclusion

From the acceptance test it is seen that detumbling B-dot controller is able to lower the angular velocity from an initial condition of 0.1 rad/s (on each axis) to below the required

0.0026 rad/s the majority of the time. Though a single axis, at a time, often is above the required (see Section 7.1).

Both reference pointing controllers fulfills the accept requirements since they were able of being in the neighborhood the given reference frame the over 90% of the time. For the nadir pointing controller the error, defined in eigenaxis angle, were under 30° 90% of the time which was significantly better than 50° accept requirement. Additionally it is noticed that the power consumption for the magnetorquers is extremely low which make it very suitable for implementation on the AAUSAT3.

From the acceptance test of the FDI in Section 7.3, it was observed that successful detection and isolation of some faults were possible. In the majority of the tests a fault was detected within 600 s, and in all the tests the fault was eventually detected.

It was suggested that the FDI, could falsely detect a fault in the ADS when the satellite is in eclipse and shortly after exiting eclipse. Thus, the FDI should not be regarded in this period.

In the test of faults in the gyroscope, it was possible to detect both faults within the time limit. However, the isolation proved incorrect. It was suggested that this was because in the system, faults happened in the SBRF frame while the UIOs are designed for faults in the CRF frame. A simulated was conducted, in which a fault was induced in the CRF frame. In this test, the FDI was able to correctly isolate the fault, though it was not able to do so until 142 s past the time limit. The FDI had most trouble, detecting and isolating if the magnetorques in one axis was short circuited to ground.

8.2 Perspective and Further Work

The acceptance tests in Chapter 7 show that the designed controllers are capable of aligning the CRF with the ECI and the ORF respectively, within an acceptable deviation. It was also observed that successful detection and isolation of some faults were possible. However, the system leaves several areas to be improved which is described in this section. Further work that should be conducted before and after launch is also described in this section.

Controllers

The B-dot controller is only tested for the case in which all three magnetorquers are working. Further study and tests with only two magnetorquers should be performed to determine if it is sufficient to stabilize the system. These studies and tests should be performed such that it can be verified that the supervisor can choose to make use of only two magnetorquers. Likewise, the constant gain controllers are only tested for the case in which all magnetorquers are working. Fault tolerant control could be designed for the scenario in which only two magnetorquers are working to study the performance and stability.

FDI

To improve the performance of the model based FDI, a model should be derived, which instead of describing ${}^c\omega_{co}$ and oq , describes ${}^s\omega_{so}$ and s_oq . This would improve the isolation probabilities, because the transducers are mounted in the SBRF and thus a transducer fault

would occur in one axis of the SBRF. The same transducer fault would appear in multiple axis of the CRF.

Through not within the time requirement, the model based FDI were able to detect all the tested faults, but the isolation proved insufficient. Alternative to trust the model based isolation, if a fault is detected, by the model based FDI, a test sequence could be started to isolate the faulty transducer. This could e.g. be an actuator testing sequence, sequentially testing each magnetorquer by using the magnetometers to measure the generated dipole moment.

Additionally, some of the mentioned simple FDI methods could be implemented, since they are capable of detecting and isolating some occurring transducer faults.

It could also be considered to include more sensors e.g. gyroscopes as these are considered relative inexpensive. It would then be possible to expand the use of the mentioned voting algorithm to detect and isolate faults.

Before Launch

The controllers and the FDI designed in this project need to be implemented on the micro-controllers which are gonna be on board AAUSAT3. The implementation should be conducted such that it is possible to alter the controller e.g. the feedback matrix and constants for the gain constant controllers and the B-dot controller respectively, after launch.

After Launch

Since most of the transducers, used on board AAUSAT3, has not been used in space before, the sensor measurements might differ from the expected and thereby the thresholds for the FDI algorithms will need some fine tuning. The gains for the different controllers are also parameters which could be fine tuned after launch. In this way, the performance of the controllers can be evaluated and changed while in flight.

Appendix A

General Rotational Kinematics

To be able to describe a rigid body with respect to an inertial frame , a general description of rotational kinematics is described.

The rotation of frame (B) seen from the inertial frame (A) is denoted by:

$${}^B\underline{\mathbf{C}}_A : \quad A \rightarrow B \quad (\text{A.1})$$

For short ${}^B\underline{\mathbf{C}}_A = \underline{\mathbf{C}}$. Frame A is spanned by a set of orthogonal unit vectors $[\mathbf{a}_1 \mathbf{a}_2 \mathbf{a}_3]^T$, likewise frame B is spanned by a set of orthogonal unit vectors $[\mathbf{b}_1 \mathbf{b}_2 \mathbf{b}_3]^T$. The matrix $\underline{\mathbf{C}}$ maps the set of vectors spanning frame A to the set of vectors spanning frame B by:

$$\begin{bmatrix} \mathbf{b}_1 \\ \mathbf{b}_2 \\ \mathbf{b}_3 \end{bmatrix} = \underline{\mathbf{C}} \begin{bmatrix} \mathbf{a}_1 \\ \mathbf{a}_2 \\ \mathbf{a}_3 \end{bmatrix} \quad (\text{A.2})$$

$$\Updownarrow \quad (\text{A.3})$$

$$\underline{\mathbf{C}} = \begin{bmatrix} \mathbf{b}_1 \\ \mathbf{b}_2 \\ \mathbf{b}_3 \end{bmatrix} \begin{bmatrix} \mathbf{a}_1 & \mathbf{a}_2 & \mathbf{a}_3 \end{bmatrix} \quad (\text{A.4})$$

$$= \begin{bmatrix} \mathbf{b}_1 \cdot \mathbf{a}_1 & \mathbf{b}_1 \cdot \mathbf{a}_2 & \mathbf{b}_1 \cdot \mathbf{a}_3 \\ \mathbf{b}_2 \cdot \mathbf{a}_1 & \mathbf{b}_2 \cdot \mathbf{a}_2 & \mathbf{b}_2 \cdot \mathbf{a}_3 \\ \mathbf{b}_3 \cdot \mathbf{a}_1 & \mathbf{b}_3 \cdot \mathbf{a}_2 & \mathbf{b}_3 \cdot \mathbf{a}_3 \end{bmatrix} \quad (\text{A.5})$$

From (A.4) it is seen that each entities in $\underline{\mathbf{C}}$ is described by an inner product of \mathbf{b}_i and \mathbf{a}_j vectors, which is the cosine of the angle between the two vectors. For this reason each entities is referred to as "direct cosines" and the matrix as the "direction cosine matrix". As $\underline{\mathbf{C}}$ maps between orthogonal unit vectors $\underline{\mathbf{C}}$ is an orthonormal matrix thus $\underline{\mathbf{C}}^T = \underline{\mathbf{C}}^{-1}$.

A.1 Euler Angles

The rotation performed by $\underline{\mathbf{C}}$ can be described by Euler angles, which rotates a coordinate system by three rotations over one body-axis at a time. Eulers rotation theorem states:

A rigid body can be moved from any orientation to an other by three successive rotations

around the coordinate body axis or by three successive rotations around the coordinate initial axis, as long as the same two rotations are not successive.

In matrix form these rotations are referred to as (when using a 3-2-1 set of Euler rotation):

$$\underline{\mathbf{C}}_3(\theta_3) : A \rightarrow A' \quad (\text{A.6})$$

$$\underline{\mathbf{C}}_2(\theta_2) : A' \rightarrow A'' \quad (\text{A.7})$$

$$\underline{\mathbf{C}}_1(\theta_1) : A'' \rightarrow B \quad (\text{A.8})$$

and given by

$$\underline{\mathbf{C}}_1(\theta_1) = \begin{bmatrix} 1 & 0 & 0 \\ 0 & \cos \theta_1 & \sin \theta_1 \\ 0 & -\sin \theta_1 & \cos \theta_1 \end{bmatrix} \quad (\text{A.9})$$

$$\underline{\mathbf{C}}_2(\theta_2) = \begin{bmatrix} \cos \theta_2 & 0 & -\sin \theta_2 \\ 0 & 1 & 0 \\ \sin \theta_2 & 0 & \cos \theta_2 \end{bmatrix} \quad (\text{A.10})$$

$$\underline{\mathbf{C}}_3(\theta_3) = \begin{bmatrix} \cos \theta_3 & \sin \theta_3 & 0 \\ -\sin \theta_3 & \cos \theta_3 & 0 \\ 0 & 0 & 1 \end{bmatrix} \quad (\text{A.11})$$

successive rotation from any attitude to any other attitude in three-dimentional space can be described by 12 different sets of Euler rotation sequences. Using a 3-2-1 set of Euler angles creates the following direction cosine matrix:

$$\underline{\mathbf{C}}(\theta_1, \theta_2, \theta_3) = \underline{\mathbf{C}}_1(\theta_1)\underline{\mathbf{C}}_2(\theta_2)\underline{\mathbf{C}}_3(\theta_3) \quad (\text{A.12})$$

$$\underline{\mathbf{C}}(\theta_1, \theta_2, \theta_3) = \begin{bmatrix} \cos \theta_2 \cos \theta_3 & \cos \theta_2 \sin \theta_3 & -\sin \theta_2 \\ \sin \theta_1 \sin \theta_2 \cos \theta_3 - \cos \theta_1 \sin \theta_3 & \sin \theta_1 \sin \theta_2 \sin \theta_3 + \cos \theta_1 \cos \theta_3 & \sin \theta_1 \cos \theta_2 \\ \cos \theta_1 \sin \theta_2 \cos \theta_3 + \sin \theta_1 \cos \theta_3 & \cos \theta_1 \sin \theta_2 \sin \theta_3 - \sin \theta_1 \cos \theta_3 & \cos \theta_1 \cos \theta_2 \end{bmatrix} \quad (\text{A.13})$$

An example of three successive rotation is illustrated in Fig. A.1. Fig. A.1 shows a (3-1-3) rotation sequence (easier to draw in perspective than a 3-2-1 sequence). The initial coordinate system A (black) is rotated around the third body-axis into A' (cyan), then tilted around the first body-axis into A'' (red) and then rotated around the third body-axis again into B (blue).

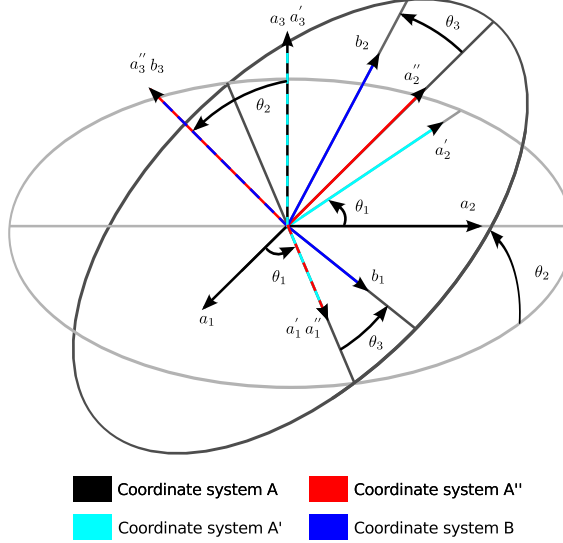


Figure A.1: Example of 3-1-3 Euler rotation sequence. $A \rightarrow A' \rightarrow A'' \rightarrow B$

A.2 Euler's Eigenaxis

Another way to describe a three-dimensional rotation in space is by the use of eigenaxis, where a rotation is described by the vector $\mathbf{e} = [e_1 \ e_2 \ e_3]^T$, and an angle θ . Euler's eigenaxis theorem states:

Rotating a rigid body about an axis that is fixed to the body and stationary in an inertial reference frame, the rigid body can be changed from any orientation to another. Such an axis is called an eigenaxis.

In other words, having a reference A and B, where the eigenvector \mathbf{e} is fixed in A, there exist a vector \mathbf{e} and a rotation of the frame B θ around that vector such that frame B can be aligned with A. For the eigenaxis the following is given:

$$\begin{aligned}\mathbf{e} &= e_1 \mathbf{a}_1 + e_2 \mathbf{a}_2 + e_3 \mathbf{a}_3 \\ &= e_1 \mathbf{b}_1 + e_2 \mathbf{b}_2 + e_3 \mathbf{b}_3\end{aligned}\tag{A.14}$$

An example of an eigenaxis rotation is seen in Fig. A.2.

In order to describe the direction cosine matrix by \mathbf{e} and θ , the rotation matrices $\underline{\mathbf{R}}$ and $\underline{\mathbf{C}}_1(\theta)$, is applied for the rotation. The matrix $\underline{\mathbf{R}}$ is given by:

$$\underline{\mathbf{R}} = {}^{A'}\underline{\mathbf{C}}_A = {}^B\underline{\mathbf{C}}_{A''} = \begin{bmatrix} e_1 & e_2 & e_3 \\ R_{21} & R_{22} & R_{23} \\ R_{31} & R_{32} & R_{33} \end{bmatrix}\tag{A.15}$$

For $\underline{\mathbf{R}}$ the orthonormality condition stands why $\underline{\mathbf{R}}^{-1} = \underline{\mathbf{R}}^T$ and

$$e_1^2 + e_2^2 + e_3^2 = 1\tag{A.16}$$

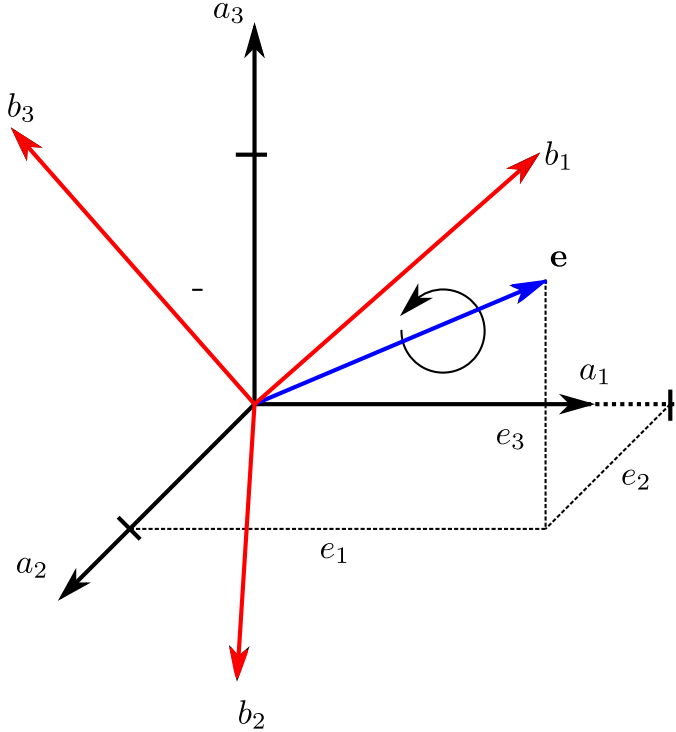


Figure A.2: Example of eigenaxis rotation. Here the eigenaxis is fixed in frame A and frame B is rotated by θ

The first rotation $\underline{\mathbf{R}}$, aligns the \mathbf{a}_1 with \mathbf{e} . For this reason when applying the matrix $\underline{\mathbf{R}}$ as described in (A.15) $\underline{\mathbf{C}}_1(\theta)$, which is defined by

$$\underline{\mathbf{C}}_1(\theta) = \begin{bmatrix} 1 & 0 & 0 \\ 0 & \cos \theta & \sin \theta \\ 0 & -\sin \theta & \cos \theta \end{bmatrix} \quad (\text{A.17})$$

must be used, as the rotations. A full rotation by eigenaxis is, by cosine direction matrices, given by:

$$\underline{\mathbf{C}}(\mathbf{e}, \theta) = \underline{\mathbf{R}}^T \underline{\mathbf{C}}_1(\theta) \underline{\mathbf{R}} \quad (\text{A.18})$$

Here the second rotation $\underline{\mathbf{C}}_1(\theta)$, rotates θ radians around \mathbf{e} , while the last rotation is done by the inverse of $\underline{\mathbf{R}}$, ($\underline{\mathbf{R}}^T$). Applying the orthogonality condition for $\underline{\mathbf{R}}$, the direction cosine matrix, can be described by \mathbf{e} and θ in the following manner:

$$\underline{\mathbf{C}}(\mathbf{e}, \theta) = \begin{bmatrix} \cos \theta + e_1^2(1 - \cos \theta) & e_1 e_2(1 - \cos \theta) + e_3 \sin \theta & e_1 e_3(1 - \cos \theta) + e_2 \sin \theta \\ e_2 e_1(1 - \cos \theta) + e_3 \sin \theta & \cos(\theta) + e_2^2(1 - \cos \theta) & e_2 e_3(1 - \cos \theta) + e_1 \sin \theta \\ e_3 e_1(1 - \cos \theta) + e_2 \sin \theta & e_3 e_2(1 - \cos \theta) + e_1 \sin \theta & \cos(\theta) + e_3^2(1 - \cos \theta) \end{bmatrix} \quad (\text{A.19})$$

A.3 Quaternions

By introducing quaternions defined by

$$q_1 = e_1 \sin\left(\frac{\theta}{2}\right) \quad (\text{A.20})$$

$$q_2 = e_2 \sin\left(\frac{\theta}{2}\right) \quad (\text{A.21})$$

$$q_3 = e_3 \sin\left(\frac{\theta}{2}\right) \quad (\text{A.22})$$

$$q_4 = \cos\left(\frac{\theta}{2}\right) \quad (\text{A.23})$$

the direction cosine matrix can be described in term of quaternions as:

$$\underline{C}(\mathbf{q}, q_4) = \begin{bmatrix} 1 - 2(q_2^2 + q_3^2) & 2(q_1q_2 + q_3q_4) & 2(q_1q_3 - q_2q_4) \\ 2(q_2q_1 - q_3q_4) & 1 - 2(q_2^2 + q_3^2) & 2(q_2q_3 + q_1q_4) \\ 2(q_3q_1 + q_2q_4) & 2(q_3q_2 - q_1q_4) & 1 - 2(q_2^2 + q_3^2) \end{bmatrix} \quad (\text{A.24})$$

Given a direction cosine matrix, the quaternions is described as:

$$q_4 = \sqrt{C_{11} + C_{22} + C_{33} + 1} \text{ for } 0 \leq \theta \leq \pi \quad (\text{A.25})$$

$$\begin{bmatrix} q_1 \\ q_2 \\ q_3 \end{bmatrix} = \frac{1}{4q_4} \begin{bmatrix} C_{23} - C_{32} \\ C_{31} - C_{13} \\ C_{12} - C_{21} \end{bmatrix} \text{ if } q_4 \neq 0 \quad (\text{A.26})$$

A.4 The Angular Velocity

In this report the angular velocity is described as a 3-dimensional vector, relative to three reference frames. Two reference frames are applied to describe the angular velocity of the object in the first frame with respect to the second frame, while the third describes in which coordinate system the velocity is expressed. This is written as

$${}^a\boldsymbol{\omega}_{bc} \quad (\text{A.27})$$

and is interpreted as the angular velocity of *b* wrt. *c*, expressed in the coordinates of *a*. Often it will only be necessary to apply two different reference frames to describe an angular velocity of an object, for instance ${}^c\boldsymbol{\omega}_{ci}$ (The angular velocity in *c* wrt. *i* expressed in *c*).

Addition of angular velocities can be described by the following. The angular velocity from frame *a* wrt. frame *c* is given by the angular velocity from *a* to *b* and that from *b* to *c*. This will of course need to be expressed in the same reference frame and the addition of angular velocities is thus given by

$${}^a\boldsymbol{\omega}_{ac} = {}^a\boldsymbol{\omega}_{ab} + {}^a\boldsymbol{\omega}_{bc} \quad (\text{A.28})$$

Appendix B

Quaternion Algebra

This appendix is based on [Kuipers 02]

B.1 Quaternion Multiplication

A quaternion can be described as hypercomplex number such that

$$\mathbf{q} = q_1 \hat{\mathbf{i}} + q_2 \hat{\mathbf{j}} + q_3 \hat{\mathbf{k}} + q_4 \quad (\text{B.1})$$

The quaternion product is defined as

$$\begin{aligned} \hat{\mathbf{i}}^2 &= \hat{\mathbf{j}}^2 = \hat{\mathbf{k}}^2 = \hat{\mathbf{i}}\hat{\mathbf{j}}\hat{\mathbf{k}} = -1 \\ \hat{\mathbf{i}}\hat{\mathbf{j}} &= -\hat{\mathbf{j}}\hat{\mathbf{i}} = \hat{\mathbf{k}} \\ \hat{\mathbf{j}}\hat{\mathbf{k}} &= -\hat{\mathbf{k}}\hat{\mathbf{j}} = \hat{\mathbf{i}} \\ \hat{\mathbf{k}}\hat{\mathbf{i}} &= -\hat{\mathbf{j}}\hat{\mathbf{k}} = \hat{\mathbf{j}} \end{aligned} \quad (\text{B.2})$$

To ease the calculations associated with the linearization the multiplication of two quaternions is performed here. It should be noted from (B.2) that the commutative law does not apply to the multiplication of quaternions.

By the multiplication of two quaternions (\mathbf{q}_B and \mathbf{q}_C) a single quaternion \mathbf{q}_A is obtained as

$$\begin{aligned} \mathbf{q}_A = \mathbf{q}_B \mathbf{q}_C &= (q_{B_1} \hat{\mathbf{i}} + q_{B_2} \hat{\mathbf{j}} + q_{B_3} \hat{\mathbf{k}} + q_{B_4}) (q_{C_1} \hat{\mathbf{i}} + q_{C_2} \hat{\mathbf{j}} + q_{C_3} \hat{\mathbf{k}} + q_{C_4}) \\ &= q_{B_1} q_{C_1} \hat{\mathbf{i}}^2 + q_{B_1} q_{C_2} \hat{\mathbf{i}}\hat{\mathbf{j}} + q_{B_1} q_{C_3} \hat{\mathbf{i}}\hat{\mathbf{k}} + q_{B_1} q_{C_4} \hat{\mathbf{i}} \\ &\quad + q_{B_2} q_{C_1} \hat{\mathbf{j}}\hat{\mathbf{i}} + q_{B_2} q_{C_2} \hat{\mathbf{j}}^2 + q_{B_2} q_{C_3} \hat{\mathbf{j}}\hat{\mathbf{k}} + q_{B_2} q_{C_4} \hat{\mathbf{j}} \\ &\quad + q_{B_3} q_{C_1} \hat{\mathbf{k}}\hat{\mathbf{i}} + q_{B_3} q_{C_2} \hat{\mathbf{k}}\hat{\mathbf{j}} + q_{B_3} q_{C_3} \hat{\mathbf{k}}^2 + q_{B_3} q_{C_4} \hat{\mathbf{k}} \\ &\quad + q_{B_4} q_{C_1} \hat{\mathbf{i}} + q_{B_4} q_{C_2} \hat{\mathbf{j}} + q_{B_4} q_{C_3} \hat{\mathbf{k}} + q_{B_4} q_{C_4} \end{aligned} \quad (\text{B.3})$$

which can be rearranged to

$$\begin{aligned} \mathbf{q}_A &= (q_{B_1} q_{C_4} + q_{B_2} q_{C_3} - q_{B_3} q_{C_2} + q_{B_4} q_{C_1}) \hat{\mathbf{i}} \\ &\quad + (-q_{B_1} q_{C_3} + q_{B_2} q_{C_4} + q_{B_3} q_{C_1} + q_{B_4} q_{C_2}) \hat{\mathbf{j}} \\ &\quad + (q_{B_1} q_{C_2} - q_{B_2} q_{C_1} + q_{B_3} q_{C_4} + q_{B_4} q_{C_3}) \hat{\mathbf{k}} \\ &\quad + (-q_{B_1} q_{C_1} - q_{B_2} q_{C_2} - q_{B_3} q_{C_3} + q_{B_4} q_{C_4}) \end{aligned} \quad (\text{B.4})$$

In matrix form this can be written as

$$\underbrace{\begin{bmatrix} q_{A_1} \\ q_{A_2} \\ q_{A_3} \\ q_{A_4} \end{bmatrix}}_{\mathbf{q}_A} = \mathbf{q}_B \mathbf{q}_C = \underbrace{\begin{bmatrix} q_{C_4} & q_{C_3} & -q_{C_2} & q_{C_1} \\ -q_{C_3} & q_{C_4} & q_{C_1} & q_{C_2} \\ q_{C_2} & -q_{C_1} & q_{C_4} & q_{C_3} \\ -q_{C_1} & -q_{C_2} & -q_{C_3} & q_{C_4} \end{bmatrix}}_{\underline{Q}_C} \underbrace{\begin{bmatrix} q_{B_1} \\ q_{B_2} \\ q_{B_3} \\ q_{B_4} \end{bmatrix}}_{\mathbf{q}_B} \quad (\text{B.5})$$

Defining $\mathbf{q}_{C_{1:3}} = [q_{C_1} \ q_{C_2} \ q_{C_3}]^T$ and a screw-symmetric matrix $\underline{\mathbf{S}}(\mathbf{q}_{C_{1:3}})$ to

$$\underline{\mathbf{S}}(\mathbf{q}_{C_{1:3}}) = \begin{bmatrix} 0 & -q_{C_3} & q_{C_2} \\ q_{C_3} & 0 & -q_{C_1} \\ -q_{C_2} & q_{C_1} & 0 \end{bmatrix} \quad (\text{B.6})$$

(B.5) can be written as

$$\mathbf{q}_A = \mathbf{q}_B \mathbf{q}_C = \underline{\mathbf{Q}}_C \mathbf{q}_B = \begin{bmatrix} -\underline{\mathbf{S}}(\mathbf{q}_{C_{1:3}}) + \underline{\mathbf{1}}_{3 \times 3} q_{C_4} & \mathbf{q}_{C_{1:3}} \\ -\mathbf{q}_{C_{1:3}}^T & q_{C_4} \end{bmatrix} \mathbf{q}_B \quad (\text{B.7})$$

From (B.7) it is seen that the product of two quaternions can be represented by a one of the quaternions and a matrix which includes the (real and complex) number of the other quaternion

B.2 Quaternion Addition and Subtraction

Given two quaternions \mathbf{q}_A and \mathbf{q}_B

$$\mathbf{q}_A = q_{A_1} \hat{\mathbf{i}} + q_{A_2} \hat{\mathbf{j}} + q_{A_3} \hat{\mathbf{k}} + q_{A_4} \quad (\text{B.8})$$

$$\mathbf{q}_B = q_{B_1} \hat{\mathbf{i}} + q_{B_2} \hat{\mathbf{j}} + q_{B_3} \hat{\mathbf{k}} + q_{B_4} \quad (\text{B.9})$$

the addition and subtraction of these are handled out as like regular complex numbers[Kuipers 02, p. 105], which yields

$$\mathbf{q}_A \pm \mathbf{q}_B = (q_{A_1} \pm q_{B_1}) \hat{\mathbf{i}} + (q_{A_2} \pm q_{B_2}) \hat{\mathbf{j}} + (q_{A_3} \pm q_{B_3}) \hat{\mathbf{k}} + (q_{A_4} \pm q_{B_4}) \quad (\text{B.10})$$

Thus addition and subtraction of quaternions is both associative and commutative.

B.3 Quaternion Complex Conjugate

The complex conjugate of a quaternion is defined by negating all imaginary parts of the quaternions such that

$$\mathbf{q}^* = -q_1 \hat{\mathbf{i}} - q_2 \hat{\mathbf{j}} - q_3 \hat{\mathbf{k}} + q_4 \quad (\text{B.11})$$

From here the following can easily be shown

$$(\mathbf{q}_A \mathbf{q}_B)^* = \mathbf{q}_B^* \mathbf{q}_A^* \quad (\text{B.12})$$

B.4 Quaternion Norm and Inverse

The norm of a quaternion is given by

$$\|\mathbf{q}\| = \mathbf{q}\mathbf{q}^* = \mathbf{q}^*\mathbf{q} = |\mathbf{q}|^2 = \sqrt{q_1^2 + q_2^2 + q_3^2 + q_4^2} \quad (\text{B.13})$$

As $\mathbf{q}\mathbf{q}^{-1} = \mathbf{q}^{-1}\mathbf{q} = 1$, the inverse of a quaternion is given by

$$\begin{aligned} \mathbf{q}^{-1}\mathbf{q}\mathbf{q}^* &= \mathbf{q}^* \\ \mathbf{q}^{-1}\|\mathbf{q}\| &= \mathbf{q}^* \\ &\Downarrow \\ \mathbf{q}^{-1} &= \frac{\mathbf{q}^*}{\|\mathbf{q}\|} \end{aligned} \quad (\text{B.14})$$

For unit quaternions (B.14) is reduced to

$$\mathbf{q}^{-1} = \mathbf{q}^* \quad (\text{B.15})$$

B.5 Quaternion Rotation of a Vector

By letting a vector \mathbf{v} be defined as a *pure quaternion* (a quaternion with real-value zero), the vector \mathbf{v} can be rotated into the vector \mathbf{w} by

$$\mathbf{w} = \mathbf{q}\mathbf{v}\mathbf{q}^* \quad (\text{B.16})$$

By the use of (B.16), the vector \mathbf{v} can be rotated between frames. In (B.17) \mathbf{v} is rotated from frame A to frame B .

$$\begin{bmatrix} {}^A\mathbf{w} \\ 0 \end{bmatrix} = \begin{bmatrix} {}^B\mathbf{v} \\ 0 \end{bmatrix} = {}^A\mathbf{q} \begin{bmatrix} {}^A\mathbf{v} \\ 0 \end{bmatrix} {}^A\mathbf{q}^* \quad (\text{B.17})$$

Appendix C

Dynamic Equations for Nadir pointing

In this appendix that dynamics for the nadir pointing is linearized by separating the constant, linear, and quadratic terms. Then all constant and quadratic terms is neglected.

$$\begin{aligned}
 {}^c\dot{\omega}_{ci} &= \underline{\mathbf{I}}^{-1}\underline{\mathbf{S}}(\underline{\mathbf{C}}({}^c\mathbf{q}){}^o\omega_{oi} + {}^c\omega_{co})\underline{\mathbf{I}}(\underline{\mathbf{C}}({}^c\mathbf{q}){}^o\omega_{oi} + {}^c\omega_{co}) \\
 &= (\underline{\mathbf{I}}^{-1}\underline{\mathbf{S}}(\underline{\mathbf{C}}({}^c\mathbf{q}){}^o\omega_{oi}) + \underline{\mathbf{I}}^{-1}\underline{\mathbf{S}}({}^c\omega_{co}))(\underline{\mathbf{I}}\underline{\mathbf{C}}({}^c\mathbf{q}){}^o\omega_{oi} + \underline{\mathbf{I}}{}^c\omega_{co}) \\
 &= \underbrace{\underline{\mathbf{I}}^{-1}\underline{\mathbf{S}}(\underline{\mathbf{C}}({}^c\mathbf{q}){}^o\omega_{oi})\underline{\mathbf{I}}\underline{\mathbf{C}}({}^c\mathbf{q}){}^o\omega_{oi}}_{(1)} + \underbrace{\underline{\mathbf{I}}^{-1}\underline{\mathbf{S}}(\underline{\mathbf{C}}({}^c\mathbf{q}){}^o\omega_{oi})\underline{\mathbf{I}}{}^c\omega_{co}}_{(2)} \\
 &\quad + \underbrace{\underline{\mathbf{I}}^{-1}\underline{\mathbf{S}}({}^c\omega_{co})\underline{\mathbf{I}}\underline{\mathbf{C}}({}^c\mathbf{q}){}^o\omega_{oi}}_{(3)} + \underbrace{\underline{\mathbf{I}}^{-1}\underline{\mathbf{S}}({}^c\omega_{co})\underline{\mathbf{I}}{}^c\omega_{co}}_{quadratic}
 \end{aligned} \tag{C.1}$$

where (1)

$$\begin{aligned}
 \underline{\mathbf{I}}^{-1}\underline{\mathbf{S}}(\underline{\mathbf{C}}({}^c\mathbf{q}){}^o\omega_{oi})\underline{\mathbf{I}}\underline{\mathbf{C}}({}^c\mathbf{q}){}^o\omega_{oi} &\approx \underline{\mathbf{I}}^{-1}\underline{\mathbf{S}}({}^o\omega_{oi} + \underline{\mathbf{S}}({}^c\mathbf{q}){}^o\omega_{oi})\underline{\mathbf{I}}({}^o\omega_{oi} + \underline{\mathbf{S}}({}^c\mathbf{q}){}^o\omega_{oi}) \\
 &\approx (\underline{\mathbf{I}}^{-1}\underline{\mathbf{S}}({}^o\omega_{oi}) + \underline{\mathbf{I}}^{-1}\underline{\mathbf{S}}(\underline{\mathbf{S}}({}^c\mathbf{q}){}^o\omega_{oi}))(\underline{\mathbf{I}}{}^o\omega_{oi} + \underline{\mathbf{I}}\underline{\mathbf{S}}({}^c\mathbf{q}){}^o\omega_{oi}) \\
 &\approx \underbrace{\underline{\mathbf{I}}^{-1}\underline{\mathbf{S}}({}^o\omega_{oi})\underline{\mathbf{I}}{}^o\omega_{oi}}_0 + \underbrace{\underline{\mathbf{I}}^{-1}\underline{\mathbf{S}}({}^o\omega_{oi})\underline{\mathbf{I}}\underline{\mathbf{S}}({}^c\mathbf{q}){}^o\omega_{oi}}_{linear} \\
 &\quad + \underbrace{\underline{\mathbf{I}}^{-1}\underline{\mathbf{S}}(\underline{\mathbf{S}}({}^c\mathbf{q}){}^o\omega_{oi})\underline{\mathbf{I}}{}^o\omega_{oi}}_{linear} + \underbrace{\underline{\mathbf{I}}^{-1}\underline{\mathbf{S}}({}^c\mathbf{q}){}^o\omega_{oi}\underline{\mathbf{I}}\underline{\mathbf{S}}({}^c\mathbf{q}){}^o\omega_{oi}}_{quadratic}
 \end{aligned} \tag{C.2}$$

where (2)

$$\begin{aligned}
 \underline{\mathbf{I}}^{-1}\underline{\mathbf{S}}(\underline{\mathbf{C}}({}^c\mathbf{q}){}^o\omega_{co})\underline{\mathbf{I}}{}^c\omega_{co} &\approx \underline{\mathbf{I}}^{-1}\underline{\mathbf{S}}(\underline{\mathbf{C}}({}^c\mathbf{q}){}^o\omega_{oi})\underline{\mathbf{I}}{}^o\omega_{oi} \\
 &\approx \underline{\mathbf{I}}^{-1}\underline{\mathbf{S}}({}^o\omega_{oi} + \underline{\mathbf{S}}({}^c\mathbf{q}){}^o\omega_{oi})\underline{\mathbf{I}}{}^c\omega_{co} \\
 &\approx \underline{\mathbf{I}}^{-1}\underline{\mathbf{S}}({}^o\omega_{oi})\underline{\mathbf{I}}{}^c\omega_{co} + \underline{\mathbf{I}}^{-1}\underline{\mathbf{S}}(\underline{\mathbf{S}}({}^c\mathbf{q}){}^o\omega_{oi})\underline{\mathbf{I}}{}^c\omega_{co} \\
 &\approx \underline{\mathbf{I}}^{-1}\underline{\mathbf{S}}({}^o\omega_{oi})\underline{\mathbf{I}}{}^c\omega_{co} - \underline{\mathbf{I}}^{-1}\underline{\mathbf{S}}(\underline{\mathbf{S}}({}^o\omega_{oi}){}^c\mathbf{q})\underline{\mathbf{I}}{}^c\omega_{co} \\
 &\approx \underbrace{\underline{\mathbf{I}}^{-1}\underline{\mathbf{S}}({}^o\omega_{oi})\underline{\mathbf{I}}{}^c\omega_{co}}_{linear} + \underbrace{\underline{\mathbf{I}}^{-1}\underline{\mathbf{S}}({}^o\omega_{oi})\underline{\mathbf{S}}({}^c\mathbf{q})\underline{\mathbf{I}}{}^c\omega_{co}}_{quadratic}
 \end{aligned} \tag{C.3}$$

where (3)

$$\begin{aligned}
 \underline{\mathbf{I}}^{-1}\underline{\mathbf{S}}({}^c\omega_{co})\underline{\mathbf{I}}\underline{\mathbf{C}}({}^c\mathbf{q}){}^o\omega_{oi} &\approx \underline{\mathbf{I}}^{-1}\underline{\mathbf{S}}({}^c\omega_{co})\underline{\mathbf{I}}({}^o\omega_{oi} + \underline{\mathbf{S}}({}^c\mathbf{q}){}^o\omega_{oi}) \\
 &\approx \underbrace{\underline{\mathbf{I}}^{-1}\underline{\mathbf{S}}({}^c\omega_{co})\underline{\mathbf{I}}{}^o\omega_{oi}}_{linear} - \underbrace{\underline{\mathbf{I}}^{-1}\underline{\mathbf{S}}({}^c\omega_{co})\underline{\mathbf{I}}\underline{\mathbf{S}}({}^o\omega_{oi}){}^c\mathbf{q}}_{quadratic}
 \end{aligned} \tag{C.4}$$

Appendix D

Linearization of Model Equations

The non-linear dynamic and kinematic equations of motion is described in Section 3.3.3 an is given by

$$\begin{bmatrix} \dot{\mathbf{q}} \\ \dot{\boldsymbol{\omega}} \end{bmatrix} = \left[\underline{\mathbf{I}}^{-1} (-^C \underline{\mathbf{S}}(\boldsymbol{\omega}) \underline{\mathbf{I}}^C \boldsymbol{\omega} + ^C \mathbf{N}_{dist} + ^C \mathbf{N}_{control}) \right] \quad (\text{D.1})$$

D.1 Linearization of Kinematics

The kinematic equations are given by

$$\begin{aligned} \dot{\mathbf{q}} &= \frac{1}{2} \underline{\Omega} \mathbf{q} \\ &= \frac{1}{2} \underbrace{\begin{bmatrix} \underline{\mathbf{S}}(\boldsymbol{\omega}) & \boldsymbol{\omega} \\ -\boldsymbol{\omega}^T & 0 \end{bmatrix}}_{\underline{\Omega}} \mathbf{q} \end{aligned} \quad (\text{D.2})$$

In the following a bar (e.g. $\bar{\mathbf{q}}$) denotes the operating point of a given quaternion while the tilde (e.g. $\tilde{\mathbf{q}}$) denotes a small-signal value of the quaternion close to the operating point. The following applies to the linearization of quaternions near a given operating point[Kuipers 02, p. 119][Bak 99, p. 61].

$$\mathbf{q} = \mathbf{q}(t + \Delta t) = \mathbf{q}(t)\mathbf{q}(\Delta t) = \bar{\mathbf{q}}\tilde{\mathbf{q}} \quad (\text{D.3})$$

as $\mathbf{q}^* = \mathbf{q}^{-1}$ why

$$\tilde{\mathbf{q}} = \bar{\mathbf{q}}^* \mathbf{q} \quad (\text{D.4})$$

By introducing the angular rate vector as a pure quaternion

$$\mathbf{q}_\omega = \bar{\mathbf{q}}_\omega + \tilde{\mathbf{q}}_\omega = \begin{bmatrix} \boldsymbol{\omega} \\ 0 \end{bmatrix} = \begin{bmatrix} \bar{\boldsymbol{\omega}} + \tilde{\boldsymbol{\omega}} \\ 0 \end{bmatrix} = \begin{bmatrix} \omega_1 \\ \omega_2 \\ \omega_3 \\ 0 \end{bmatrix} = \begin{bmatrix} \bar{\omega}_1 + \tilde{\omega}_1 \\ \bar{\omega}_2 + \tilde{\omega}_2 \\ \bar{\omega}_3 + \tilde{\omega}_3 \\ 0 \end{bmatrix} \quad (\text{D.5})$$

The multiplication of quaternions can be expressed as a matrix-vector product as described by (B.7) in Section B.1, why the matrix-vector product in (D.2) can also be described by a quaternion multiplication. (D.2) can thus be rewritten as

$$\dot{\mathbf{q}} = \frac{1}{2} \mathbf{q} \mathbf{q}_\omega \quad (\text{D.6})$$

It should be noticed that the contribution from q_{C_4} in (B.7) is omitted in (D.6) as the last entry in \mathbf{q}_ω is zero. Taking the time derivative of (D.4) yields by the product rule

$$\dot{\tilde{\mathbf{q}}} = \dot{\bar{\mathbf{q}}}^* \mathbf{q} + \bar{\mathbf{q}}^* \dot{\mathbf{q}} \quad (\text{D.7})$$

It is now desirable to manipulate the equation such that the derivative small-signal value of the positioning quaternion ($\dot{\tilde{\mathbf{q}}}$) solemnly depends on operating point and small-signal values of the positioning and angular velocity quaternions. By inserting (D.6) into (D.7) and applying (D.4), the following is obtained:

$$\begin{aligned} \dot{\tilde{\mathbf{q}}} &= \left(\frac{1}{2} \bar{\mathbf{q}} \bar{\mathbf{q}}_\omega \right)^* \mathbf{q} + \bar{\mathbf{q}}^* \left(\frac{1}{2} \mathbf{q} \mathbf{q}_\omega \right) \\ &= \frac{1}{2} ((\bar{\mathbf{q}} \bar{\mathbf{q}}_\omega)^* \mathbf{q} + \bar{\mathbf{q}}^* \mathbf{q} \mathbf{q}_\omega) \\ &= \frac{1}{2} ((\bar{\mathbf{q}} \bar{\mathbf{q}}_\omega)^* \mathbf{q} + \tilde{\mathbf{q}} \mathbf{q}_\omega) \end{aligned} \quad (\text{D.8})$$

and by applying the quaternion properties $(\mathbf{q} \mathbf{q}_\omega)^* = \mathbf{q}_\omega^* \mathbf{q}^*$, $\mathbf{q}_\omega^* = -\mathbf{q}_\omega$ (only true for pure quaternions), and (D.4) yields

$$\begin{aligned} \dot{\tilde{\mathbf{q}}} &= \frac{1}{2} (\bar{\mathbf{q}}_\omega^* \bar{\mathbf{q}}^* \mathbf{q} + \tilde{\mathbf{q}} \mathbf{q}_\omega) \\ &= \frac{1}{2} (-\bar{\mathbf{q}}_\omega \tilde{\mathbf{q}} + \tilde{\mathbf{q}} \mathbf{q}_\omega) \end{aligned} \quad (\text{D.9})$$

By substituting \mathbf{q}_ω in (D.9) by (D.5) yields

$$\begin{aligned} \dot{\tilde{\mathbf{q}}} &= \frac{1}{2} (-\bar{\mathbf{q}}_\omega \tilde{\mathbf{q}} + \tilde{\mathbf{q}} (\bar{\mathbf{q}}_\omega + \tilde{\mathbf{q}}_\omega)) \\ &= \frac{1}{2} (-\bar{\mathbf{q}}_\omega \tilde{\mathbf{q}} + \tilde{\mathbf{q}} \bar{\mathbf{q}}_\omega + \tilde{\mathbf{q}} \tilde{\mathbf{q}}_\omega) \end{aligned} \quad (\text{D.10})$$

In (D.10) the differential equations for small-signal values are obtained. Expressing this as a matrix-vector product (as described in Section B.1) the first two terms are thus given by

$$\begin{aligned} \bar{\mathbf{q}}_\omega \tilde{\mathbf{q}} &= \begin{bmatrix} -\underline{\mathbf{S}}(\tilde{\mathbf{q}}_{1:3}) + \underline{\mathbf{1}}_{3x3} \tilde{q}_4 & \tilde{\mathbf{q}}_{1:3} \\ -\tilde{\mathbf{q}}_{1:3}^T & \tilde{q}_4 \end{bmatrix} \begin{bmatrix} \bar{\boldsymbol{\omega}} \\ 0 \end{bmatrix} \\ &= \begin{bmatrix} (-\underline{\mathbf{S}}(\tilde{\mathbf{q}}_{1:3}) + \underline{\mathbf{1}}_{3x3} \tilde{q}_4) \bar{\boldsymbol{\omega}} \\ -\tilde{\mathbf{q}}_{1:3}^T \bar{\boldsymbol{\omega}} \end{bmatrix} \\ &= \begin{bmatrix} \underline{\mathbf{S}}(\bar{\boldsymbol{\omega}}) \tilde{\mathbf{q}}_{1:3} + \underline{\mathbf{1}}_{3x3} \tilde{q}_4 \bar{\boldsymbol{\omega}} \\ -\tilde{\mathbf{q}}_{1:3}^T \bar{\boldsymbol{\omega}} \end{bmatrix} \end{aligned} \quad (\text{D.11})$$

In (D.11) the identity $-\underline{\mathbf{S}}(\tilde{\mathbf{q}}_{1:3}) \bar{\boldsymbol{\omega}} = \underline{\mathbf{S}}(\bar{\boldsymbol{\omega}}) \tilde{\mathbf{q}}_{1:3}$ is used.

$$\begin{aligned} \tilde{\mathbf{q}} \bar{\mathbf{q}}_\omega &= \begin{bmatrix} -\underline{\mathbf{S}}(\bar{\boldsymbol{\omega}}) & \bar{\boldsymbol{\omega}} \\ -\bar{\boldsymbol{\omega}}^T & 0 \end{bmatrix} \begin{bmatrix} \tilde{\mathbf{q}}_{1:3} \\ \tilde{q}_4 \end{bmatrix} \\ &= \begin{bmatrix} -\underline{\mathbf{S}}(\bar{\boldsymbol{\omega}}) \tilde{\mathbf{q}}_{1:3} + \bar{\boldsymbol{\omega}} \tilde{q}_4 \\ -\bar{\boldsymbol{\omega}}^T \tilde{\mathbf{q}}_{1:3} \end{bmatrix} \end{aligned} \quad (\text{D.12})$$

Noting the following property of quaternions:

$$\lim_{\theta \rightarrow 0} \mathbf{q} = \lim_{\theta \rightarrow 0} \begin{bmatrix} e \sin\left(\frac{\theta}{2}\right) \\ \cos\left(\frac{\theta}{2}\right) \end{bmatrix} = \begin{cases} \mathbf{q}_{1:3} \rightarrow 0 \\ q_4 \rightarrow 1 \end{cases} \quad (\text{D.13})$$

The third term ($\tilde{\mathbf{q}}\tilde{\mathbf{q}}_\omega$) can be rewritten by the use of (B.7), and afterwards approximated using (D.13).

$$\begin{aligned} \tilde{\mathbf{q}}\tilde{\mathbf{q}}_\omega &= \begin{bmatrix} -\underline{\mathbf{S}}(\tilde{\boldsymbol{\omega}}) & \tilde{\boldsymbol{\omega}} \\ -\tilde{\boldsymbol{\omega}}^T & 0 \end{bmatrix} \begin{bmatrix} \tilde{\mathbf{q}}_{1:3} \\ \tilde{q}_4 \end{bmatrix} = \begin{bmatrix} -\underline{\mathbf{S}}(\tilde{\boldsymbol{\omega}})\tilde{\mathbf{q}}_{1:3} + \tilde{\boldsymbol{\omega}}\tilde{q}_4 \\ -\tilde{\boldsymbol{\omega}}^T\tilde{\mathbf{q}}_{1:3} + 0\tilde{q}_4 \end{bmatrix} \\ &\approx \begin{bmatrix} [0] \\ [0] \\ [0] \\ [0] \end{bmatrix} + \begin{bmatrix} \tilde{\omega}_1 \\ \tilde{\omega}_2 \\ \tilde{\omega}_3 \\ 0 \end{bmatrix} \tilde{q}_4 \approx \begin{bmatrix} \tilde{\omega}_1 \\ \tilde{\omega}_2 \\ \tilde{\omega}_3 \\ 0 \end{bmatrix} = \tilde{\mathbf{q}}_\omega \end{aligned} \quad (\text{D.14})$$

By substituting (D.11), (D.12), and (D.14) into (D.10) gives

$$\begin{aligned} \dot{\tilde{\mathbf{q}}} &= \frac{1}{2} \left(- \begin{bmatrix} \underline{\mathbf{S}}(\bar{\boldsymbol{\omega}})\tilde{\mathbf{q}}_{1:3} + \mathbf{1}_{3x3}\tilde{q}_4\bar{\boldsymbol{\omega}} \\ -\tilde{\mathbf{q}}_{1:3}^T\bar{\boldsymbol{\omega}} \end{bmatrix} + \begin{bmatrix} -\underline{\mathbf{S}}(\bar{\boldsymbol{\omega}})\tilde{\mathbf{q}}_{1:3} + \bar{\boldsymbol{\omega}}\tilde{q}_4 \\ -\bar{\boldsymbol{\omega}}^T\tilde{\mathbf{q}}_{1:3} \end{bmatrix} + \tilde{\mathbf{q}}\tilde{\mathbf{q}}_\omega \right) \\ &= \begin{bmatrix} -\underline{\mathbf{S}}(\bar{\boldsymbol{\omega}}) \\ \mathbf{0}_{1x3} \end{bmatrix} \tilde{\mathbf{q}}_{1:3} + \frac{1}{2} \tilde{\mathbf{q}}\tilde{\mathbf{q}}_\omega \\ &\approx \begin{bmatrix} -\underline{\mathbf{S}}(\bar{\boldsymbol{\omega}}) \\ \mathbf{0}_{1x3} \end{bmatrix} \tilde{\mathbf{q}}_{1:3} + \frac{1}{2} \tilde{\mathbf{q}}_\omega \end{aligned} \quad (\text{D.15})$$

Removing the zeroes from (D.15) yields

$$\dot{\tilde{\mathbf{q}}}_{1:3} = -\underline{\mathbf{S}}(\bar{\boldsymbol{\omega}})\tilde{\mathbf{q}}_{1:3} + \frac{1}{2}\tilde{\boldsymbol{\omega}} \quad (\text{D.16})$$

D.2 Linearization of Dynamics

The non-linear dynamic equation is given by

$$\dot{\boldsymbol{\omega}} = \underline{\mathbf{I}}^{-1}(-\underline{\mathbf{S}}(\boldsymbol{\omega})\underline{\mathbf{I}}\boldsymbol{\omega} + \mathbf{N}_{dist} + \mathbf{N}_{control}) \quad (\text{D.17})$$

The angular velocity vector can be described as a small signal value $\tilde{\boldsymbol{\omega}}$ around an operating point $\bar{\boldsymbol{\omega}}$ thus

$$\boldsymbol{\omega} = \bar{\boldsymbol{\omega}} + \tilde{\boldsymbol{\omega}} \quad (\text{D.18})$$

The linearization of $\dot{\boldsymbol{\omega}}$ is conducted by a first order Taylor-approximation. For notational simplicity the following notation is used

- $x = (\boldsymbol{\omega}, \mathbf{N}_{dist}, \mathbf{N}_{control})$ - the parameters which $\dot{\boldsymbol{\omega}}$ is a function of.
- $\bar{x} = (\bar{\boldsymbol{\omega}}, \bar{\mathbf{N}}_{dist}, \bar{\mathbf{N}}_{control})$ are the small signal values of x
- $\tilde{x} = (\tilde{\boldsymbol{\omega}}, \tilde{\mathbf{N}}_{dist}, \tilde{\mathbf{N}}_{control})$ are the small signal values of x

The first order Taylor-approximation is given by

$$\begin{aligned}\dot{\omega}(x) &\approx \dot{\omega}(\bar{x}) + \nabla \dot{\omega}(x)|_{x=\bar{x}} \tilde{x} \\ &= \dot{\omega}(\bar{x}) + \frac{\delta \dot{\omega}(x)}{\delta \omega}|_{x=\bar{x}} \tilde{\omega} + \frac{\delta \dot{\omega}(x)}{\delta \mathbf{N}_{dist}}|_{x=\bar{x}} \tilde{\mathbf{N}}_{dist} + \frac{\delta \dot{\omega}(x)}{\delta \mathbf{N}_{control}}|_{x=\bar{x}} \tilde{\mathbf{N}}_{control}\end{aligned}\quad (\text{D.19})$$

Now the stationary equation ($\dot{\omega}(\bar{x})$) is subtracted from (D.19) to archive a linearized small signal equation and the applying (D.17).

$$\begin{aligned}\dot{\tilde{\omega}}(\omega, \mathbf{N}_{control}, \mathbf{N}_{dist}) &\approx \frac{\delta}{\delta \omega} \dot{\omega}(\omega, \mathbf{N}_{control}, \mathbf{N}_{dist})|_{\omega=\bar{\omega}} \tilde{\omega} \\ &\quad + \frac{\delta}{\delta \mathbf{N}_{control}} \dot{\omega}(\omega, \mathbf{N}_{control}, \mathbf{N}_{dist})|_{\mathbf{N}_{control}=\bar{\mathbf{N}}_{control}} \tilde{\mathbf{N}}_{control} \\ &\quad + \frac{\delta}{\delta \mathbf{N}_{dist}} \dot{\omega}(\omega, \mathbf{N}_{control}, \mathbf{N}_{dist})|_{\mathbf{N}_{dist}=\bar{\mathbf{N}}_{dist}} \tilde{\mathbf{N}}_{dist} \\ &\Updownarrow \\ \dot{\tilde{\omega}}(\omega, \mathbf{N}_{control}, \mathbf{N}_{dist}) &\approx -\underline{\mathbf{I}}^{-1} \frac{\delta}{\delta \omega} \underline{\mathbf{S}}(\omega) \underline{\mathbf{I}} \omega|_{\omega=\bar{\omega}} \tilde{\omega} \\ &\quad + \underline{\mathbf{I}}^{-1} \frac{\delta}{\delta \mathbf{N}_{control}} \mathbf{N}_{control}|_{\mathbf{N}_{control}=\bar{\mathbf{N}}_{control}} \tilde{\mathbf{N}}_{control} \\ &\quad + \underline{\mathbf{I}}^{-1} \frac{\delta}{\delta \mathbf{N}_{dist}} \mathbf{N}_{dist}|_{\mathbf{N}_{dist}=\bar{\mathbf{N}}_{dist}} \tilde{\mathbf{N}}_{dist} \\ &\Updownarrow \\ \dot{\tilde{\omega}}(\omega, \mathbf{N}_{control}, \mathbf{N}_{dist}) &\approx -\underline{\mathbf{I}}^{-1} \left[\frac{\delta}{\delta \omega} \underline{\mathbf{S}}(\omega)|_{\omega=\bar{\omega}} \underline{\mathbf{I}} \bar{\omega} + \underline{\mathbf{S}}(\bar{\omega}) \frac{\delta}{\delta \omega} \underline{\mathbf{I}} \omega|_{\omega=\bar{\omega}} \right] \tilde{\omega} \\ &\quad + \underline{\mathbf{I}}^{-1} \tilde{\mathbf{N}}_{control} + \underline{\mathbf{I}}^{-1} \tilde{\mathbf{N}}_{dist}\end{aligned}\quad (\text{D.20})$$

By applying the identity $\underline{\mathbf{S}}(\omega) \underline{\mathbf{I}} \bar{\omega} = -\underline{\mathbf{S}}(\underline{\mathbf{I}} \bar{\omega}) \omega$, (D.20) can be rewritten to

$$\begin{aligned}\dot{\tilde{\omega}}(\omega, \mathbf{N}_{control}, \mathbf{N}_{dist}) &\approx \underline{\mathbf{I}}^{-1} \left[\underline{\mathbf{S}}(\underline{\mathbf{I}} \bar{\omega}) \frac{\delta}{\delta \omega} \omega|_{\omega=\bar{\omega}} - \underline{\mathbf{S}}(\bar{\omega}) \frac{\delta}{\delta \omega} \underline{\mathbf{I}} \omega|_{\omega=\bar{\omega}} \right] \tilde{\omega} \\ &\quad + \underline{\mathbf{I}}^{-1} \tilde{\mathbf{N}}_{control} + \underline{\mathbf{I}}^{-1} \tilde{\mathbf{N}}_{dist}\end{aligned}\quad (\text{D.21})$$

This yields the following linearized equations

$$\dot{\tilde{\omega}} = \underline{\mathbf{I}}^{-1} [\underline{\mathbf{S}}(\underline{\mathbf{I}} \bar{\omega}) - \underline{\mathbf{S}}(\bar{\omega}) \underline{\mathbf{I}}] \tilde{\omega} + \underline{\mathbf{I}}^{-1} \tilde{\mathbf{N}}_{control} + \underline{\mathbf{I}}^{-1} \tilde{\mathbf{N}}_{dist} \quad (\text{D.22})$$

D.3 The Linearized Model

By the use of (D.16) and (D.22) the equations for the linearized kinematic and dynamic is combined to

$$\begin{bmatrix} \dot{\tilde{\mathbf{q}}}_{1:3} \\ \dot{\tilde{\omega}} \end{bmatrix} = \begin{bmatrix} -\underline{\mathbf{S}}(\bar{\omega}) & \frac{1}{2} \underline{\mathbf{1}}_{3 \times 3} \\ \underline{\mathbf{0}}_{3 \times 3} & \underline{\mathbf{I}}^{-1} [\underline{\mathbf{S}}(\underline{\mathbf{I}} \bar{\omega}) - \underline{\mathbf{S}}(\bar{\omega}) \underline{\mathbf{I}}] \end{bmatrix} \begin{bmatrix} \tilde{\mathbf{q}}_{1:3} \\ \tilde{\omega} \end{bmatrix} + \begin{bmatrix} \underline{\mathbf{0}}_{3 \times 3} \\ \underline{\mathbf{I}}^{-1} \end{bmatrix} \begin{bmatrix} \tilde{\mathbf{N}}_{control} \\ \tilde{\mathbf{N}}_{dist} \end{bmatrix} \quad (\text{D.23})$$

Appendix E

The State Transition Matrix

This section is based on [Mohler 99, chap. 3 and 4] and [Ward 10].

E.1 The Time-independent System

Given a homogeneous linear differential equation with n states and constant coefficients

$$\dot{\mathbf{x}}(t) = \underline{\mathbf{A}}\mathbf{x}(t) \quad (\text{E.1})$$

(E.1) can be rewritten to a matrix differential equation by the use of the fundamental matrix $\underline{\mathbf{X}}(t)$, which contains a basis of the vector space. In this way $\underline{\mathbf{X}}(t)$ contains n linearly independent solutions to (E.1). The matrix differential equation is thus given by

$$\dot{\underline{\mathbf{X}}}(t) = \underline{\mathbf{A}}\underline{\mathbf{X}}(t) \quad (\text{E.2})$$

With the initial time $t_0 = 0$ and the initial state $\mathbf{x}(t_0) = \mathbf{x}_0$, (E.1) is solved by

$$\mathbf{x}(t, \mathbf{x}_0, t_0) = e^{\underline{\mathbf{A}}(t-t_0)} \mathbf{x}_0 = e^{\underline{\mathbf{A}}t} \mathbf{x}_0 \quad (\text{E.3})$$

Here the exponential in (E.3) can be seen as a transition in state space from the initial state vector \mathbf{x}_0 to the state vector at time t ($\mathbf{x}(t)$) and is thus called the state transition matrix. The state-transition matrix is a fundamental matrix with $\underline{\mathbf{X}}(t_0) = \mathbf{1}_{n \times n}$. From (E.3), the stability of (E.1) is evaluated by the eigenvalues of $\underline{\mathbf{A}}$.

E.2 Time-dependent Periodic System and Floquet Theory

To ensure stability for the time-variant, continuous and linear system

$$\dot{\mathbf{x}}(t) = \underline{\mathbf{A}}(t)\mathbf{x}(t) \quad (\text{E.4})$$

is studied. Here $\underline{\mathbf{A}}(t)$ is an $n \times n$ matrix, which is periodic with time T , such that

$$\underline{\mathbf{A}}(t) = \underline{\mathbf{A}}(t+T) \quad (\text{E.5})$$

With the initial time t_0 and the initial state $\mathbf{x}(t_0) = \mathbf{x}_0$. The state-transition matrix for (E.4) is denoted $\underline{\Phi}_A$ and contains n linearly independent solution to (E.4). The matrix differential equation for the time-dependent system is thus given by

$$\dot{\underline{\Phi}}_A(t, t_0) = \underline{\mathbf{A}}(t)\underline{\Phi}_A(t, t_0) \quad (\text{E.6})$$

Here $\underline{\Phi}_A(t, t) = \underline{\Phi}_A(t_0, t_0) = \underline{1}$. In general, if (E.5) holds and if $\underline{\Phi}(t, t_0)$ is a fundamental matrix, then $\underline{\Phi}(t + T, t_0)$ will also be a fundamental matrix and a non-singular constant matrix \underline{C} exist such that

$$\underline{\Phi}(t + T, t_0) = \underline{\Phi}(t, t_0)\underline{C} \quad (\text{E.7})$$

(E.7) can be proven by calculating the differential of $\underline{\Phi}(t + T, t_0)$

$$\dot{\underline{\Phi}}(t + T, t_0) = \dot{\underline{\Phi}}(t, t_0)\underline{C} = \underline{A}(t)\underline{\Phi}_A(t, t_0)\underline{C} = \underline{A}(t + T)\underline{\Phi}_A(t + T, t_0) \quad (\text{E.8})$$

From (E.7) it is easily seen that \underline{C} is given by

$$\underline{C} = \underline{\Phi}^{-1}(t, t_0)\underline{\Phi}_A(t + T, t_0) \quad (\text{E.9})$$

As \underline{C} is a constant matrix and thus time-independent, it can be computed by setting $t = t_0$ which yields

$$\underline{C} = \underline{\Phi}^{-1}(t_0, t_0)\underline{\Phi}_A(t_0 + T, t_0) = \underline{1}\underline{\Phi}_A(t_0 + T, t_0) = \underline{\Psi}(t_0) \quad (\text{E.10})$$

$\underline{\Psi}(t_0)$ is called the Monodromy matrix, and it can be seen that the eigenvalues of $\underline{\Psi}(t_0)$ are independent of the initial time t_0 . A constant matrix \underline{R} exist that satisfies

$$\underline{C} \equiv e^{\underline{R}T} \quad (\text{E.11})$$

Here the eigenvalues of \underline{R} are the characteristic multipliers of (E.6). For asymptotic stability all characteristic multipliers must be positioned in the left half plane. Likewise the characteristic exponents (the eigenvalues of \underline{C}), should be enclosed by the unit circle for asymptotic stability.

Appendix F

Lyapunov Stability

To prove that a system is stable the Lyapunov stability criteria is used. A system can be unstable, Lyapunov stable, asymptotically stable or exponentially stable. To test if the system is stable, a positive definite continuously differentiable function $V(x)$ describing the closed loop system, φ , must be found. This can for instance be a function describing the energy in the system. The system is then defined to be stable if the energy in the system goes towards zero as the time goes to infinity. The Lyapunov Stability theorem [Khalil 96, p. 100]:

$$\begin{aligned} \text{if } & \exists \quad V : D \subset \mathbb{R}^n \rightarrow \mathbb{R} \text{ s.t. :} \\ & 1 : \quad V(0) = 0 \\ & 2 : \quad V(x) > 0 \quad \forall x \in D, x \neq 0 \\ & 3 : \quad \dot{V}(x) \leq 0 \quad \forall x \in D \\ \text{then } & x = 0 \text{ is a stable equilibrium for } \varphi. \end{aligned}$$

$$\begin{aligned} \text{and if } & 4 : \quad \dot{V}(x) < 0 \quad \forall x \in D, x \neq 0 \\ \text{then } & x = 0 \text{ is an asymptotically stable equilibrium for } \varphi. \end{aligned}$$

$$\begin{aligned} \text{and if } & 5 : \quad \|x\| \rightarrow \infty \implies V(x) \rightarrow \infty \\ \text{then } & x = 0 \text{ is a globally stable equilibrium for } \varphi. \end{aligned}$$

$V(x)$ is often found such that it is on the quadratic form, known as Lyapunov function (F.1)[Khalil 96, p. 160]:

$$V(x) = x^T Q x \tag{F.1}$$

$$\dot{V}(x) = \dot{x}^T Q x + x^T Q \dot{x} \tag{F.2}$$

Appendix G

Fault Propagation Calculations

By observing Fig. 5.1 it can been seen that:

$$\mathbf{e}_g = \underline{\mathbf{A}}_{f_g} \otimes \mathbf{f}_g \quad (\text{G.1})$$

$$\underline{\mathbf{A}}_{f_g} = \begin{bmatrix} 0 & 1 & 0 & 1 \\ 1 & 0 & 0 & 1 \\ 0 & 0 & 1 & 0 \end{bmatrix} \quad (\text{G.2})$$

$$\mathbf{e}_{ads} = \underline{\mathbf{A}}_{f_{ads}} \otimes \begin{bmatrix} \mathbf{f}_{ads} \\ \mathbf{e}_g \end{bmatrix} = \underline{\mathbf{A}}_{f_{ads}} \otimes \begin{bmatrix} \mathbf{1} & \mathbf{0} \\ \mathbf{0} & \underline{\mathbf{A}}_{f_g} \end{bmatrix} \otimes \begin{bmatrix} \mathbf{f}_{ads} \\ \mathbf{f}_g \end{bmatrix} \quad (\text{G.3})$$

$$\underline{\mathbf{A}}_{f_{ads}} = \begin{bmatrix} 1 & 1 & 1 & 1 \\ 1 & 1 & 1 & 1 \end{bmatrix} \quad (\text{G.4})$$

$$\mathbf{e}_{mt} = \underline{\mathbf{A}}_{f_{mt}} \otimes \mathbf{f}_{mt} \quad (\text{G.5})$$

$$(\text{G.6})$$

$$\underline{\mathbf{A}}_{f_{mt}} = \begin{bmatrix} 0 & 1 & 0 & 0 & 0 & 1 \\ 1 & 0 & 1 & 0 & 0 & 1 \\ 0 & 0 & 0 & 1 & 1 & 0 \end{bmatrix} \quad (\text{G.7})$$

$$\mathbf{e}_{pm} = \underline{\mathbf{A}}_{f_{pm}} \otimes \mathbf{f}_{pm} \quad (\text{G.8})$$

$$(\text{G.9})$$

$$\underline{\mathbf{A}}_{f_{pm}} = [1] \quad (\text{G.10})$$

$$\mathbf{e}_{sc} = \underline{\mathbf{A}}_{f_{sc}} \otimes \begin{bmatrix} \mathbf{e}_g \\ \mathbf{e}_{ads} \\ \mathbf{e}_{mt} \\ \mathbf{e}_{pm} \end{bmatrix} \quad (\text{G.11})$$

$$\underline{\mathbf{A}}_{f_{sc}} = \begin{bmatrix} 0 & 0 & 0 & 1 & 1 & 1 & 1 & 1 & 1 \\ 1 & 1 & 1 & 0 & 0 & 0 & 0 & 1 & 0 \end{bmatrix} \quad (\text{G.12})$$

The system fault vector is defined as :

$$\mathbf{f}_{sys} = \begin{bmatrix} \mathbf{f}_g \\ \mathbf{f}_{ads} \\ \mathbf{f}_{mt} \\ \mathbf{f}_{pm} \end{bmatrix} \quad (\text{G.13})$$

For later calculation it is convenient to define a conversion matrix $\underline{\mathbf{C}}$:

$$\begin{bmatrix} \mathbf{f}_g \\ \mathbf{f}_{ads} \\ \mathbf{f}_g \\ \mathbf{f}_{mt} \\ \mathbf{f}_{pm} \end{bmatrix} = \underline{\mathbf{C}} \otimes \mathbf{f}_{sys} \quad (\text{G.14})$$

$$\Downarrow \quad (\text{G.15})$$

$$\underline{\mathbf{C}} = \begin{bmatrix} \underline{\mathbf{1}} & \underline{\mathbf{0}} & \underline{\mathbf{0}} & \underline{\mathbf{0}} \\ \underline{\mathbf{0}} & \underline{\mathbf{1}} & \underline{\mathbf{0}} & \underline{\mathbf{0}} \\ \underline{\mathbf{1}} & \underline{\mathbf{0}} & \underline{\mathbf{0}} & \underline{\mathbf{0}} \\ \underline{\mathbf{0}} & \underline{\mathbf{0}} & \underline{\mathbf{1}} & \underline{\mathbf{0}} \\ \underline{\mathbf{0}} & \underline{\mathbf{0}} & \underline{\mathbf{0}} & \underline{\mathbf{1}} \end{bmatrix} \quad (\text{G.16})$$

The propagation of faults from its origin to the end effect can now be derived.

$$\mathbf{e}_{sc} = \underline{\mathbf{A}}_{f_{sc}} \otimes \begin{bmatrix} \mathbf{e}_g \\ \mathbf{e}_{ads} \\ \mathbf{e}_{mt} \\ \mathbf{e}_{pm} \end{bmatrix} = \underline{\mathbf{A}}_{f_{sc}} \otimes \begin{bmatrix} \underline{\mathbf{A}}_{f_g} \otimes \mathbf{f}_g \\ \underline{\mathbf{A}}_{f_{ads}} \otimes \begin{bmatrix} \underline{\mathbf{1}} & \mathbf{0} \\ \mathbf{0} & \underline{\mathbf{A}}_{f_g} \end{bmatrix} \otimes \begin{bmatrix} \mathbf{f}_{ads} \\ \mathbf{f}_g \end{bmatrix} \\ \underline{\mathbf{A}}_{f_{mt}} \otimes \mathbf{f}_{mt} \\ \underline{\mathbf{A}}_{f_{pm}} \otimes \mathbf{f}_{pm} \end{bmatrix} \quad (\text{G.17})$$

$$= \underline{\mathbf{A}}_{f_{sc}} \otimes \begin{bmatrix} \underline{\mathbf{A}}_{f_g} & \mathbf{0} & \mathbf{0} & \mathbf{0} \\ \mathbf{0} & \underline{\mathbf{A}}_{f_{ads}} \otimes \begin{bmatrix} \underline{\mathbf{1}} & \mathbf{0} \\ \mathbf{0} & \underline{\mathbf{A}}_{f_g} \end{bmatrix} & \mathbf{0} & \mathbf{0} \\ \mathbf{0} & \mathbf{0} & \underline{\mathbf{A}}_{f_{mt}} & \mathbf{0} \\ \mathbf{0} & \mathbf{0} & \mathbf{0} & \underline{\mathbf{A}}_{f_{pm}} \end{bmatrix} \otimes \underline{\mathbf{C}} \otimes \mathbf{f}_{sys} \quad (\text{G.18})$$

$$= \underline{\mathbf{A}}_{f_{sys}} \otimes \mathbf{f}_{sys} \quad (\text{G.19})$$

Appendix H

CUSUM Algorithm Calculations

This section is based on [Blanke 06].

Given a sequence of independent stochastic variables $z(i)$, where $z(i)$ is a Gaussian sequence with mean μ and standard deviation σ , the probability density function (pdf) is given by[Leon-Garcia 09, p. 164]:

$$p_{\mu,\sigma}(z) = \frac{1}{\sqrt{2\pi}\sigma} e^{-\frac{1}{2} \left(\frac{\mu-z}{\sigma}\right)^2} \quad (\text{H.1})$$

Two hypothesis are defined. One which states that the process is normal (\mathcal{H}_0) and a hypothesis stating that the process is faulty (\mathcal{H}_1). To determine whether the process is faulty or not a log-likelihood ratio of the two pdfs ($s(z)$) is studied. In this way the probability for $z(i)$ being a normal or faulty process can be described by the sign of $s(z)$. This means that $z(i)$ will be most likely to belong to $p_{\mathcal{H}_0(z)}$, if $s(z)$ is negative, and more likely to belong to $p_{\mathcal{H}_1(z)}$ if $s(z)$ is positive. $s(z)$ is given by

$$s(z(i)) = \ln \left(\frac{p_{\mathcal{H}_1(z)}}{p_{\mathcal{H}_0(z)}} \right) \quad (\text{H.2})$$

To detect a change of a single parameter the probability density function is simplified such that the change of only one parameter is studied (here the mean-value μ), thus the variance σ^2 is assumed to be the same for a faulty and non-faulty process. $s(z)$ is

then rewritten to

$$\begin{aligned}
s(z) &= \ln \left(\frac{p_{\mu_1}(z)}{p_{\mu_0}(z)} \right) \\
&= \ln \left(\frac{\frac{1}{\sqrt{2\pi}\sigma} e^{-\frac{1}{2} \left(\frac{\mu_1-z}{\sigma} \right)^2}}{\frac{1}{\sqrt{2\pi}\sigma} e^{-\frac{1}{2} \left(\frac{\mu_0-z}{\sigma} \right)^2}} \right) \\
&= -\frac{1}{2} \left(\frac{\mu_1-z}{\sigma} \right)^2 + \frac{1}{2} \left(\frac{\mu_0-z}{\sigma} \right)^2 \\
&= \frac{1}{2\sigma^2} \left(-(\mu_1-z)^2 + (\mu_0-z)^2 \right) \\
&= \frac{1}{2\sigma^2} \left(-(\mu_1^2 + z^2 - 2\mu_1 z) + (\mu_0^2 + z^2 - 2\mu_0 z) \right) \\
&= \frac{2z(\mu_1 - \mu_0) + (\mu_0^2 - \mu_1^2)}{2\sigma^2} \\
&= \frac{\mu_1 - \mu_0}{\sigma^2} \left(z - \frac{\mu_0 + \mu_1}{2} \right)
\end{aligned} \tag{H.3}$$

A function $S(k)$ is obtained by the cumulative sum of (H.2)

$$S(k) = \sum_{i=1}^k s(z(i)) \tag{H.4}$$

(H.4) will now have a negative drift when $z(i)$ has higher probability belonging to a non-faulty process and a positive drift when $z(i)$ is most likely to be a faulty process. In practise $z(i)$, will not be perfectly Gaussian, nor have means or variance that fits the model exact (will be estimated). Most significantly the algorithm is based on probabilities. For this reason the value of $S(k)$ can at given samples provide the wrong information. For this reason a fault-threshold is introduced, such that minor misinformations from $S(k)$ is ignored. To make the threshold independent of time (number of samples k), $S(k)$ is biased and the decision function is given by

$$g(k) = S(k) - m(k) \tag{H.5}$$

where

$$m(k) = \min_{j=[i;k]} S(j) \tag{H.6}$$

In this way the minimum value of the decision function $g(k)$ will always be zero and thus a threshold h can be chosen as a constant positive value. The following decision rule is thus obtained

$$\begin{aligned}
&\text{if } g(k) \leq h \text{ accept } \mathcal{H}_0 \\
&\text{if } g(k) > h \text{ accept } \mathcal{H}_1
\end{aligned} \tag{H.7}$$

The threshold parameter h should be chosen with care as too low a value will result in the detection of faults when no faults have occurred. On the other hand too high a h will cause the CUSUM algorithm not to detect the occurring faults. I.e. determining h is a compromise between the mean delay for detection a fault (T_d) and the mean time between false alarms (T_{fa}). The value of T_d and T_{fa} can be estimated by the Average

Run Length (ARL) which provides the expected value of the alarm time, given that the sequence has a Gaussian distribution. When interested in detecting a change of mean the ARL can be estimated by

$$L(\mu_s) = \frac{\sigma_s^2}{2\mu_s^2} \left[e^{-2\left(\frac{\mu_s h}{\sigma_s^2} + 1.166\frac{\mu_s}{\sigma_s}\right)} - 1 + 2\left(\frac{\mu_s h}{\sigma_s^2} + 1.166\frac{\mu_s}{\sigma_s}\right) \right] \quad (\text{H.8})$$

where

$$\sigma_s^2 = \frac{(\mu_1 - \mu_0)^2}{\sigma^2} \quad (\text{H.9})$$

the estimated mean delay for detecting a fault, T_d is given as

$$T_d = L(E_{\mu_1}(s(z))) = L\left(\frac{(\mu_1 - \mu_0)^2}{2\sigma^2}\right) \quad (\text{H.10})$$

and the estimated mean time between false alarms, T_{fa} is found by

$$T_{fa} = L(E_{\mu_0}(s(z))) = L\left(-\frac{(\mu_1 - \mu_0)^2}{2\sigma^2}\right) \quad (\text{H.11})$$

Appendix I

Simulation Environment

The simulink implementation of the nadir controller and the unknown input observer is shown in this appendix. The rest of the simulations can be found on the CD in Appendix J.

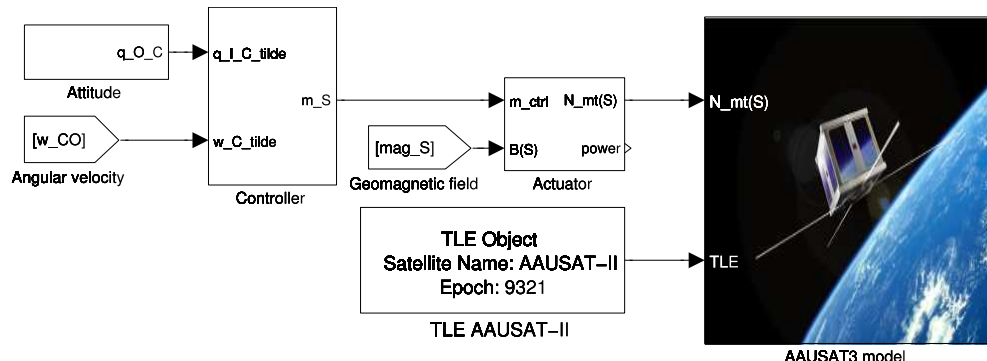


Figure I.1: The nadir controller setup include the actuator model and the satellite model

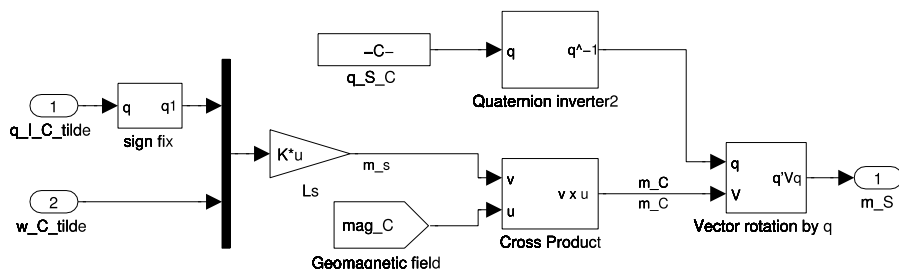


Figure I.2: The controller box in Fig. I.1

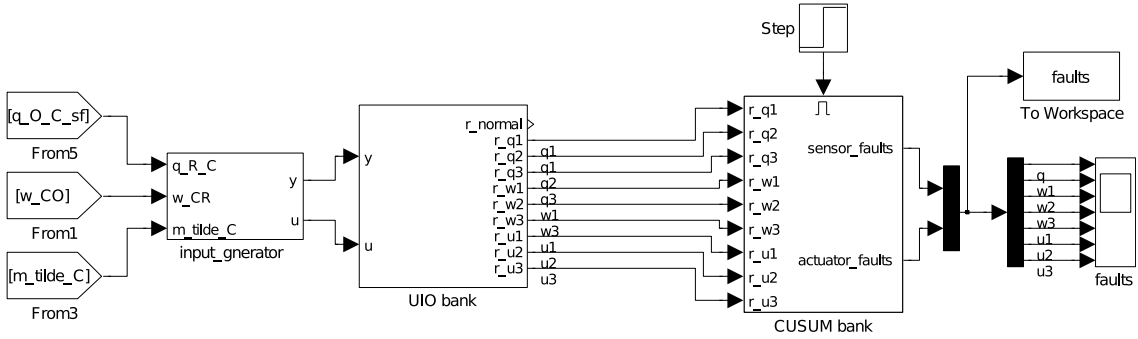


Figure I.3: The implementation of the UIO in simulink

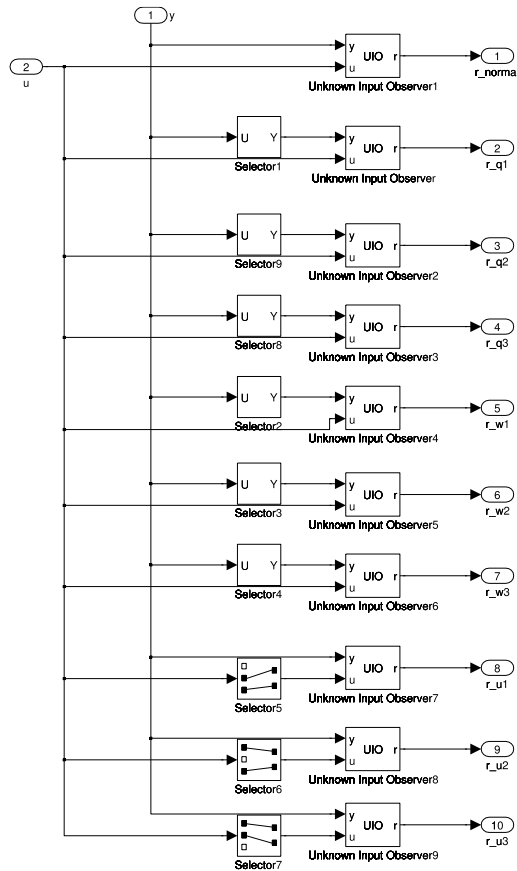


Figure I.4: The internal structure of the UIO bank from Fig. I.3

Appendix J

CD Content

```
cd_10gr832
├── bibliography
│   ├── datasheets.....Downloaded version of the datasheets
│   └── internet .....Downloaded version of the web pages
├── matlab_scripts
│   ├── bdot .....Scripts used for designing the B-dot
│   └── constant_gain.....Scripts for constant gain
├── simulink_models
│   ├── bdot .....Implementation of the B-dot controller
│   └── constant_gain.....Implementation of the nadir pointing controller
└── svn.....Checkout of the SVN source this is messy
```

Bibliography

- [Atmel 06] Atmel. *8-bit AVR Microcontroller with 128K Bytes of ISP Flash and CAN controller*, 2005/2006. <http://www.alldatasheet.com/datasheet-pdf/pdf/83728/ATMEL/AT90CAN128.html>.
- [Bak 99] Thomas Bak. Spacecraft Attitude Determination - a Magnetometer Approach. AAU Centertrykkeriet, 1999.
- [Bak 02] Thomas Bak. *Lecture Notes - Modeling of Mechanical Systems*, 2002.
- [Blanke 06] M. Blanke, M. Kinnaert, J. Lunze & M. Staroswiecki. Diagnosis and fault-tolerant control. Springer, 2006.
- [Chen 99] Jie Chen & R.J. Patton. Robust Model-based Fault Diagnosis For Dynamic Systems. Kluwer Academic Publishers, 1999.
- [Graversen 02] Torben Graversen, Michael Kvist Frederiksen & Søren Vejlgaard Vedstesen. Attitude control system for aau cubesat. 2002.
- [Green 06] Martin Green, Martin Nygaard Kragelund & Mads Sletten. Robust disturbance rejecting attitude control for the north observer satellite. 2006.
- [Hor 08] Honeywell. *HMC 6343*, October 2008. Magnotometer (big).
- [Hor 09] Honeywell. *HMC 5843*, February 2009. Magnotometer (small).
- [Inv 08] InvenSense. *IDG-1215*, July 2008. Two Axis Gyro.
- [Inv 09] InvenSense. *ISZ-1215*, July 2009. One Axis Gyro.
- [Izadi-Zamanabadi 99] Roozbeh Izadi-Zamanabadi. Fault-tolerant Supervisory Control-System Analysis and Logic Design. AAU Centertrykkeriet, 1999.
- [Izadi-Zamanabadi 06] R. Izadi-Zamanabadi & J. A. Larsen. *A Fault Tolerant Control Supervisory System Development Procedure for Small Satellites the AAUSAT-II Case*. 2006.
- [Jensen 10] Kasper Fuglsang Jensen & Kasper Vinther. *Attitude Determination and Control System for AAUSAT3*, 2010.
- [Khalil 96] Hassan K. Khalil. Nonlinear Systems, Second Edition. Prentice-Hall, 1996.
- [Korhonen 10] Kimmo Korhonen. *The IGRF-Applet Homepage*, 2010. <http://www.geo.fmi.fi/MAGN/igrf/>.

-
- [Kuipers 02] Jack B. Kuipers. Quaternions and Rotation Sequence. Princeton University Press, 2002.
- [Leon-Garcia 09] Alberto Leon-Garcia. Probability, Statistics, and Random Processes for Electrical Engineering, Third Edition. Pearson Prentice Hall, 2009.
- [Max 07] Maxim. *DS75LX*, March 2007. Temperature Sensor.
- [Mohler 99] Ronald R. Mohler. Nonlinear Systems VOLUME 1 Dynamics and Control. Prentice-Hall, Inc., 1999.
- [Schacht 09] Jörg Schacht. *Design-FMEA*, 2009. <http://www.i-q.de/dokumente/downloads/Bewertungstabellen\DFMEA\SAE-J1739\engl.pdf>.
- [Serway 04] Serway & Jewett. Physics for Scientist and Engineers 6ed. Thomson Books/Cole, 2004.
- [Sil 04] Silonex. *SLCD-61N8*, October 2004. Sun Photo Diode.
- [team 10a] The AAUSAT3 team. *Cubesat*, 2010. <http://www.aausat3.space.aau.dk/pmwiki.php?n=Site.AISPayload>.
- [team 10b] The AAUSAT3 team. *Cubesat*, 2010. <http://www.aausat3.space.aau.dk/pmwiki.php?n=Site.AISPayload>.
- [team 10c] The AAUSATII team. *2 ÅRS FØDSELSDAG og still going strong !!!*, 2010. <http://aausatii.space.aau.dk/>.
- [team 10d] The AAUSATII team. *2 ÅRS FØDSELSDAG og still going strong !!!*, 2010. <http://en.wikipedia.org/wiki/CubeSat>.
- [Tex 09] Texas Instruments. *ADS1115*, May 2009. ADC used for Gyros.
- [Vedstesen 02] Torben Graversen Michael Kvist Frederiksen Søren Vejlgaard Vedstesen. *Attitude Control system for AAU CubeSat*, 2002.
- [Vis 04] Vishay. *Si9988*, April 2004. Magnetorque drivers.
- [Ward 10] Michael Jeffrey Ward. *Basic Floquet Theory*, 2010. www.math.ubc.ca/~ward/teaching/m605/every2\floquet1.pdf.
- [Wertz 78] J.R. Wertz. Spacecraft attitude determination and control. Kluwer Academic Pub, 1978.
- [Wie 98] Bong Wie. Space vehicle dynamics and control. AIAA educational series, 1998.
- [Wiśniewski 96] Rafal Wiśniewski. Satellite Attitude Control Using Only Electromagnetic Actuation. AAU Centertrykkeriet, 1996.